DESIGN AND FABRICATION OF BIOCOMPATIBLE COPPER BASED SHAPE MEMORY ALLOY BY SPARK PLASMA SINTERING

by
Auditee Majumder Momo
Student ID: 0419112013

MASTER OF SCIENCE IN MATERIALS AND METALLURGICAL ENGINEERING

Supervisor: Dr. Fahmida Gulshan
Co-Supervisor: Dr. Syed Ansar Md. Tofail

Department of Materials and Metallurgical Engineering

Bangladesh University of Engineering and Technology

Dhaka-1000, Bangladesh

July 2022

Approval page

The thesis titled "DESIGN AND FABRICATION OF BIOCOMPATIBLE COPPER BASED SHAPE MEMORY ALLOY BY SPARK PLASMA SINTERING" submitted by Auditee Majumder Momo, Roll No: 0419112013, Session: April/2019, has been accepted as satisfactory in partial fulfillment of the requirement for the degree of Master's of Science in Materials and Metallurgical Engineering on 3rd July, 2022.

BOARD OF EXAMINERS

1. .....

Dr. Fahmida Gulshan — Chairman
Professor — (Supervisor)
Department of MME, BUET, Dhaka

2. .....

Dr. Syed Ansar Md. Tofail — Member
Associate Professor — (Co-Supervisor)
Department of Physics,
Bernal Institute, University of Limerick, Ireland

3. .....

Head/Director, Dr. Mahbub Hasan — Member
Professor — (Ex-Officio)
Department of MME, BUET, Dhaka

4. .....

Dr. Kazi Mohammad Shorowordi — Member
Professor
Department of MME, BUET, Dhaka

5. .....

Dr. Hossain Mohammad Mamun Al Rashed — Member
Associate Professor
Department of MME, BUET, Dhaka.

6. .....

Dr. Sheikh Manjura Hoque — Member
Chief Scientific Officer and Head — (External)
Materials Science Division, Atomic Energy Center, Dhaka.

Declaration

I, Auditee Majumder Momo, hereby declare that this thesis is entirely my work, and any part of it has not been submitted anywhere else for the award of any degree. All quotations, figures, and results from other sources are duly acknowledged and referenced.

.....

Student ID- 0419112013
Auditee Majumder Momo
Department of Materials and Metallurgical Engineering
BUET, Dhaka-1000

Dedication.....
To Dr. Fahmida Gulshan, whose constant warmth and companionship I could not repay.

ACKNOWLEDGEMENTS

I would like to thank the almighty God, who provided me with the opportunity to complete this study and always guided me towards achieving my goal.

My supervisor Prof. Dr. Fahmida Gulshan was my guardian angel throughout this journey. She inspired me to embark on this journey, shared her incredible experience and knowledge throughout the study, and provided support whenever I needed it. I would like to thank her for teaching me about proper research methodologies. I would also like to show my gratitude to my co-supervisor, Dr. Syed Ansar Md. Tofail. While working with the MOSAIC group of the Bernal Institute of the University of Limerick, his supervision, constant encouragement, and motivation were invaluable.

I am blessed to have met two of the most wonderful souls I know - Garry Warren and Sarah Markham from the University of Limerick, Ireland. Their kindness and hospitality mesmerized me, while their enthusiasm and work ethic inspired me to be a better researcher and a better human being.

Last but not certainly the least, I would like to thank my family and friends. My parents have been my support system throughout my educational career, and the number of times they have inspired me to carry on cannot be counted. My brother has always been my knight in shining armor, his care and support instilled in me the optimism I needed to finish this study. I thank my friends, peers, and colleagues for always being there for me, I could not have completed my research without them.

Auditee Majumder Momo acknowledges European Commission Erasmus International Credit Mobility 2018-2023 between the University of Limerick, Ireland, and Bangladesh University of Engineering and Technology, Dhaka, Bangladesh, for a six-month secondment at the Modeling, Simulation, and Innovative Characterization (MOSAIC) group of the Bernal Institute of the University of Limerick, where a part of the research leading to the current thesis was conducted. Neither the European Commission nor the University of Limerick holds any responsibility for this thesis's content and conclusion

Abstract

Copper based shape memory alloys are at the forefront of R&D for biomedical applications due to their good shape recovery, ease of fabrication, excellent thermal and electrical conductivity, antibacterial properties, and corrosion resistance. Spark plasma sintering (SPS) is a consolidated powder metallurgy process, which offers biocompatibilities to the materials by controlling grain growth, forming desired phases and controlled number of porosities. In the present study, two type of shape memory alloys- CuAlNi and NiTiCu have been fabricated by the SPS method. Studying the ternary phase diagram of the alloys, the composition has been chosen. The SPS parameters have been determined through multiple trials. CuAlNi and NiTiCu alloys have been sintered respectively at 475℃ and 730℃. The present study aims to find out the effectiveness of lower sintering temperature and pressure for sintering the shape memory alloys. After selecting the material and experimental parameters, the sample powders have been prepared by wet ball milling at lower ball powder ratio (BPR) and lower milling hour. DSC analysis of the powder has been done to find out the melting point of the alloy powders and the temperatures for different phase formations. XRD, SEM and EDS analysis of the sintered CuAlNi and NiTiCu samples have been carried out to identify the phases and to see the morphology of the samples. Micro hardness of the sintered alloys has been measured and static corrosion test have been done on the sample to find out the corrosion rate. The DSC analysis of the alloy powders provides evidence that successful sintering of CuAlNi and NiTiCu is possible at lower SPS and ball milling parameters. XRD, SEM and EDS results also confirm the presence of desired phases in the sintered alloys. The Vickers hardness values of CuAlNi and NiTiCu refer to the further modification of CuAlNi sample is required whereas the hardness of NiTiCu alloys already have the desired values. The corrosion rates of presently studied CuAlNi alloys are lower. But corrosion resistance of NiTiCu samples in the present study requires further improvement.

Table of Contents

Abstract ..... ***v***

Chapter 1 : Introduction ***1***

1.1 Introduction **1**

1.2 Research Aim: **1**

1.3 Research Questions: **2**

1.4 Research Hypothesis: **2**

1.5 Methodological Approach: **3**

1.6 Structure of the thesis: **4**

Chapter 2 : Literature Review ***6***

2.1 Introduction: **6**

2.2 Contribution to the State of the Art: **6**

2.3 Shape memory alloys: **7**

2.4 Biocompatibility: **8**

2.5 Recent developments in metals for biomedical devices: **13**

Metal selection for Biomedical application: 13

Metals and Alloys used in Biomedical application: 15

New generation of metallic biomaterials: 17

2.6 Structure and transformation of CuAlNi and NiTiCu: **18**

2.6.1 CuAlNi: 18

2.6.2 NiTiCu: 21

2.7 Properties of CuAlNi and NiTiCu: **23**

2.7.1 CuAlNi: 23

2.7.2 NiTiCu: 25

2.8 Biocompatibility and cytotoxicity of CuAlNi and NiTiCu: **27**

2.8.1 Biocompatibility of Copper: 27

2.8.2 Biocompatibility of Aluminium: 29

2.8.3 Biocompatibility of Nickel: 29

2.8.4 Biocompatibility of Titanium: 30

2.8.5 Biocompatibility of CuAlNi: 31

2.8.6 Biocompatibility of NiTiCu: 31

2.8.7 Cytotoxicity of different elements: 32

2.9 Corrosion resistance of CuAlNi and NiTiCu: **33**

2.9.1 Corrosion of CuAlNi: 33

2.9.2. Corrosion of NiTiCu: 34

2.10 Different Corrosion Media: **34**

2.11 Biomedical applications of copper-based shape memory alloys: **35**

2.12 Production methods of shape memory alloys: **42**

2.13 Spark plasma sintering of CuAlNi and NiTiCu: **43**

2.13.1 Principle of Spark Plasma Sintering: 44

2.13.2 Mechanism of solid-state sintering: 45

2.14 Biocompatibility and Spark Plasma Sintering: **46**

Chapter 3 : Experimental Design: ***48***

3.1 Material selection: **48**

3.2 Ball milling parameter selection: **50**

3.3 SPS Temperature profile and pressure selection: **51**

3.4 Corrosion Media Selection: **53**

Chapter 4 : Methodology: ***54***

4.1 Ball milling for producing the powders: **54**

(a) CuAlNi: 55

(b) NiTiCu: 55

4.2 DSC: **56**

4.3 Spark Plasma Sintering and characterizations: **56**

4.3.1 Die preparation: 56

4.3.2 Sintering of the samples in the SPS machine: 57

4.3.3 XRD: 59

4.3.4 SEM: 59

4.3.5 Hardness Test: 59

4.3.6 Corrosion Test: 59

Chapter 5 : Results and Discussions: ***63***

5.1 DSC of ball milled powder: **63**

5.2 Hardness: **66**

5.3 SEM results of the Samples: **69**

5.4 XRD analysis of the samples: **78**

5.5 Corrosion rate: **81**

Conclusion: ***83***

Future Scope of work: ***83***

References ***84***

Table of Figures

Figure 2.1:Shape memory effect and Pseudo elasticity 8
Figure 2.2: Binary Cu-Al phase Diagram 19
Figure 2.3: Crystal structures of austenite, orthorhombic, monoclinic phases respectively from the left and their lattice correspondence 20
Figure 2.4: Binary Ni-Ti phase diagram 22
Figure 2.5: Crystal structure during the transformation of NiTiCu 23
Figure 2.6: Pseudo elasticity of CuAlNi 24
Figure 2.7: Illustration of the schematic phase occurred after sintering [24] 26
Figure 2.8: Shape memory alloy made eyeglasses 36
Figure 2.9: Wagner's thermolock spring 36
Figure 2.10: Medical guidewire 37
Figure 2.11: Simon Filter 38
Figure 2.12: Nitinol Stent 38
Figure 2.13: Spinal Vertebrae Spacer 39
Figure 2.14: Orthopedic staples, staples placed in human bone 39
Figure 2.15: Shape memory alloy plate 40
Figure 2.16: Gloves made of shape memory alloy wire 40
Figure 2.17: Sequence of opening the shape memory basket 41
Figure 2.18: Intra-aortic balloon pump 41
Figure 2.19: Laparoscopy tools used for gripping in surgery 42
Figure 2.20: Localized heating and neck formation by joule heating [48] 44
Figure 2.21: Schematic diagram of spark plasma sintering principle 44
Figure 2.22: Initial stage of spark discharging by ON-OFF pulse energization, Generation of spark plasma, Vaporization and melting action to the particle surface, Generation of spark impact pressure, sputtering of Enhanced neck growth in the presence of vaporized/mol [49] 45
Figure 3.1: CuAlNi ternary phase diagrams (a) isothermal section at 800℃, (b) pseudo-binary phase diagram [52] 48
Figure 3.2: Ternary phase diagram of NiTiCu with the liquids and primary crystallization phases [53] 50
Figure 4.1 Measuring the (a)round, (b) Cylindrical ZrO_2 balls, powder, ethanol and taking into the (c) HDPE plastic container (d) ball milling in NECO SYSTEM, (e) Evaporating alcohol for getting dry powders 54
Figure 4.2: Die preparation before Sintering 56
Figure 4.3: Dr. Sinter, SPS-515S, SPS Syntax Inc., Kawasaki, Japan Model SPS-511 with optional High Vacuum System and no Analysis Unit 58
Figure 4.4: CuAlNi and NiTiCu submerged in PBS solution before corrosion 60
Figure 4.5: CuAlNi and NiTiCu submerged in PBS solution after corrosion 60
Figure 5.1: DSC Curve (Heating cycle) of ball milled CuAlNi (a) sample-1 (b) sample-2 powders ball milled for 8hrs 63
Figure 5.2: DSC curves of heating and cooling cycle of ball milled CuAlNi powder 64
Figure 5.3: DSC Curve (heating cycle) of ball milled NiTiCu (a) Sample-1 (b) Sample-2 powders ball milled for 8hrs 65
Figure 5.4: DSC Curve (heating and cooling cycle) of ball milled NiTiCu powder 66
Figure 5.5: Comparison of the hardness of CuAlNi SMAs with the existing biomaterials 67
Figure 5.6: Comparison of the hardness of NiTiCu SMAs with the existing biomaterials 68
Figure 5.7: SEM micrograph of CuAlNi Sample-1 sintered at 475℃ (a) 10000x (b) 10,000 x (c) 2,000x 69

Figure 5.8: EDS of CuAlNi sample 1 70
Figure 5.9: SEM micrograph of CuAlNi sample 2 sintered at 475℃ (a) 500x, (b) 5000x, (C) 2000x....71
Figure 5.10: EDS of CuAlNi sample 2 72
Figure 5.11: SEM image of NiTiCu Sample-1 sintered at 730℃ (a) 300x, (b) 500x, (c) 1000x. 74
Figure 5.12: EDS result of NiTiCu Sample-1....75
Figure 5.13: SEM image of NiTiCu sample 2 sintered at 730℃- (a)300x, (b) 1000x, (c) 500x 76
Figure 5.14: EDS result of NiTiCu sample 2....77
Figure 5.15: XRD pattern of (a) Sample 1, (b) Sample 2 79
Figure 5.16: XRD pattern of NiTiCu (a) sample 1 (b) sample 2 80
Figure 5.17: Comparison of the corrosion rate of prepared CuAlNi samples 81
Figure 5.18: Comparison of the corrosion rate of NiTiCu with NiTi....82

Lists of Tables:

Table 2.1: Different Biomaterials applied to medical science [16] 16
Table 2.2: Physical properties of CuAlNi.....25
Table 2.3: Physical properties of NiTiCu 27
Table 3.1: Chosen composition of CuAlNi alloys.....49
Table 3.2: Chosen composition for NiTiCu alloy.....50
Table 3.3: SPS Temperature profile for CuAlNi alloys.....52
Table 3.4: SPS Temperature profile for NiTiCu alloys 53
Table 4.1: weight of pure elements and prepared CuAlNi alloy powder 55
Table 4.2: weight of pure elements and prepared NiTiCu alloy powder.....55
Table 4.3: Theoretical density wise weight of each CuAlNi sample's powder before sintering.....57
Table 4.4: Theoretical density wise weight of each NiTiCu sample's powder before sintering.....57
Table 4.5: Initial specifications of the CuAlNi samples.....61
Table 4.6: Specifications of CuAlNi Samples after 20 days of Corrosion 61
Table 4.7: Initial specifications of NiTiCu samples 62
Table 4.8: Specifications of NiTiCu Samples after 20 days of Corrosion.....62
Table 5.1: Hardness data of CuAlNi and NiTiCu Samples 67
Table 5.2: Elemental Composition Analysis of CuAlNi Sample 1 by EDS.....70
Table 5.3: Elemental Composition Analysis of CuAlNi Sample 2 by EDS.....73
Table 5.4: Elemental Composition Analysis of NiTiCu Sample 1 by EDS 76
Table 5.5: Elemental Composition Analysis of NiTiCu Sample 2 by EDS 78
Table 5.6: After 20 days corrosion rate of the CuAlNi samples.....81
Table 5.7: After 20 days corrosion rate of the NiTiCu samples 82

Chapter 1 : Introduction

1.1 Introduction

Shape memory alloys (SMAs) are smart materials that respond to external stimuli- thermal, mechanical, chemical, electric, electro-magnetic effects, and change their temporarily deformed structures and related properties. There are three main types of SMAs- NiTi-based, Cu-based, and Fe-based. The multifunctional alloys are at the center of attention for many decades due to their diverse functionality applicable to electrical, fire protection, automatic, aerospace, robotics, and biomedical appliances. The shape memory effect, pseudo elasticity, biocompatibility, and electrochemical stability of the SMAs is applied to bioengineering [1]. The significant medical application of SMAs lies in orthopedic, orthodontic, vascular, neuro-surgical, and surgical fields [2]. NiTi alloys have been used in manufacturing biomedical apparatus for a long period of time. The NiTi alloys have their limitations in shape memory, pseudo elastic, and mechanical properties. In addition, from the biological perspective, these alloys have moderate corrosion resistance and cell culture compatibility. The essential amount of Ni in the human body is around 0.1ppm for biological functionality. But the harmful release of the Ni ions from the medical implants may cause allergic, carcinogenic harm to the body. Optimization of the thermo-mechanical processing parameters and surface processing may improve the mechanical properties and biocompatibility of the alloys [3]. The applicability of these alloys depends on the protective TiO_2 so that, toxic Ni ions can't be released. Although NiTi SMAs are extensively being utilized in medical devices and equipment, the use of copper based SMAs was limited to electronic applications in the past. However, at present copper based SMAs are used in external biomedical applications. The significant applications of the alloys include- different biologically inspired robotic systems, especially as micro-actuators, or artificial muscles [4, 5]. Among the copper based SMAs the Cu-Al-Ni alloys have comparatively low cost, reasonable shape memory properties, less vulnerability to phase stabilization, flexible phase transformation temperature. The properties of Cu-Al-Ni alloys have been improved by the addition of alloying elements previously [5]. The elongation of the alloys is almost identical to the NiTi alloys. Copper based SMAs can also show the two-way shape memory effect if the alloys are given thermomechanical treatment training. The challenge in applying these alloys in biomedical applications is the corrosion behavior and toxicity of the copper element. Analysis of the compositional effect on the alloys, and spark plasma sintering parameters is important to evaluate the applicability of the alloys.

1.2 Research Aim:

The aims of this work can be enlisted as follows-

I. Selecting the composition of the CuAlNi and NiTiCu SMAs by analyzing the binary and ternary phase diagrams and previous works on those SMAs.
II. Optimizing the SPS method parameters for fabricating CuAlNi and NiTiCu alloys

III. Observing the microstructural, mechanical, and corrosion properties to evaluate the feasibility of the SMAs for biomedical application.

1.3 Research Questions:

CuAlNi with high transformation temperature gives excellent functional properties but its application in the biomedical field is not noteworthy. The Spark Plasma Sintering (SPS) method is a rapid solidification technique that eliminates many limitations of casting techniques and produces favorable morphology beneficial for biocompatibility. Already studies have been carried out to evaluate the microstructures, and physical and mechanical properties of SPS made CuAlNi. But the surface morphology analysis and biocompatibility checking of the CuAlNi have not been studied yet. Another shape memory alloy, NiTiCu by SPS has also been studied. But the biocompatibility study of the alloys has not been carried out.

So, the study aims to find the answers to the following questions-

I. What are the potentials of the SPS method to produce biocompatible SMAs?
II. What are the effects of composition on the properties, the sintering temperature, and biocompatibility of the SMAs?
III. What is the surface morphology and composition of the SPS-made Cu-based and Cu containing SMAs?
IV. What is the corrosion rate of Cu-based and Cu containing SMAs in the human body fluid condition?

1.4 Research Hypothesis:

The research work has been carried out based on the following hypothesis-

I. Al_2O_3 on the Cu-Al-Ni SMAs plays the same role as TiO_2 on the NiTiCu.
II. As the milling time increases the Ni and Al content gets reduced due to the dissolution of these in Cu.
    a) After 32 hr of milling: A solid solution of Ni-Ti-Al forms
    b) After 48 hrs of milling: A single phase FCC structured phase forms, disordered single-phase solid solution

A rapid decrease in the grain size and increase in lattice strain occur within 10 hrs of milling as a part of grain refining. The severe plastic deformation results in lattice defects that disintegrate the particles to form nanocrystalline structures inside micron-sized particles, grain size refining is not severe after 12 hrs of milling. Excessive time milling may lead to the formation of an amorphous structure, severely deformed, having large dislocation densities, contains a very fine equiaxed substructure.

III. Effect of the elements in the alloy-

Effect of Copper:

- Cu in the range from 5 to 15 wt% changes the crystallographic structure of the low-temperature phase. Cu >7.7 wt% results in a two-way shape memory effect and Cu<7.7 wt% results in a one-way shape memory effect in NiTiCu. The thermal hysteresis is reported to decrease from 40 K for the binary alloy to 11 K for NiTi-10 wt% Cu.
- The stress of the super elastic hysteresis is decreased. Higher unloading plateau is beneficial for medical applications.
- The fatigue resistance during thermal cycling is increased.
- The hardness of the NiTi alloys increases after adding copper.

Effect of Ni:

- Ni>56wt% results in brittle precipitation phase.
- An increase in Ni results in a decrease in transformation temperature.
- At higher sintering temperature the Ni gets induced to Ti later than Cu that results in porosity formation and decrease in hardness.
- 0.5wt% change in Ni content from 56wt% may result in losing the SMA effect.

Effect of Al:

- When the alloy contains Al~11wt%, an ordered structure is found.
- When the alloy contains Al>11wt%, a disordered structure is found.

Effect of Ti:

- The element has a positive impact on its oxide on the surface as the oxide layer prevents Ni ion release.

1.5 Methodological Approach:

The study aims to investigate the biocompatibility of copper based SMAs. The effect of the composition and process parameters on the properties of these alloys has been evaluated by studying the surface properties, the transformation temperatures, mechanical properties, and corrosion behavior. Design of copper based SMAs has been done based on the following requirements-

- Biocompatibility-
  - Improved surface property
  - Proper alloy composition
  - Phase formation
- Improved mechanical properties-
  - SMA effect
  - Corrosion property
  - Microstructure

Two types of samples have been made- CuAlNi and NiTiCu. Among the two types, one type is copper based, and another type is the addition of the copper to the NiTi alloys. The purpose of the preparation of two types of samples is to investigate the compatibility of the copper elements both as the prime alloying element and minor alloying element. The composition of the alloys has been determined from the phase diagram. From the binary Ni-Ti phase diagram, the near equiatomic composition of Ni and Ti generally shows the shape memory behavior, when the β phase is present in the sample. So that in the NiTiCu alloys copper's composition has been varied from 7 wt% to 10 wt% and the composition of the Ni and Ti has been kept nearly identical to each other. From the Cu-Al phase diagram (Figure 2.2), generally, the 70-80% Cu-Al binary alloys show the shape memory properties.

All the samples have been prepared by the powder metallurgy method. The powder metallurgy is better than the traditional casting method because the cast samples are brittle, highly contaminated by the gasses and mold materials in casting, and hard to process further. SPS is one of the powder metallurgy processing techniques for preparing samples. The process requires a short time to sinter due to which grain growth does not occur. The controlled amount of micro and nanosized pores can be introduced to the samples which assist in several biomedical applications i.e.- orthodontics and orthopedic. Additionally, control in the formation of pores also makes the sintered sample lightweight. This is a method of producing the samples without the contamination of oxygen, nitrogen, and carbon. For the fabrication of the alloys, the powders have been prepared by the wet ball milling process. The transformation temperature of the prepared sample powders, the mechanical properties, corrosion rates and the phase analysis for checking the biocompatibility have been carried out. Besides CuAlNi samples, NiTiCu samples have also been investigated to evaluate particularly the effect of copper in the traditional NiTi alloys.

1.6 Structure of the thesis:

This book contains the introduction, literature review, experimental design, methodology, results and discussion, and conclusion.

Chapter one gives the overview of the research aim, research questions, the outline of the research work. Along with these, the research hypothesis has also been outlined in the chapter. The research hypothesis includes the logical reasons, principles, and findings of previous studies which justify the research's working principles. In addition, the structure of this thesis has been described in this section.

Chapter two discusses the review of previous related works to this thesis work along with the findings of those studies, and contribution of the present study to the existing literature. In this chapter, the crystal structures, properties, shape memory effects, pseudo elasticity, biocompatibility and cytotoxicity, corrosion resistance, biomedical applications, and spark plasma sintering (SPS) of CuAlNi and NiTiCu have been discussed in detail. Besides

justification for choosing the SPS method for fabricating the SMAs for biomedical applications has also been given in this section.

In chapter three, the process of experimental design has been delineated. The materials selection from phase diagram and previous studies, ball milling parameter selection, selection of SPS parameters, and simulated human body fluid selection for corrosion test have been described.

Chapter four contains the methodological approach stepwise. All the steps for powder formation by wet ball milling, die preparation, SPS machine operation and sample making, different characterization techniques, and the parameters for the tests have been included.

In chapter five, all the obtained experimental results and relevant explanations have been summarized.

Finally, in chapter six, a conclusion has been drawn from the main empirical results.

Chapter 2 : Literature Review

2.1 Introduction:

The literature review provides an overview of copper-based shape memory alloys, their fabrication, biocompatibility, and challenges in their biomedical application. In this review, these challenges and the solutions focused on compositional control and the powder metallurgy technique.

The advantages of the Cu-Al-Ni include ease of melting, casting, composition control, machining, higher young modulus, and the potential for giving a two-way shape memory effect. Besides these advantages, more advantages can be gained if the alloys are synthesized by the rapid solidification technique [6]. If the excellent physical properties of the shape memory alloys are integrated with the biocompatibility, then these alloys would be the most promising alloys for biomedical alloys. Nitinol alloys have limitations in biomedical applications. Elementwise, Titanium is a biocompatible element with a medium amount of corrosiveness, but Nickel has poor biocompatibility with the carcinogenic, genotoxic, mutagenic, cytotoxic, allergenic, and corrosiveness. Copper also has less biocompatibility but like nitrogen, it does not have the carcinogenic effect [7]. In the previous studies of ternary alloy addition, it has been found that the copper and tantalum addition to the nitinol alloys increase the corrosion resistance and the powder metallurgy has a significant role in the increment of the corrosion resistance [8].

2.2 Contribution to the State of the Art:

Cristiana et al. [9] have investigated the effect of copper addition on the mechanical properties and microstructures of the traditional nitinol shape memory alloys. The samples were prepared in the study by one step and multiple step sintering. The effect of heat-treatment in the multiple-step sintering process and copper addition on the hardness of the samples have been investigated. The hardness of the copper alloyed samples had given higher hardness than the non-alloyed samples. The effect of sintering rate and temperature on pre-alloyed spark erosion powders of Ti-Ni-Hf, Ni-Al, and Cu-Al- Ni-Ti-Cr shape memory alloys have been studied by *Monastyrsky et al.* [10]. According to the work, the pre-alloyed and powder by spark erosion method requires a higher temperature to be sintered and the higher rate of sintering is not the only solution for preventing the precipitate formation in the samples. *Thiruppath et al.* [11] have studied the densification behavior of the Cu-Al-Ni powders during the spark plasma sintering process. In the research work, the density of the sintered samples was measured and compared with the traditional process-made alloys. The findings of the research work are a 13.8 % increase in relative density through spark plasma sintering. So, the SPS process is efficient for producing higher-density Cu-Al-Ni alloys. Optimization of the temperature, heating rate, and applied pressure during the sintering is very important to get the desired physical and mechanical properties. The optimization of the SPS parameters for NiTiCu alloys

was done by C. *Velmurugan et al.* [12]. The study showed the control of density and hardness of the SMAs by controlling the SPS parameters, and particle sizes of the powders. The transformation behavior, mechanical properties, and biocompatibility after copper addition in the traditional Ni-Ti shape memory alloys have been investigated by *Mohammed et al*. [13]. Copper added Ni-Ti alloys show a narrow hysteresis loop and direct transformation from the austenite to B19 martensite. The results of the work carried out by Xianyang et al. [14] suggest that the shape-memory behavior of NiTi results from the storage of the shape information in the internal stresses, which also stabilize the observed B19′structure. The research work explains the reason behind the martensitic stabilization, the structural parameters play an important role in inscribing the shape memory properties in these alloys. *Trepanier et al.* [3] have done a comparative corrosion study between NiTi and stainless steel. The in-vitro potentiodynamic test results indicate superior passivation quality of nitinol than the stainless steel and the Ni ion release for the NiTi alloys was found tens of ppb (parts per billion). The amount of Ni ion released in NiTi alloys varies from study to study. *Miodrag et al.* [6] have done the in-vitro biocompatibility tests of the casted Cu-Al-Ni and jet spun Cu-Al-Ni alloys. The ribbons made in the controlled environment show better cell viability and less release (around 10-12 times) of the copper ion.

The spark plasma sintering method has been studied for producing the CuAlNi and NiTiCu shape memory alloys. But the previous studies had analyzed the CuAlNi and NiTiCu made by high temperature SPS method. The powder preparation method also differs from the present study for these compositions' alloys. The present study focuses on phase formation varying with sintering temperature, and the corrosion behavior, and hardness of the shape memory alloys.

2.3 Shape memory alloys:

In metallurgy, a shape-memory alloy (SMA) is an alloy that can be deformed when cold but returns to its pre-deformed ("remembered") shape when heated. It may also be called memory metal, memory alloy, smart metal, smart alloy, or muscle wire.

The property of recalling shapes can be classified in two-

(a) Shape memory effect: Shape memory effect (SME) is a phenomenon, in which a material recovers to its original size and shape when heated above a certain characteristic transformation temperature. When the alloys are heated then they can change their deformed Martensite shape and transform to the Austenite structure. For the phase transformation application of heat is required. So, the shape memory property is thermally induced. The property can be one way or two ways. When just being heated the martensite transforms to austenite which is called one-way shape memory effect. On the other hand, if while cooling the austenite also transforms back to the martensite structure then the given property is two-way shape memory effect.

(b) Pseudo elasticity: The stress induced shape memory property is called pseudo elasticity. It is sometimes called super elasticity, is an elastic (reversible) response to an applied stress, caused by a phase transformation between the austenitic and martensitic phases of a crystal. It is exhibited in shape-memory alloys. Super elastic alloys belong to the larger family of shape-memory alloys. When mechanically loaded, a super elastic alloy deforms reversibly to very high strains (up to 10%) by the creation of a stress-induced phase. When the load is removed, the new phase becomes unstable, and the material regains its original shape. Unlike shape-memory alloys, no change in temperature is needed for the alloy to recover its initial shape. The shape memory effect and pseudo elasticity of shape memory alloys are represented in Figure 2.1.

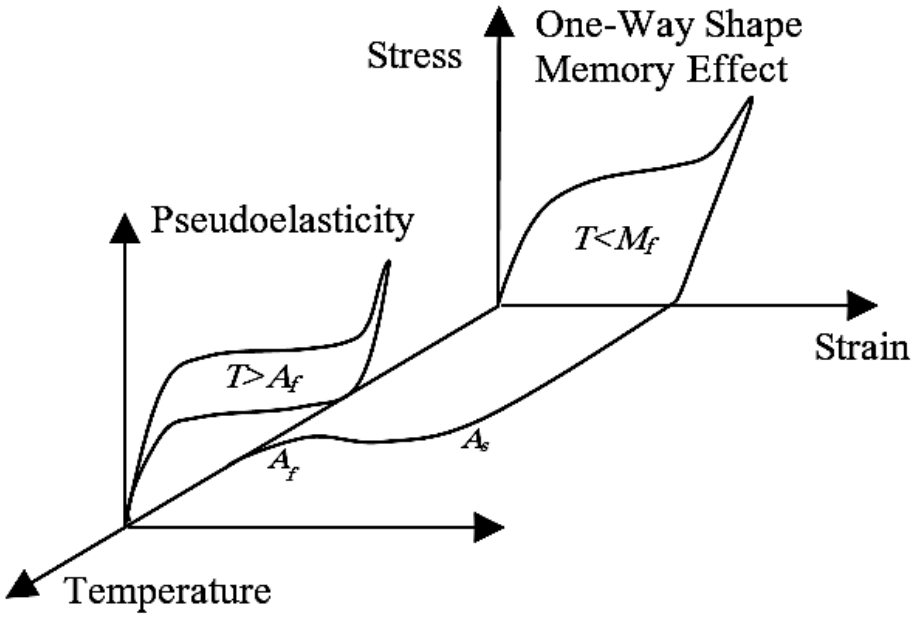

Figure 2.1:Shape memory effect and Pseudo elasticity

2.4 Biocompatibility:

The understanding of biocompatibility has been focused for long-term implantable devices, which are biologically inactive and chemically inert so that they give no harmful effect to the human tissues. However, with recent development in biotechnology, some level of biological activity is needed research areas, such as tissue engineering, drug, and gene delivery systems, where direct interactions between biomaterials and tissue components are very essential. One of the recent definitions of biocompatibility is "the ability of a biomaterial to perform its desired function with respect to a medical therapy, without eliciting any undesirable local or systemic effects in the recipient or beneficiary of that therapy but generating the most appropriate beneficial cellular or tissue response in that specific situation and optimizing the clinically relevant performance of that therapy". In metals, biocompatibility involves the acceptance of an artificial implant by the surrounding tissues and by the body as a whole. The metallic implants do not irritate the surrounding structures, do not incite an excessive inflammatory response, do not stimulate allergic and immunologic reactions, and do not cause cancer. Other

functional characteristics that are important for metallic devices include adequate mechanical properties such as strength, stiffness, and fatigue properties and appropriate density. Since many applications of metallic devices are for the structural implant, metal biocompatibility is of considerable concern since metals can corrode in an in vivo environment. The corrosion of metallic implants gives adverse effects to the surrounding tissues and to the implant itself. It produces chemical substances that are harmful for human organs and deteriorates the mechanical properties of the implant. Therefore, corrosion resistance of a metallic implant is an important aspect of its biocompatibility. Even though, in special cases, metals which can degrade are proposed for temporary implants but certainly without ignoring the biocompatibility requirement.

A fabrication process of metal implants is powder metallurgy. The process includes blending and mixing of ingredient materials, compaction, sintering and in most cases followed with HIP process. This process is relatively expensive; therefore, it is suitable to produce highly loaded implants like femoral stems of total hip prostheses. One of the important requirements for implant materials is porosity which is expected in the range between 20-50% volume fractions. This condition can be achieved by controlling the sintering process parameters. In addition, improvement in the mechanical properties of the implant by this method can be achieved by conducting HIP process after sintering by decreasing defects like gas or shrinkage pores.

Failure of materials for biomedical devices:

(a) Corrosion:

Metal implant is prone to corrosion during its services due to corrosive medium of implantation site and in most cases subjected to cyclic loading. Types of corrosion that frequently found in implant applications are fretting, pitting and fatigue. Fretting corrosion most frequently happens in hip joint prostheses due to small movement in corrosive aqueous medium.

Fretting corrosion refers to corrosion damage at the small area of contact surface due to repeated load, the mechanism of which frequently refers to corrosion which is activated by friction. Corrosive medium, chemical composition of alloy and level of stress at the contact surfaces are among important parameters that determine fretting corrosion behavior of metallic implants. It was reported that the presence of chlorides influences the degradation acceleration of the stainless-steel surface. On the other hand, it was observed that corrosion resistance of Ti15Mo alloy is strongly dependent on the concentration of fluoride ions for dental application [15].

General corrosion is a process that describes the uniform loss of material across its entire surface-environment interface. In metallic materials used in vivo, general corrosion takes the form of passive corrosion, the rate of which is defined as the difference between the rates of passivation versus that of passive layer dissolution. Typically, for implants, this rate is low, often not exceeding 1 pm per year, and is unlikely to affect the mechanical properties of the implant.

A much greater rate of corrosion can occur when the passive layer is removed, e.g., due to physical damage or changes in the local pH, resulting in the localized corrosion of affected areas. Certain chemical sites in the passivation layer can make it more susceptible to pitting corrosion due to increased levels of dissolution at these sites, especially when in contact with liquids containing halide ions. Presence of impurities, formation of metal hydroxide, localized drop in pH are the main drivers of corrosion and pit growth. The resulting inter-pit environment is highly conducive to corrosion processes, and the pits themselves can provide a source of metal ions at potentially toxic concentrations. When considering the impact of pitting corrosion of an implant, it is important to consider the susceptibility of the material to de-passivation as well as the frequency of pit formation over time. where stainless steel is more prone to de-passivation compared to Ti and as such has a greater frequency of pit nucleation, over time this frequency reduces to zero as the repeated nucleation and metastable propagation eliminate the sites at which pits tend to form, e.g., sulfide inclusions on the surface of stainless steel. On the surface of Ti, however, the pit nucleation remains at a low frequency over time, suggesting that for this metal, nucleation is not driven by inclusions but rather by the inherent properties of the titanium oxide layer, and events such as explosive microscopic rupture of the layer perpetrated by the accumulated chloride at its interface. The consequences of pitting corrosion in the case of NiTi are more concerning and may result in significant levels of ion release.

Another type of localized corrosion, i.e., **crevice corrosion**, takes place when the inflow and outflow of chemical species is reduced due to the geometry of the space created by two surfaces coming into proximity with each other, for example at the interface between the head of fixing screws and bone or plate. This is because the formation of the protective oxide relies on the availability of dissolved oxygen, whereas the dissolution processes are promoted by increased concentrations of halide species.

When coupled with mechanical stress, the above-described corrosion reactions can lead to crack propagation and eventual failure of the material, a process termed as stress **corrosion cracking or corrosion fatigue** depending on whether the loading is static or cyclic in nature.

Under conditions that favor increased hydrogen evolution at the surface of the intact passivation layer, e.g., when the metal in question is galvanically coupled to another metal with greater activity, hydrogen atoms can interact with the metal lattice, leading to the formation of brittle metal hydrides that are prone to cracking under applied or residual stress. In vivo **hydrogen embrittlement** was suggested to be the cause of severe corrosion attack on the mating interfaces of retrieved hip-implants with Ti-6% Al-4%V/Ti-6%Al-4%V modular taper interfaces in the stem. The surfaces of the modular connections showed signs of etching, pitting, delamination, and surface cracking, as well as the precipitation of brittle hydrides because of crevice and fretting corrosion, where the oxide layer was mechanically damaged. Naturally, Ti and other materials that rely on the protective effects of an oxide layer are subject to a considerable reduction in fatigue strength under fretting conditions, with the nature of the environment playing a less important role when the damage from fretting is more severe. Increasing the fretting resistance, changes to the alloy grain structure through heat treatment,

may reduce the susceptibility of some materials to fretting corrosion. This is because cracks are observed to propagate along the boundary lines between the acicular α and β phases.

The loss of material may also compromise the mechanical integrity of the site where the implant is fixed to the bone, leading to implant loosening and compromising the correct load transfer across the interfaces and the bulk of the implant. Thus-stressed materials can be more susceptible to failure due to corrosion fatigue processes. The debris generated in the process of fretting corrosion, e.g., oxide particles of various dimensions, tend to accumulate in the peri-implant milieu, thereby increasing stress. If trapped in between the two rubbing surfaces, these particles may enhance damage via abrasion. Although increasing the hardness of the material reduces the damage it is likely to sustain from fretting wear, most Ti and Co–Cr alloys, and stainless steels are subject to fretting due to shearing micro-movements at the implant–cement or implant–bone interface. Mixed phase α/β alloys, such as Ti-6%Al-4%V and Ti-6%Al-7%Nb, may display better characteristics with respect to resistance to corrosion and wear, whereas commercially pure titanium and the near-β, Ti-13%Nb-13%Zr and β Ti-15% Mo alloys may show superior corrosion resistance among the group.

In some applications, e.g., in restorative dentistry, it may be necessary to place two dissimilar metallic materials into direct electrical contact. In the presence of a corrosive fluid, e.g. saliva rich in acids, salts, proteins and enzymes, **galvanic corrosion** may take place. This type of corrosion is characterized by changes in the rate of the corrosion on these materials, with the corrosion being promoted on a less immune material and suppressed on a more noble material. This is because the difference in the corrosion potential of these materials drives a flow of electric current through the metal/metal junction, as well as through fluids in the peri-implant milieu and in tissues. This can lead to the formation of a galvanic cell that promotes corrosion on the less noble metal. The reactions involved include cathodic reactions that reduce dissolved oxygen in the electrolyte (i.e., $O_2 + 4e^- + 2H_2O \rightarrow 4OH^-$ and $O_2 + 4H^+ + 4e^- \rightarrow 2H_2O$) and anodic reactions that dissolve the metal following $M \rightarrow M^{n+} + ne^-$.

Galvanic coupling is held responsible for the intergranular corrosion of dental amalgams, i.e. the multiphase alloys commonly used in restorative dentistry.

The passivation of metals greatly reduces the probability and practical consequences of galvanic coupling since the corrosion potential of the passivation layer on the less noble metal would be that of a more noble metal. Having said that, physical or chemical damage to the protective layer would expose the underlying metal, thereby increasing the probability of galvanic corrosion.

Prevention of corrosion will be greatly assisted by evaluation of corrosion behavior using methods which resemble the service condition of the metal implants. Since stress and corrosive media play an important role, special devices that combine these two factors should be developed. Ultrasonic frequency was used in corrosive medium to evaluate the fatigue corrosion of metallic implants which enables the application of a very-high stress cycle within reasonable testing period. On the other hand, the fretting corrosion behavior of metallic

implants can be evaluated by a typical pin-on disc method in an artificial physiological medium. Parameters that are needed to be set include concentration of corrosive medium, load or friction forces, frequency, and number of fretting cycles. In the case of pitting corrosion, it can be evaluated with the absences of applied forces. It was reported that a good example of pitting corrosion evaluation was obtained in a buffered saline solution using anodic polarization and electrochemical impedance measurements.

Titanium nitride coating on the metallic implant has been a popular method to improve corrosion resistance of metallic implants such as Ti alloy and Co based alloy by physical vapor deposition, plasma spray process, etc. Modification of metallic implant surface by electropolishing, sand blasting or shot peening method were also reported to improve the corrosion resistance of the implant. It is known that a significant improvement of corrosion resistance can be achieved for the electropolished surfaces and sand blasted surfaces, where the former surfaces are corroded most slowly. The modification of corrosion resistance properties by the two methods are considered due to the increasing surface area and the introduction of compressive stress on the surface. In addition, chemical composition modification is also possible by sand blasting process with the introduction of sand particles that form a certain layer on the surface being blasted.

(b) Fatigue and fracture:

During its service most, metallic implants are subjected to cyclic loading inside the human body which leads to the possibility for fatigue fracture. Factors determining the fatigue behavior of implant materials include microstructure of the implant materials. It was reported that Ti6Al4V with equiaxed structure has better fatigue strength properties than the elongated structure. Another important parameter is the frequency of the cyclic loading or the cycling rate.

Design of the implants also plays an important role on the fatigue failure characteristics. It was reported that fatigue failure of femoral screw had initiated near a keyway, and suggestion on design improvement has been proposed by lengthening the barrel around the lag screw. In addition, beside the type of fluid medium of the implant, the existence of other substances such as protein was also reported to have significant influence on the surface reaction and fatigue resistance of Ti implant.

Like corrosion failure, various surface modification methods give beneficial influences in improving the fatigue resistance of implant materials. These surface modifications include shot blasting and shot peening that were observed to work well in any medium or environment. Beside improvement in the fatigue resistance, this method was also observed to improve the osseointegration on the implant materials.

(C) Wear:

Together with the corrosion process, wear is among the surface degradation that limits the use of metallic implants such as Ti alloy. Removal of dense oxide film which naturally formed on the surface of this metallic implant in turn caused wear. In fact, the major factor that causes premature failure of hip prostheses is due to the wear process with multiple variables interacting and thus increasing the resultant wear rates. Since wear is a type of failure due to surface contact, thus surface modification is an appropriate method to improve wear resistance.

(d) Metal ions release:

It is realized that high strength alloys possess good mechanical strength but have relatively poor corrosion resistance properties. In most situations it is worse if metal ion release follows a corrosion process which can be a toxic contaminant inside the human body. As an example, the vanadium ions release Ti alloys that are preceded with a corrosion process. Similar condition was found on CoCrMo alloys which are used as orthopedic implant materials, that these alloys release Co, Cr, Mo ions to host tissues. There are several factors which play an important role on the metal ion release. First, the existence of passive oxide films where once it is broken, metal ions release will be easier to occur. Second, pH factors where ion release in both stainless steel and Co are affected by pH of the body fluid at a degree that higher for stainless steel. Similar situation was reported in that Co based alloys show less ions released during the test using natural and synthetic saliva for dental alloys.

To reduce the metal ion release from metallic implant, coating is the appropriate method to reduce this process. Nitrogen ion implantation on the CoCrMo alloys enables modification of the near surface region of this alloy by forming a protective layer on the surface. Titanium nitride layer was found to have an excellent biocompatibility and the formation of hard nitride layer showed a lower ion release on the metallic implant. Therefore, coating of titanium nitride has been implemented on the Ti alloy and Co based alloy. Hydroxyapatite coating was also reported to decrease the metal ion release. On the other hand, significant improvement was also reported by Ti coating on Co base alloy using plasma spraying method. One point to be noted here is the morphology and surface roughness of the coating layer also determine the corrosion resistance and in turn the metal ion release behavior. Therefore, proper coating process as well as substrate preparation is required to obtain optimum results.

2.5 Recent developments in metals for biomedical devices:

Metal selection for Biomedical application:

(a) Consideration of Metal Toxicity:

When choosing suitable alloying elements, the individual and cumulative toxicity of elements within an alloy should be low, with a preference given to the essential trace elements Co and Fe (as these elements are already present in healthy tissues of living organisms), and highly corrosion resistant active elements, such as Ti. Ti alloys are considered most biocompatible,

with the greatest corrosion resistance and specific strength. This statement is of course a generalization, as the properties of alloys within each group can differ considerably based on their composition, fabrication method and post-processing treatment, and the environment within which they operate. For some time, Ni was one of the most popular alloying elements due to its ability to enhance the formability, weldability, ductility, and, in some instances, corrosion resistance of stainless steels and Co–Cr alloys. The subsequent discovery of the potential acute and chronic adverse effects of exposure to Ni that leached out from the implants, including delayed hypersensitivity, headaches, vertigo, vision changes, altered iron metabolism and homeostasis of Ca, Mg, Mn, and Zn, has led to the reduction in the use of Ni in biomedical alloys. The use of another popular alloying element, Al, has been suspected to cause osteomalacia, hepatic dysfunction, anemia, and neurological effects. While Ni and Al are non-essential metals for the human body, even for essential metals that the body requires for the proper functioning of many of its proteins and enzymes, their quantities are tightly controlled via homeostatic regulation, with the presence of excessive amounts of these metals often causing local and systemic toxicity. For example, although vanadium is considered essential for proteins that participate in phosphate and lipid metabolism, and insulin enhancement, the presence of excess vanadium may result in the development of headaches, weakness, tremor and gastrointestinal issues in patients. This holds true for excess Mo, which can cause urinary tract stones, acute renal failure, and myositis, as well as for Co, Cu, Fe, Mn, Zn and Cr essential metals. Undesirable physiological effects have also been reported for other non-essential metals frequently found in biomedical implants, including Ti, Ag, Au, Pt, Pd, Sn, Hf, Zr, W and Ir. Nb, Ta and Zr are often considered among the least toxic alloying elements, yet are expensive. Also, expensive, precious metals, including Au and Au alloys with Pt and Pd, Ag and its alloys, and Pt and Pt alloys are used in restorative dentistry, in antimicrobial treatments (Ag) and as electrodes for electrically active devices.

(b) Bulk Properties:

The bulk properties of metals are defined by their chemical composition, crystalline structure, and bond strength. The 3D arrangement of closely packed atoms in metals, where the nuclei of positively charged ions are immersed in a delocalized cloud of freely moving valence electrons, is responsible for the excellent electrical and thermal conductivities of metals, and their high density (in the case of most metals). Greater amounts of delocalized electrons correspond to stronger metallic bonds, i.e., stronger electrostatic interactions between the electron cloud and the ions. The strength of the metallic bonds defines the tensile strength of the material, whereas the non-directional nature of metallic bonds is responsible for the malleability and ductility of metals, which allows them to undergo a significant amount of plastic deformation (plastic strain) without failure (cleaving). The strength of the metallic bonds is greater for metals made of atoms of greater nuclear charge, which have a greater number of electrons they can release into the cloud, and of smaller atom size; the greater strength of the metallic bonds is also responsible for the higher melting temperature and hardness of such metals. As such, atoms with half-filled valence shells (such as W and other transition metals with valence-level d electrons) make solids that are stronger than those made of elements with nearly empty or nearly full valence subshells. While the Young's modulus, ultimate tensile strength and

toughness define the application of metallic biomaterials,8 their hardness and melting temperature prescribe the kind of techniques that can be used for their processing into implants and devices.

(c) Metal vs. Bone:

Among the key drivers behind the development of new alloys is the growing understanding of how different properties of materials affect their behavior in vivo, the interactions between materials and cells. For example, the nature of a cellular response is not only determined by the surface chemistry of the material, but also its surface topography and surface and bulk mechanical properties, including the material's Young's modulus, its specific strength (expressed as the ratio between its strength and ductility) and others. This is in part because to perform their load-bearing function, they need to have a suitable level of stiffness. The consequences of this difference include non-homogeneity in the implant–bone load transfer and reduced stress stimulation of the bone, resulting in bone loss, limited bone remodeling and sub-optimal implant integration, which affect implant performance and lifetime in vivo. Importantly, the measurement of the distribution of stress and strain in dental implants and in bones when the implant is loaded under normal occlusal loading conditions is difficult to conduct in vivo, and thus such information often comes from modeling studies or those involving human cadavers. Among the Ti alloys, those that have β-type phase constitution, i.e., metals with a bcc structure, are characterized by significantly lower Young's moduli when compared to α-type alloys, i.e., those with a close-packed hexagonal crystal structure and (α + β)-type alloys. The phase constitution can be controlled through the selection of alloying elements, with Nb and Ta frequently used to stabilize the β-phase, with some Zr introduced due to its ability to dissolve in the β-phase and increase the strength of the material [16].

Metals and Alloys used in Biomedical application:

Pure metals have relatively limited properties; however, these properties can be enhanced by alloying the metals. Most of the metals used in engineering applications are in the form of their alloy. Most alloys consist of two or more solid phases in the form of either solid solutions or intermetallic compounds that depend on the alloying composition and temperature. A phase is defined as a homogenous portion in a material that has its own physical and chemical characteristics and properties. Every pure metal is considered as a phase, as also is every solid solution and intermetallic compound. Alloying a metal with finely dispersed particles as a second phase is one of the important methods of strengthening alloys and enhancing their properties. The second-phase particles present as obstacles to the movement of dislocations thus increase the overall strength and hardness of the alloys.

Table 2.1: Different Biomaterials applied to medical science [16]

Type	Primary Use
Routinely Applied Materials	
• Stainless Steel	Temporary fracture plates, screws, hip nails etc
	Total hip replacement
• Cobalt-based Alloys	Total joint replacement
	Dentistry casting
• Titanium-based Alloys	Stem and cup of total hip replacements with CoCrMo or ceramic femoral heads
	Other permanent devices (nails, pacemakers)
Emerging Food and Drug Administration (FDA) Approved Materials	
• NiTi	Orthodontic dental archwires
	Vascular Stents
	Vena Cava Filter
	Intracranial Aneurysm Clips
	Catheter guide wires
	Orthopedic staples
• Tantalum	Wire sutures for plastic surgery and neurosurgery
	Radiographic markers for diagnostic application
Materials in Clinical Trials and Research	
• NiTi	Contractile artificial muscles for an artificial heart
• Mg	Biodegradable orthopedic implants

According to Table 2.1, the application of shape memory alloys has different biomedical applications, both in existing applications as well as in new emerging applications. The copper-based shape memory alloys are also under critical investigations. Several studies have been being carried out on their radiopacity, thermal conductivity, corrosion resistance and shape memory properties.

Along with the advances in biomedical technology and tissue engineering, biomaterials are desired to exhibit low elastic modulus, shape memory effect or super elasticity, wear resistance, super plasticity, and workability. In addition, they are required to eliminate all possibility of toxic effects from leaching, wear, and corrosion. One of the concerns is avoiding the use of Ni in fabricating metal alloys. This demand leads to the development of a new generation of metallic biomaterials and their novel processing.

New generation of metallic biomaterials:

Shape Memory Alloys In recent years, shape memory effects and pseudoelasticity in some alloys (e.g., NiTi alloys) have been recognised as valuable properties that can advance a few surgical procedures. When used as implants and surgical tools, NiTi and other shape memory alloys are designed so that the temperature at which the material finishes the martensite to austenite transition is well below that of the human body. The alloy composition will have a direct effect on the transformation of Austenite (TA) start, TA finish, Transformation of Martensite (TM) start and TM finish temperatures, the maximum value of strain that can be thermally recovered, and the hysteresis characteristics, with TM start and TM finish being particularly affected by the nature and relative amounts of the alloying elements. For example, adding Cu (10 wt%) to NiTi reduces transformation and pseudoelastic hysteresis, and limits the sensitivity of TM to the elemental composition of the alloy; in contrast, the addition of Nb widens thermal hysteresis, and the introduction of Pt, Pd, Hf, Au or Zr shifts the transformation temperatures significantly higher compared to TiNi. The addition of Ag may provide antibacterial activity against common implant-associated pathogens, while also slightly increasing the corrosion resistance, elongation, and tensile strength of the alloy, whereas Hf implantation may render TiNi more wear resistant owing to the presence of HfO_2 in the protective oxide layer. Increasing the fraction of Hf may positively contribute towards fatigue resistance. Corrosion resistance may also improve with the addition of Mo.

Apart from NiTi (developed in the 1960s), shape memory behavior has also been observed in AgCd and AuCd (developed in 1930s), Cu-based alloys (e.g., CuAlNi, CuAlBe, CuSn, CuZr), Fe-based FePt and FePd, and others, e.g., InTi, NiAl, MnCu, FeMnSi, and magnetic NiMnGa, etc. However, the manipulation of alloy chemistry is limited by the need for the material to remain biocompatible and resistant to corrosion. The alloy microstructure will also affect both its transformation temperatures and key properties. NiTi alloys with a small grain size (< 100 nm) have been shown to have lower transformation temperatures, with a grain size below 50 nm effectively suppressing transformation to martensite because of nanoscale grains on B19′ martensite morphology. Crystallinity also affects the shape of the stress–strain response, with polycrystalline coarse-grained NiTi showing a plateau, as opposed to a sharp rise that is evident in the nanocrystalline NiTi response. When compared to other metallic implants, the plateau stress of NiTi is on par with their yield strength, but it is more corrosion resistant and biocompatible than stainless steel. In addition to the use of solid NiTi implants as rods, nails, plates, and vertebrae spacers, scaffolds made of porous shape memory alloys are being investigated for their ability to promote bone tissue remodeling and vascularization while being strong and lightweight [16].

Stainless steels for metal implants have been further developed to be Ni-free. Replacing Ni with other alloying elements while maintaining the stability of austenitic phase, corrosion resistance, magnetism, and workability, has led to the use of nitrogen creating Fe-Cr-N, Fe-Cr-Mo-N and Fe-Cr-Mn-Mo-N systems. The high strength which has been achieved opens the

possibility for reduction of implant sizes where limited anatomical space is often an issue, for example, coronary stents with finer meshes,

In **CoCr alloys** system, maximizing C content to its upper limit and addition of Zr and N with optimal precipitation hardening permit the formation of fine and distributed carbides and the suppression of -phase which in turn improves the wear resistance of cast CoCr alloy. Contrary, for wrought CoCr alloys, addition of N and suppression of carbides and intermetallic results in the desired better workability.

– type **Ti alloy** exhibits a lower elastic modulus than type and + type which makes it considered to be the first candidate for low elastic modulus metallic biomaterials. In Ti-Nb systems such as Ti-29%Nb-13%Ta-4.6%Zr and Ti-35%Nb-4%Sn, the elastic moduli can be reduced to 50-60 GPa which are closer to that of cortical bone (10-30 GPa) [15].

2.6 Structure and transformation of CuAlNi and NiTiCu:

2.6.1 CuAlNi:

Phases in the CuAlNi alloys are responsible for their shape memory properties. The Austenitic and martensitic phases have their identical crystal structures. Only when the alloys contain the favorable crystal structures and phases, they can give the pseudo elastic and thermal shape memory effect.
The ternary phase diagram of CuAlNi for a certain composition has been developed from the binary Cu-Al phase diagram shown in the following Figure 2.2 and the reaction kinetics for the formation of different phases.

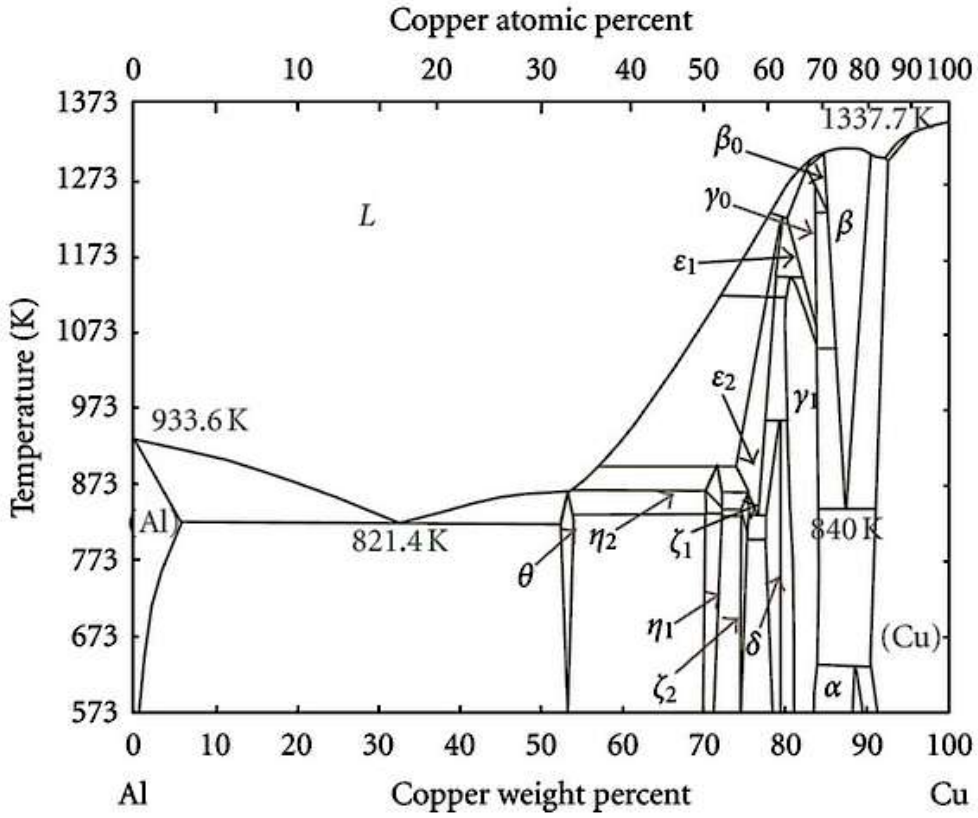

Figure 2.2: Binary Cu-Al phase Diagram

The β phases are responsible for the shape memory property of the Cu-Al-Ni alloys. From the binary and ternary phase diagram, for Nickel amount 4wt% the amount of copper can lie in between 70%-80% and the Aluminium amount can vary in between 11 wt% to 15 wt%.

Generally, the following compositions are maintained for these alloys-

(a) Cu (82.3 wt%) - (13.7 wt%) Al - (4 wt%) Ni
(b) Cu (82.42 wt%) - (13.58 wt%) Al - (3.94 wt%) Ni
(c) Cu (82.5 wt%) - (13.5 wt%) Al - (4 wt%) Ni
(d) Cu (84.3 wt%) - (11.92 wt%) Al - (3.78 wt%) Ni
(e) Cu (82.6 wt%) - (13.4 wt%) Al - (4 wt%) Ni
(f) Cu (80.38 wt%) - (13.58 wt%) Al - (6.04 wt%) Ni
(h) Cu (82.5 wt%) - 13.5 wt% Al - 4 wt% Ni

The SME of Cu-based SMAs is associated with thermoelastic transformation from β phase to 9R (or 18R), 3R and 2H martensite, depending on the composition and heat-treatment of the alloy. The β phase, i.e., the high-temperature phase or parent phase, has a bcc structure, while the martensite phase has a hexagonal structure or an orthorhombic structure.

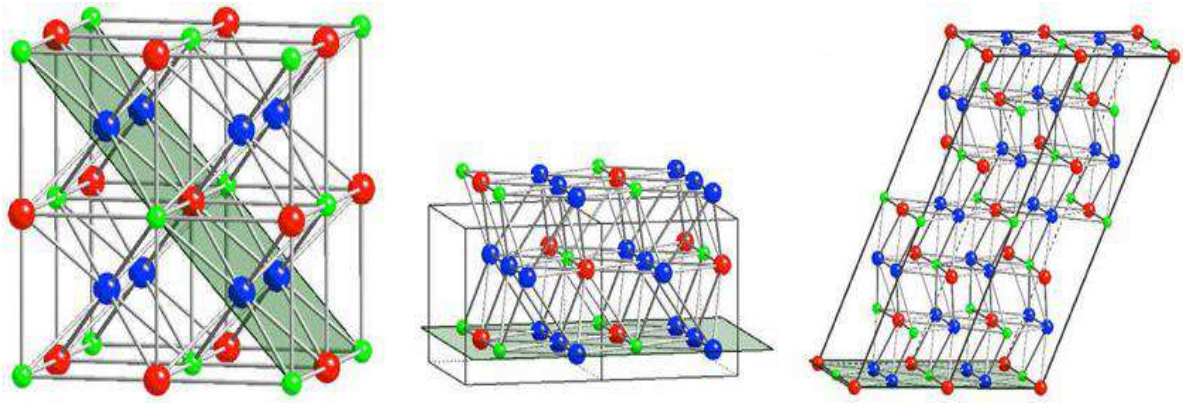

Figure 2.3: Crystal structures of austenite, orthorhombic, monoclinic phases respectively from the left and their lattice correspondence

It was reported that the 9R (or 18R) type martensite has a monoclinic unit cell. When martensite stabilization occurs, the structure of the martensite transforms from monoclinic to orthorhombic and the orthorhombic distortion is attributed to the reordering of the martensitic phase. If the monoclinic angle of the quenched martensite, is 90° (orthorhombic) or very close to 90°, the transition from monoclinic to orthorhombic, the crystal structures shown in figure 2.3 would be restrained and it would be difficult for the martensite stabilization to occur during aging in the martensite state. The martensitic stabilization effect is sensitive to the thermal treatment and the aging effect. Generally aging results in martensitic stabilization. Different milling times give an insight into the structural evolution during mechanical alloying for a Cu–Al–Ni alloy. When analyzing the milled powders different intermetallic phases have been found at a small amount after an insufficient amount of milling time [17]. On the other hand, in SPS, the type of precipitates depends on the temperature of sintering mainly. Two phases are well recognized inside the particles: matrix phase and precipitated phase sized of several microns with a composition close to Cu_9Al_4. Superficial and interspaces phases between the particles are also well recognized. The phase on the surface of particles (superficial) and the phase from the interspaces between the particles are rather the mixture of copper and aluminum oxides [10]. So, the phases of the Cu-Al-Ni samples are highly sensitive to the processing conditions and the composition.

According to the ternary phase diagram, the analyzed contents of the three major elements Cu, Al, and Ni in the control alloy almost correspond to the eutectoid composition. Therefore, in the microstructure of the slowly solidifying control alloy all three phases could be expected a NiAl and precipitates, all uniformly distributed, forming no large crystals. The phase is a Cu-rich solid solution having a face-centered cubic structure. NiAl is an intermetallic compound, having an ordered body-centered cubic structure of the CsCl type and a B2 superlattice. Its equiatomic chemical composition corresponds to 69 wt.% Ni and 31 wt.% Al. The $\gamma_2$is a complex cubic compound (52 atoms per unit cell) Cu_9Al_4. It consists of 84 wt.% Cu and 16 wt.% Al.

In a ternary alloy with Ni, the γ_2 phase primarily contains Ni atoms in the crystal structure, substituting Cu. The matrix is a product of eutectoid decomposition during the high-temperature transition of the (parent) phase to the α and γ_2 phases. According to the phase diagram, in hypereutectoid Cu–Al–Ni alloys the $\gamma_2$phase partially precipitates in the form of proeutectoid crystals, and at low temperatures no NiAl is present.

In the martensitic structure of the SMA ribbons, according to the literature, two kinds of martensite are possible. In Cu–Al–Ni alloys containing <13 wt.% Al β_1 martensite prevails, having a monoclinic 18R structure, while in alloys containing >13 wt.% Al, orthorhombic 2H-type martensite prevails [18].

The unique properties of Cu–Al–Ni SMA are mainly attributed to the thermoelastic martensitic transformation that takes place in a temperature range of (173–473 K) depending on the composition of the alloy. These properties are significantly affected by the movements of interfaces (twin boundaries, martensitic variants, and parent/martensite phase boundaries). Some other parameters also exhibited a significant influence on the properties of these alloys, for instance, the formation of vacancies, dislocations, grain boundaries, and precipitates, along with the way of their distribution and volume fraction. On the other hand, the Cu–Al–Ni alloys are liable to aging treatment, which it leads to the form of different types, volume fractions. and distributions of precipitates in the microstructure, associated with the successive of martensitic transformation from β_1 martensite to other martensite phases. However, it is well established that different types of martensitic phases, 2H, 18R, and 6R form in the Cu–Al–Ni SMAs, depending on the chemical composition, mode of applied load, test temperature, and crystal orientation. Furthermore, a proper aging process may produce a favorable combination of features, such as high strength and a large strain recovery. As these alloys are susceptible to post-quench aging at high-temperature service conditions, their transformation temperatures, martensitic phases, and mechanical properties can change with the time of treatment. Consequently, many studies were conducted on various aspects of aging in these alloys and their influence on the shape memory properties [19].

2.6.2 NiTiCu:

The addition of smaller amount of copper to the NiTi does not affect much to the formed phases. The phases responsible for the shape memory effect in the NiTinol also are present in the NiTiCu alloys.

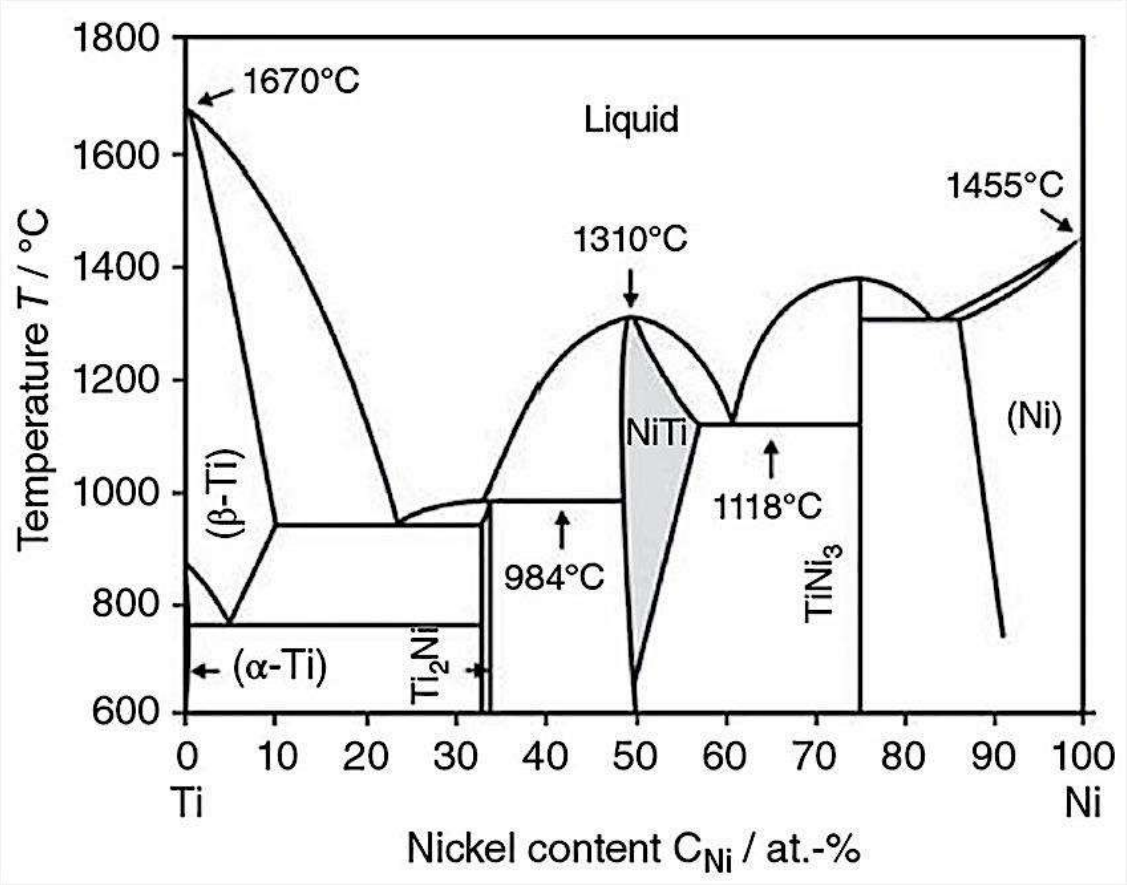

Figure 2.4: Binary Ni-Ti phase diagram

The Cu-Ti binary system has a very similar phase diagram to the Ni-Ti phase diagram as shown in Figure 2.4. However, the NiTi phase has the austenitic cubic structure whereas the CuTi has a tetragonal crystal structure. So, the addition of copper more than 30% may result in the presence of both austenitic and cubic structures. To get the shape memory properties from the alloys the Ti amount should be nearly 50 at% [20]. Several ternary NiTi-X alloys have been introduced to improve the fatigue properties and to decrease the thermal hysteresis range. Among those, the well-known ternary alloying elements are Cu and Fe. Particularly. Cu has been shown to dissolve in the B(austenite) phase in a concentration of up to 30 at%. However, NiTiCu solid solutions containing more than 10 at% are characterized by poor formability so alloys of technical interest usually contain Cu in the range from 5 to 10 at% [13]. With an increasing copper level, the orthorhombic martensite becomes continuously more stable over the monoclinic morphology that is typically observed in binary NiTi. Analysis of the diffraction pattern of the NiTiCu alloy by the SPS method revealed the presence of B2, B19, and/or B19' phases and typical precipitates like Ni_3Ti, Ni_2Ti, $NiTi_2$, and $Ti_2(Ni, Cu)$ [9].

NiTiCu shows a direct transformation from austenite to martensite, probably B19 whereas the binary NiTi alloy transforms to the trigonal R-phase before the B19 transformation occurs at a lower temperature. The transformation path changes from B2–B19' into B2–R–B19' in Ni-rich NiTi alloys when Ni_4Ti_3 precipitates are present in the B2 matrix [13]. Figure 2.5 shows the phase transformations in NiTiCu ternary alloys.

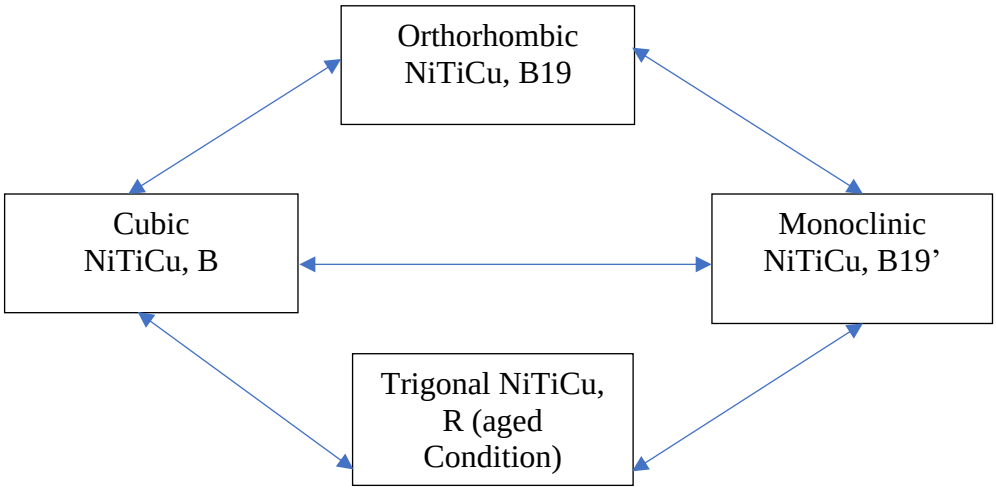

Figure 2.5: Crystal structure during the transformation of NiTiCu

The stable BCO structure, centered rectangular structure in 2D has dramatic consequences for the interpretation of the shape-memory effect at the atomistic level. The conventional picture of how shape memory is stored is that each martensitic variant has an atom-to-atom correspondence with the austenite because of lying in the 'Ericksen–Pitteri' neighborhood (EPN) of its austenite parent. Thus, while a particular austenite state gives rise to several martensite variants, which may be interconverted in twinning deformation, each martensite returns to a unique austenite state: the material never escapes from its EPN, and this stores the information necessary for shape memory. Although all B19, B19′, and R variants lie in the same B2 EPN, the ground-state BCO structure of NiTi lies on the boundary between the two neighborhoods. Specifically, the Ti atom has three in-plane near neighbors and four out-of-plane neighbors. To transform back to B2, one of the two in-plane second neighbors has to become a near neighbor, and the other a second neighbor. Because they are symmetrically equivalent, the B2–BCO–B2 transformation is not uniquely reversible at the atomistic level: BCO alone cannot store the memory of the original austenite [14].

2.7 Properties of CuAlNi and NiTiCu:

2.7.1 CuAlNi:

Cu-Al based shape memory alloys offer better properties and have lower fabrication cost than existing Nitinol alloys. The shape memory properties of CuAlNi are nearly identical to the NiTi alloys.

2.7.1.1 Shape memory properties:

SME results from a displacive, first-order phase transition called Martensitic Transformation (MT), which is one of the most interesting variants of structural phase transition in solids. The so-called "shape memory effects" are the direct result of thermoelastic MT. In this kind of transformation, a balance is struck between chemical-free energy change which accompanies

the transformation and the elastic energy built up around the martensite crystallites. The parent-to-product transformation can be induced by either decreasing the temperature or applying induced stress on the specimen [17].

In normal use, metal acts as an elastic material, with minimal displacement. In unusual conditions, if stress rises above a critical level, the metal displaces without exerting additional force, and the displacement can be as much as 9% strain. This has two advantages: the device is not so likely to fracture, and it protects the bone or other body tissue to which the implanted device is attached from stresses that are beyond its fracture stress. Various copper based SMAS, including Cu, Al, Ni, or Minor Be, may be used. These biocompatible alloys may be used to take advantage of their hyper elastic properties (having recoverable strains greater than 8% with a relatively flat stress plateau). Devices having a martensitic transformation with A, between 10 and 40^0C. may be useful. Such devices may be useful for intravascular use, intramuscular use, intraocular use, etc. The anisotropic single crystal shape memory alloy material formed is deformable at a constant force at a recoverable strain of at least 9% with a very narrow loading-unloading hysteresis, a recovery that is completely repeatable and complete and very low yield strength when martensitic [21]. The pseudo elasticity of the single phase CuAlNi is shown in Figure 2.6.

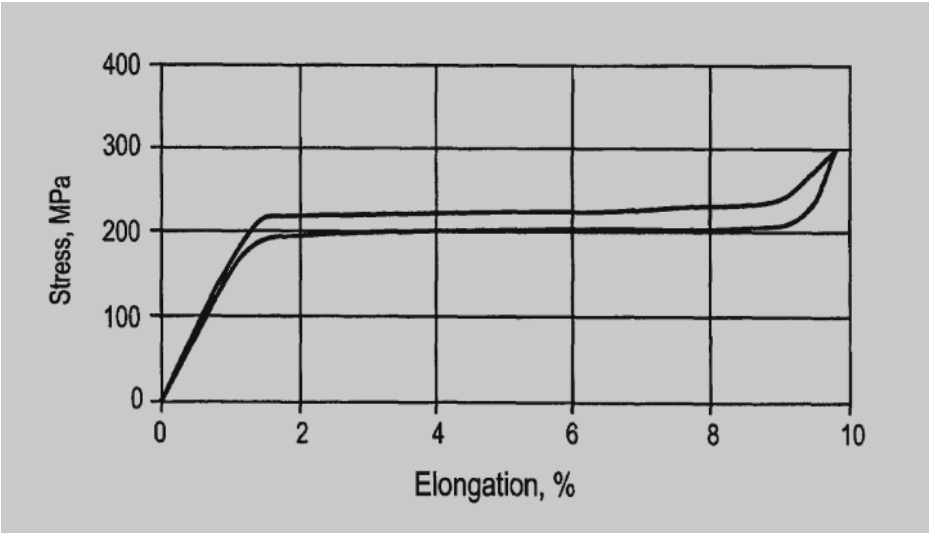

Figure 2.6: Pseudo elasticity of CuAlNi

However, Cu-based pseudo elastic alloys have not been seriously considered for such investigations since the degree of pseudo elasticity associated with them is not as high as that of (Ni-Ti)-based pseudo elastic (8%) alloys. They are also prone to stress corrosion cracking, have low strength, short fatigue life, and are not amenable to the manufacture wires of diameter less than 1 mm. characteristics of the Ti-based alloys in different applications. Yet, considering the very high price (about 1dollar/g) of the Ni-Ti alloys, the Cu-based alloys remain a good economical alternative, due to their price being 100 times lower. To the above economic arguments, one must add those concerning their physical properties, such as the 6% SME or 2% TWSME, a 1 J/g mechanical work developed by SME by heating, as well as the pseudo elastic effect (PSE) of 5% developed during the isothermal mechanical unloading [17].

2.7.1.2 Mechanical properties:

a) *Cyclic fatigue properties:* The main issue of concern of the potential offered by the thermomechanical properties of SMAs is the long-term predictability of the material behavior and the fatigue lifetime of the macrostructural elements (as different from the one of wire segments). Repeated use of the shape memory effect may lead to a shift of the characteristic transformation temperatures. This effect is known as functional fatigue, as it is closely related to a change of microstructural and functional properties of the material. Cu-based alloy presents the main advantage of avoiding undesirable creep phenomena. This capability is mainly achieved by preliminarily performing a suitable thermal treatment and it could be improved by applying adequate mechanical training.

b) *Physical properties of CuAlNi:* The physical properties of the CuAlNi shape memory alloys are listed in the following table-

Table 2.2: Physical properties of CuAlNi

Material Parameter	CuAlNi (4wt%)
Thermal Conductivity (20°C) (W/mK)	30-75
Phase transformation temperature(°C)	No finite range
Normal working stress (MPa)	70
Melting temperature	around 1100^0C
Young's Modulus (MPa)	80-100

So, the copper-based shape memory alloys have- low cost, reasonable shape memory, good pseudo elastic behavior, brittle in tension, stable phase precipitation near 200°C, reordering causes shift in transformation temperature in the quenched specimen [5].

2.7.2 NiTiCu:

The addition of a third or fourth element to the NiTi alloys provides a powerful tool for controlling the properties of these shape memory alloys. The control of the transformation temperature, the stabilization of the transformation temperature, control of the hysteresis width, control the austenitic strength, increase or decrease the martensitic strength, an increase of the two-way shape memory effect can be introduced by the addition of these elements.

2.7.2.1 Shape memory properties:

In this ternary alloy system, the metastable pre-martensitic rhombic phase doesn't occur which results in the lower hysteresis which is beneficial to electronic applications like actuators. The

hysteresis reduction is highly dependent on the cu amount. Ternary alloys with copper addition less than 7% results in the one-step transformation (cubic to monoclinic) whereas adding more than 8% results in more stability and the transformation is two-step (Cubic to orthorhombic to monoclinic). NiTiCu alloys show stable super elasticity characteristics when cyclically loaded with small stress-hysteresis. On the other hand, it is the hysteresis is smaller and the change of stress-strain curve by cyclic deformation is more stable in· the Ni-Ti-Cu alloy [20].

F.J.GIL et. Al [22] have investigated the shape memory properties of the NiTiCu alloys in orthodontic archwire applications. The findings indicate how the ternary addition improves the mechanical behavior of the biomaterials. Compared to the NiTi shape memory alloys NiTiCu alloys are less sensitive to composition which makes them easier to be produced industrially. For NiTi binary alloys the composition variation around 0.1% can result in the transformation temperature change to around 10%. For the NiTi Cu samples, the general transformation temperature range is between -100 to 100^0C. The two-way shape memory effect of the NiTiCu alloys is dependent on the composition and the pre-strain in the alloys [23].

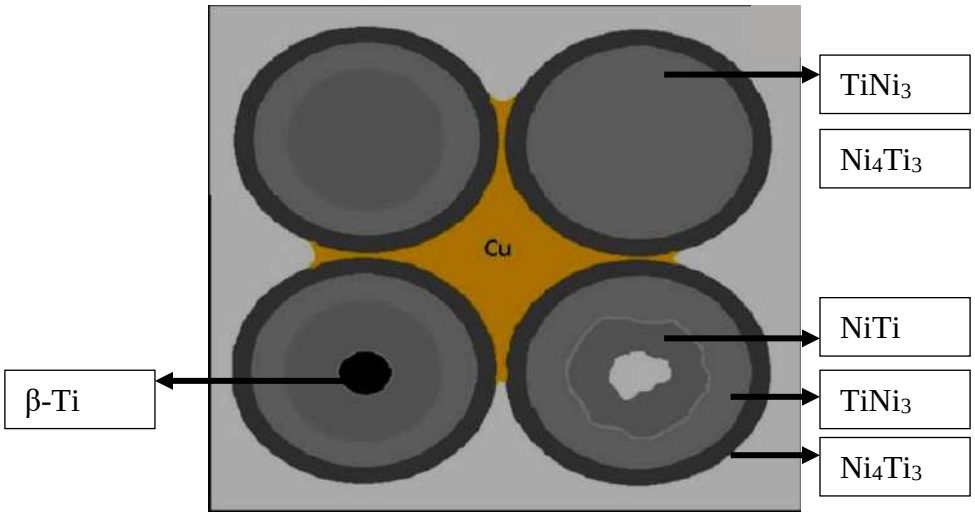

Figure 2.7: Illustration of the schematic phase occurred after sintering [24]

Figure 2.7 represents the phase formation while solid state sintering of NiTiCu. During solidification, a Ti_2(Ni, Cu) phase forms between NiTi cells/dendrites through a peritectic reaction [28,46]. Ti_2Ni is known to be detrimental to the shape-memory effect because it promotes brittle fracture. Within the Ti_2(Ni, Cu) phase, SEM/EDX reveals three variants of the corresponding $(Ni, Cu)_4Ti_3$ precipitates, lighter lenticular disc like shapes [25].

2.7.2.2 Mechanical properties:

a) *Cyclic fatigue properties:* The stability of the properties during cyclic loading is a major concern for the shape memory alloys. A reliable shape memory alloy should show a constant martensitic temperature with cyclic loading. Secondly, the amount of recovered shape should be independent of the cyclic loading. An inability to show stability in

mechanical and transformation temperature are fatigue prone. So, from the previous section as the NiTiCu shows the stability so these alloys have superior fatigue properties [14].

b) *Physical properties of NiTiCu:* The physical properties of the NiTiCu shape memory alloys are listed in Table 2.3

Table 2.3: Physical properties of NiTiCu

Material Parameter	**NiTiCu**
Thermal Conductivity (20°C) (W/mK)	9-18
Phase transformation temperature(°C)	-10-150^{o}C
Normal working stress (MPa)	100-130
Melting temperature	1264-1321^{o}C
Young's Modulus (MPa)	30-90

Various studies have shown that the hardness of the Nitinol shape memory alloys increases with the addition of copper. Comparison of the mechanical properties shows the superior behavior of the ternary NiTiCu alloy, particularly on loading-unloading cycles. The addition of copper reduces the super elastic hysteresis stress and allows higher unloading plateaus to be obtained which is of particular interest for medical applications. The resistance to softening during loading and unloading cycles at higher temperatures is also considerably improved [13].

2.8 Biocompatibility and cytotoxicity of CuAlNi and NiTiCu:

2.8.1 Biocompatibility of Copper:

The total amount of Cu in normal adults is 50–150 mg, of which 50%–70% is distributed in muscle and bone, 20% in liver, and 5%–10% in blood. Cu mainly exists in the ceruloplasmin and cuprase in vivo, and there are few free Cu ions in the body. Cu in the diet is mainly absorbed in the stomach and small intestine, especially the duodenum, which absorbs about 40% of the total. After absorption, Cu is transported into the liver and throughout the body through the blood. Apart from some Cu-containing proteins are stored in the liver, and the rest are synthesized in the liver or other human tissues, such as cytochrome oxygenase and monoamine enzyme. More than 90 different enzymes and proteins have been found to contain Cu to various extents.

Both the overload and the deficiency of Cu can influence human health through multiple mechanisms. Disorders featuring an overload of Cu mainly include two aspects:

(1) Acute Cu toxicity: The acute toxic reaction caused by exposure to many copper-containing substances in a short period of time. Nausea, vomiting, headache, diarrhea, hemolytic anemia, gastrointestinal hemorrhage, and liver and kidney failure, as well as death, may occur with an increase of the Cu dose.

(2) Chronic Cu toxicity: The chronic toxic reaction caused by the long-term repeated entry of low-dose copper-containing substances into the body. This can cause Wilson disease. This background underlines the fact that Cu is a trace element that is essential for life and good health.

Copper-containing biomaterials have beneficial effects on bone fracture repairing, cardiovascular system, antibacterial effect. Cu-bearing SS, L605-Cu, 316L-Cu stent promotes the adhesion, proliferate of VEC (Valvular Endothelial Cell), reduce the early apoptosis ratio of VEC, inhibit the proliferation of VSMC (Vascular smooth muscle cells), inhibit the proliferation of VSMC, reduce the formation of thrombosis. These biomaterials also show the best effect on endothelialization with good biosafety. Copper ion helps in Increasing the expression of VEGF (VEGF-A plays an important role in cardiac morphogenesis, cardiac contractility, and wound healing within the myocardium), increasing the eNOS activity.

In recent years, Cu-containing titanium alloys have attracted increasing attention since titanium alloy is one of the most used materials in orthopedics. In orthopedic applications, enhancing the adhesion and proliferation of osteoblasts, the gene expression of collagen, Upregulating the expression of alkaline phosphatase, Collagen I, osteopontin, and osteocalcin can be attained by 317L-Cu, 316L-Cu, Ti-Cu, Nano-copper-bearing 317L SS, Cu-containing ceramic coatings on titanium.

Based on the strong antibacterial performance of Cu, which is one of the most essential trace elements present in the human body, researchers have increasingly focused on fabricating Cu-containing implantable materials to inhibit the occurrence of infections. Stainless steel is one of the most used materials in the biomedical field. Related research demonstrated that the strong and broad-spectrum antibacterial ability of Cu-containing SS is mainly due to the Cu ions released from the steel's surface, which damage bacterial cell walls and cell membranes, adsorb electrons from bacteria, and generate reactive oxygen species (ROS), resulting in severe damage to and death of bacteria and fungi, such as Staphylococcus haemolyticus, Escherichia coli, and Candida albicans. Besides 317 L-Cu SS, other Cu-containing materials also exhibited satisfactory antibacterial abilities.

In addition to copper-containing biomaterials, Ghosh Deepanjan et al. [26] found that delivery of ionic copper from sutures could promote incisional wounds healing, and copper-eluting fibers may have translational potential for accelerating repair on surgical and trauma wounds. L. A. Volodina et al. [27] developed ointment containing copper nanoparticles (NPs), which could provide a high level of reparation of skin wounds. Some studies suggest that copper-containing materials have a certain role in the treatment of cancer. Based on the previous studies, colloidal Cu NPs have been proven to be one of the effective inorganic materials

against various cancer cell lines. As reported by Mayor et al. [28] Cu NPs were toxic to human lung carcinoma cell line (A549), human liver hepatoma (HepG2), Chinese hamster ovary (CHO), human osteosarcoma, and mouse embryonic fibroblast (3T3L1) cells in a dose-dependent manner. The study revealed that the capped Cu NPs by nontoxic aqueous extract of latex could be directly used for administration/in vivo delivery for cancer therapy. Anticancer studies demonstrated the in vitro cytotoxicity values of Cu NPs against the tested human colon cancer Caco-2 cells, human hepatic cancer HepG2 cells, and human breast cancer Mcf-7 cells, which can be used as a photothermal treatment to kill cancer cells.

Copper has several radioisotopes, and $_{60}$Cu, $_{61}$Cu, $_{62}$Cu, $_{64}$Cu, and $_{67}$Cu are particularly interesting for radiotherapy and imaging applications. Decay characteristics of copper radionuclides make them suitable for numerous medical applications, such as Positron Emission Tomography (PET) imaging, neuroimmunology tracing, and radiotherapy of cancer [29].

2.8.2 Biocompatibility of Aluminium:

Biologically reactive aluminum is present throughout the human body and while, rarely, it can be acutely toxic, much less is understood about chronic aluminum intoxication [30]. In the human body, the total amount is 30–50 mg. is in the skeleton and 25% is in the lungs.

Al_2O_3 is an inert material with a well-known application mostly in dentistry. The protective effect of Al_2O_3 helps with corrosion and at the same time can reduce the friction on articular surfaces. Aluminum oxide obtained through the process of anodization has the qualities needed for it to be more and more widely used in the production of biomaterials. Its porous structure allows it to be filled with a bioactive material, which enhances the compatibility and the antibacterial action of the metal pad [31].

Anodized aluminum is a popular choice in manufacturing medical devices for several reasons. i.e.- lightweight, because of its structure there is almost no limit to extrusion geometries that can be achieved with aluminum, can be machined easily, accept many different types of colors, coatings, and finishing, highly biocompatible, no significant investment requirement to the tool, recyclable. For these reasons, it is a common material for machined parts, stethoscopes, and other medical devices. Aluminum's malleability also makes it useful for tubing. Whereas steel tubes are too stiff to be bent by hand, surgeons can bend aluminum tubing easily and quickly by hand to the desired shape.

2.8.3 Biocompatibility of Nickel:

According to Anke et al. [32] Nickel is an essential element in the human body it can be found in food, water, and air, although it is only required in small amounts. Nickel deficiency may cause several symptoms to occur such as weight loss, reduction in growth, and degeneration of

muscle. Laing et al. [33] and Ryhänen et al. [34] have studied those High levels of nickel in the body can cause toxic effects and allergic reactions. Studies have shown that nickel implants can cause tissue irritation, inhibition to mitosis, necrosis, and toxic reactions to occur.

Nickel toxicity in the body can display itself in a few different ways such as acute pneumonia, cancer of the nostrils, and dermatitis. However, there is not enough data to classify nickel as a genotoxic element. If the concentration of nickel in the body is too high, it starts to accumulate in the lungs and kidneys first. The accumulation rate is related to the amount of nickel present in the body. Nickel can be removed in the urine and faces. How fast the nickel can be removed not only relates to the concentration of nickel in the body but also depends on the metabolism of the person [35]. The link between nickel and cancer is not clear but now it is thought that it is nickel compounds that can cause cancer and not the nickel ions [34].

2.8.4 Biocompatibility of Titanium:

Titanium and titanium alloys exhibit a high specific strength, which makes titanium an excellent choice for biomedical applications. Furthermore, titanium is biocompatible because it has a low electrical conductivity which contributes to the electrochemical oxidation of titanium leading to the formation of a thin passive oxide layer. The oxide layer in turn leads to high resistance to corrosion. This protective passive layer is retained at pH values of the human body due to titanium having an oxide isoelectric point of 5–6. In aqueous environments, Ti and its oxides have a low ion-formation tendency and low reactivity with macromolecules.

Titanium alloys are used in biomedical implant devices which replace damaged hard tissue. Some examples of Ti use in biomedical applications are dental and orthopedic implants, artificial hearts, pacemakers, artificial knee joints, bone plates, cardiac valve prostheses, screws for fracture fixation, artificial hip joints, and cornea backplates. Titanium and titanium alloys have therefore been used widely as biomedical implant materials since the early 1970s and the implants have been available as machined and cast components [36]. Matsuno et al. [37] evaluated the biocompatibility and osteogenesis of many metals. Titanium wires were implanted in rats. These titanium wires were implanted in both the soft and hard tissue of rats for either 2 or 4 weeks. It was found that titanium had good biocompatibility and osteogenesis. It was also found that there was no titanium ion dissolution into the soft or hard tissue, and this is due to titanium's excellent corrosion resistance which in turn contributes to its biocompatibility. T. Albrektsson et al. [38] showed that osseointegration can occur between the titanium implant and bone. Osseointegration occurs when the bone and implant form an interface and it's nearly impossible to remove the implant [39].

Titanium and its alloys have a proven track record as biomedical implants due to their excellent biocompatibility. This is related to the presence of an oxide layer that is typically present on the surface of the material in an oxidizing environment [36].

2.8.5 Biocompatibility of CuAlNi:

Due to stable mechanical properties, aging resistance, and shape memory properties, CuAlNi could potentially be used for the preparation of medical devices. CuAlNi shape memory alloys (SMAs) have been investigated as materials for medical devices, but little is known about their biocompatibility. The explanation for the different biocompatibility and corrosion stability of the control alloy and SMA ribbons can be found in their different microstructures. In addition, the formation of oxide layers on the surfaces of both materials after prolonged conditioning further decreases the release of metal ions. The hypothesis is that the martensitic structure of CuAlNi alloys is predominantly responsible for their corrosion resistance. Similar treatment of control CuAlNi platelets (double heating/quenching) partly resulted in the martensitic transformation of the alloy and its higher corrosion resistance compared to nontreated CuAlNi platelets. Besides literature shows that rapid solidification techniques for the synthesis of the shape memory alloys can result in reduced cytotoxicity because of the controlled release of the copper ion from the alloys. The release of copper around 4-10ppm is catastrophic for the human body [6].

It has been discovered that a continuous layer of Al_2O_3 and CuO forms, on the surface of the control alloy sample, without Ni, while on the surfaces of the rapidly solidified SMAs the layer also contained Ni [18]. Biocompatibility may be attributed to the formation of a durable oxide surface layer analogous to the TiO_2 layer that inhibits body fluid reaction to titanium nickel alloys, and/or the non-existence of crystal domain boundaries may inhibit corrosive chemical attack.

In general, these methods include forming a single crystal copper-based (e.g., copper, aluminum) shape memory alloy and forming a controlled layer of aluminum oxide on the single crystal copper-based shape memory alloy. In general, the controlled layer of aluminum oxide is actively applied or formed, in contrast to the thin, and likely irregular (accidental) layer of Aluminum oxide that may be formed. The controlled layer is formed by further modification of the single-crystal material (e.g., by controlling the concentration of Al near the outer Surface, etc.) [21].

2.8.6 Biocompatibility of NiTiCu:

The biocompatibility of the as cast Ni-42Ti-7Cu and SPS made $Ni_{45}Ti_{50}Cu_5$ and $Ni_{40}Ti_{50}Cu_{10}$ has been investigated. According to the study of Mohammed et al. [13], the SEM and LM studies of cells grown in the presence of the binary alloy did not show any significant morphological difference to the control sample. Adherence and growth were similar on both coverslip and metal, although the adherence on the metal seemed less pronounced than on the coverslip. Nevertheless, a normal morphology of the cells adhering to the NiTi was observed, which stresses the biocompatibility of this alloy.

The results of the Mean Transit Time (MTT) -biotoxicity test confirm this fact. The formazan (toxic and corrosive chemical) formation, which denotes the dehydrogenase activity and thus the intact mitochondrial content of the cells tested, decreases only by 10% after a 24 h incubation period, and by an additional 5% when incubated for 48 or 72 h. This decrease might be attributed to a release of Ni ions which have been shown in a recent study to be highest in the first 2 days. The results of the ternary alloy tested differ from those obtained for the binary alloy. Cell adhesion and growth are less pronounced in the presence of NiTiCu. SEM investigations of cells grown on coverslips in the presence of the metal show a higher number of spherical, sometimes detached cells.

These effects are more pronounced on the alloy. The MTT-test confirms these findings. There is a 30-38% decline of the dehydrogenase activity obtained for incubation periods of 24 and 48 or 72 h, respectively. F.J. Gil et al. [22] has showed that Cu ions are released to a higher concentration than Ni and Ti ions and that the release rate is maximum in the initial incubation phase. Therefore, it is thought that the higher cytotoxicity of the ternary alloy arises from the release of Cu ions which are known for their cytotoxic effects. Evidence for the release of the Cu ions could be also found in this work using AAS. However, it should be mentioned that for both alloys no significant change was observed between an incubation period of 48 and 72 h. This points to a time-dependent build-up of a passive layer on the alloy surfaces, which usually follows a parabolic law. This explains why the MTT results remain almost constant with increasing incubation time.

The effect of copper in the NiTi has not been established yet. For a definite conclusion, the passive layer can be investigated in more detail using electron spectroscopic surface analysis methods. So, this study aims to investigate the surface compositions of the ternary alloy and do the corrosion test to learn the passivation of the shape memory alloys.

2.8.7 Cytotoxicity of different elements:

Table 2.4 summarizes the findings of different in vivo studies on the cytotoxicity of the elements-

Table 2.4: Cytotoxicity of various elements [40]

Cytotoxic Ranking of Various Metal Ions Evaluated in L-929[a] or 3T3[b] Mouse Fibroblast Cultures

Wataha *et al.*, 1991[bb*]	Wataha *et al.*, 1994[aa]	Schmalz *et al.*, 1997[ba]	Sauvant *et al.*, 1997[a*]	Yamamoto *et al.*, 1998[a]		Kappert *et al.*, 1998[a]
Cd^{2+}	Cd^{2+}	Ag^{+}	**Cu^{2+}**, V^{5+}	K^{2+} (most toxic)	**Zn^{2+}**	In^{3+}
Ag^{+}	Ag^{+}	**Zn^{2+}**	Hg^{2+}, **Zn^{2+}**	Cd^{2+}	Y^{3+}	Ga^{3+}
Zn^{2+}	**Zn^{2+}**	Cd^{2+}	Co^{2+}	V^{3+}	$W6^{+}$	**Zn^{2+}**
Cu^{2+}	V^{3+}	Hg^{2+}	Cd^{2+}	Ag^{+}	Fe^{3+}	**Cu^{2+}**
Ga^{3+}	Au^{3+}	Au^{3+}	Ti^{4+}	Hg^{2+}	Pd^{2+}	Au^{3+}
Au^{4+}	**Cu^{2+}**	Pt^{4+}	Nb^{5+}	Sb^{3+}	Fe^{2+}	Co^{2+}
Ni^{2+}	Co^{2+}	Co^{2+}	Fe^{3+}	Be^{2+}	Ti^{4+}	Ni^{2+}
Pd^{2+}	Pd^{2+}	**Cu^{2+}**	Sb^{3+}	In^{3+}	Hf^{4+}	Pd^{2+}
In^{3+}	Ti^{4+}	Ni^{2+}	Sn^{4+}	Cr^{3+}	Ru^{3+}	Sn^{2+}
	Be^{2+}	Pd^{2+}	Mn^{3+}, Ge^{4+}	Hg^{+}	Sr^{2+}	Mo^{5+}
	Ga^{3+}	Mn^{2+}	Cr^{3+}	**Cu^{2+}**	Sn^{4+}	La^{3+}
	Ni^{2+}	Nb^{5+}	Pb^{2+}	Rh^{3+}	Ba^{2+}	
	Ti^{4+}	Ga^{3+}	Ba^{2+}	Ti^{3+}	Cs^{+}	
	Cr^{3+}	Cr^{3+}		Sn^{2+}	Nb^{5+}	
	Al^{3+}	In^{3+}		Ga^{3+}	Ta^{5+}	
		Sn^{2+}		Pb^{2+}	Zr^{4+}	
				Cu^{+}	Al^{3+}	
				Mn^{2+}	Mo^{5+}	
				Tl^{+}	Rb^{+}	
				Ni^{2+}	Li^{+} (least toxic)	

Analyzing the cytotoxicity of different cast specimens, studies have found that cytotoxicity and biocompatibility are sensitive to the composition, phase formation, and fabrication methods.

2.9 Corrosion resistance of CuAlNi and NiTiCu:

2.9.1 Corrosion of CuAlNi:

The corrosion resistance of Cu-Al alloys has been attributed to the formation of a protective layer of alumina along with copper chlorides and oxides on the alloy surface. Aluminium has a greater affinity towards oxygen than copper, and higher stability of the Al_2O_3 than Cu_2O. Some researchers have attributed the enhanced corrosion resistance to the formation of duplex-layered surface oxides composed of $Cu_2O.Al_2O_3.xH_2O$. The presence of nickel is also important in the passivation of CuNi alloys because of its incorporation in the Cu(I) oxide, which reduces the number of cation vacancies that normally exist in Cu(I) oxides.

The corrosion behavior of Cu-Al-Ni alloy in inorganic 0.5 mol dm^{-3} H_2SO_4 varying temperature has been investigated in an electrochemical cell. Increasing the temperature led to a decrease in the polarization resistance value and an increase in the corrosion current density value, indicating more intense corrosion of the CuAlNi alloy. The surface image of the CuAlNi alloy after polarization measurements by light and SEM microscopy indicated the appearance of intergranular corrosion along with pitting corrosion. Increasing the electrolyte temperature led to greater damages to the surface. EDS elemental surface analysis at a certain point revealed the presence of all alloying elements on the surface. At higher temperatures, the copper content

was slightly higher and the aluminium content lower, which could indicate its higher dissolution from the surface [41].

Cast Cu-Al-Ni (4.1 wt%) has the better cavitation erosion resistance. The damage level was significantly higher, with more and larger pits created. Self-accommodating zig-zag martensite provides benefits to alloys in terms of lower cavitation resistance, while the presence of orthorhombic martensite provides benefits to alloys in terms of better cavitation resistance [42].

Several studies have been carried out to improve the corrosion resistance of the alloys i.e.- Titanium, boron addition to the alloys, different coating techniques. All the investigations indicate that the improvement of the corrosion resistance can be gained if the phase formation and orientation of the martensitic phases can be controlled properly. No investigation for evaluating the corrosion resistance in bio media has been carried out for these alloys.

2.9.2. Corrosion of NiTiCu:

The corrosion behavior of the sputtered NiTiCu has been studied by Nan Ye et. al. Corrosion behaviors of the four films in phosphate buffered saline (PBS) solutions at 37˚C were examined using electrochemical impedance spectroscopy (EIS) method. It was found that the corrosion resistance of the NiTi film is superior to the three NiTiCu films. The EIS data were fitted using a parallel resistance-capacitance (as a constant phase element) circuit associated with the surface oxide film. The thickness of the surface oxide layer of the three NiTiCu films increases with applied potential till 0.8 V, while that of the NiTi film can reach to 1.2 V. [41] NiTiCu fabricated by powder metallurgy method has been studied by Neeraj et. al. [42]. The corrosion resistance of the compacted ball milled NiTiCu powder shows that addition of copper to NiTi alloy improves wear resistance of the alloys [43].

2.10 Different Corrosion Media:

Generally, alloys show lower corrosion compared to other materials. The component's corrosion behavior is the most important factor for understanding the corrosion behavior of the alloys. Even for a given composition, the corrosion behavior of a material is highly dependent on the grain size. Generally, high corrosion resistance is found in alloys with amorphous or nanocrystalline structures.

Dissolved phosphates, cholesterol, bi-carbonates, oxygen, and phospholipids generally don't play role in the corrosion process and exist at an insignificant amount. Therefore, the in-vitro experiments can be conducted in saline or standard isotonic solutions like- Ringer's Solution, and Hank's solution. Compared to saline calcium chloride and bicarbonate are the main differences. Blood sometimes has been utilized for the corrosion study where sodium citrate has been used as an anticoagulant. But the sodium citrate sometimes disrupts the passivation behavior of some alloys. Compositions of some simulated body fluid is given in Table 2.5.

Table 2.5: Chemical composition of different simulated body fluid [16]

Component	PBS	Ringer's solution	Hank's Solution
NaCl	8	8.60	8
$CaCl_2$	- -	0.33	0.14
KCl	0.20	0.30	0.40
$MgCl_2.6H_2O$	- -	- -	0.10
$MgSO_4.7H_2O$	- -	- -	0.10
$NaHCO_3$	- -	- -	0.35
NaH_2PO_4	1.15	- -	- -
$NaHPO_4.12H_2O$	- -	- -	0.12
KH_2PO_4	0.20	- -	0.06
Phenol Red	- -	- -	0.02
Glucose	- -	- -	0.1

2.11 Biomedical applications of copper-based shape memory alloys:

NiTi alloys are the mostly used shape memory alloys in medical science. The Cu-containing shape memory alloys don't have significant medical applications. However, in some caseswhere biocompatibility is not an issue, Cu-based SMAs find application. These include:

(a) Optometry: These frames are usually made from SMAs that have their transition temperature set below the expected room temperature. This allows the frames to undergo large deformation under stress yet regain their intended shape once the metal is unloaded again. The very large apparently elastic strains are due to the stress-induced martensitic effect, where the crystal structure can transform under loading, allowing the shape to change temporarily under load. This means that eyeglasses (Figure 2.9) made of SMAs are more robust against being accidentally damaged [17].

Figure 2.8: Shape memory alloy made eyeglasses

(b) Medical accessories like in an example of Wagner's thermolock (Figure 2.9), where a SM spring is used to lock sterilization containers. During sterilization the SM spring seals the container automatically, and once opened the container must be resterilized to seal the thermolock again [17].

Figure 2.9: Wagner's thermolock spring

(c) Cu–Al–Mn-based guidewire (Figure 2.10) has a unique characteristic, i.e., a functionally graded characteristic which can be obtained by controlling the microstructure. The tip of the guide wire shows excellent flexibility and shape effect (SE) properties which are obtained by control of the relative grain size, while the end of guidewire shows high stiffness and strength and hardly exhibit the SE property. Furthermore, those properties

gradually vary in the range from 100 to 500 mm. Such enhancements of the stiffness and strength are caused by bainitic transformation induced by aging at around 200–400°C.The graded properties can be obtained by aging treatment using a furnace with a temperature gradient. This guidewire with functionally graded properties shows excellent push ability and torqueability. These graded properties realized by microstructure control cannot be achieved in the other guidewires of Ni–Ti and stainless steels. This Cu–Al–Mn based guidewire is now under evaluation by doctors [17].

Figure 2.10: Medical guidewire

CuAlNi SMAs are being investigated for utilization in the biomedical field. The Aluminium oxide is considered a biocompatible compound the presence of which at the surface can make the alloys suitable for application in fabrication of medical implants. The addition of copper to the NiTi shape memory alloys offers interesting properties to the Nitinol alloys. The application of this NiTiCu is in producing actuators. There are no biomedical applications for the CuAlNi and NiTiCu. But the shape memory alloys have remarkable biomedical applications. So, these two potential shape memory alloys will also be applied for medical devices in future. The remarkable properties of SMA have promoted several investigations related to their applications in different fields of human knowledge as follows-

(a) *Cardiovascular applications:* Because of the intrinsic risks of cardiovascular surgery, several problems might occur. The atrial septal occlusion device is an alternative to this surgery. This device is composed of SMA wires and a waterproof film of polyurethane. As is the case for the Simon filter, the surgery to place this device exploits the shape memory effect, being much less invasive than the traditional one. First, one-half of the device is inserted through a catheter by the vena cava up to the heart, in its closed form. Then, it is placed on the atrial hole and opened, recovering its original shape. Next, the second half of the device is placed by the same route as the first one, and then both halves are connected. This procedure seals the hole, avoiding blood flow from one atrium to the other. It is expected that the device will stay in the heart for an indefinite period since the heart tissue regenerates.

Figure 2.11: Simon Filter

Self-expanding stents, named after the dentist C.T. Stent, are another important cardiovascular application that is used to maintain the inner diameter of a blood vessel. These devices are used in several situations to support any tubular passage such as the esophagus and bile duct, and blood vessels such as the coronary, iliac, carotid, aorta and femoral arteries. In this type of application, a cylindrical scaffold with shape memory is placed, for example, inside a blood vessel through a catheter. Initially, this scaffold is pre-compressed in its martensitic state. As the scaffold is heated, due to the body temperature, it tends to recover its original shape, expanding itself. This device can be used not only in the angioplasty procedure, in order to prevent another obstruction of a vessel, but also in the treatment of aneurysms for the support of a weakened vessel.

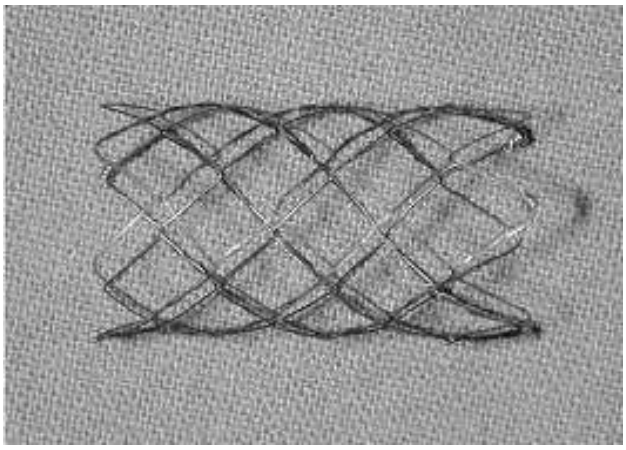

Figure 2.12: Nitinol Stent

(b) *Orthopedic applications:* SMA has many orthopedic applications. The spinal vertebrae spacer is one. The insertion of this spacer between two vertebrae assures the local reinforcement of the spinal vertebrae, preventing any traumatic motion during the healing

process. The use of a shape memory spacer permits the application of a constant load regardless of the position of the patient, who preserves some degree of motion. This device is used in the treatment of scoliosis.

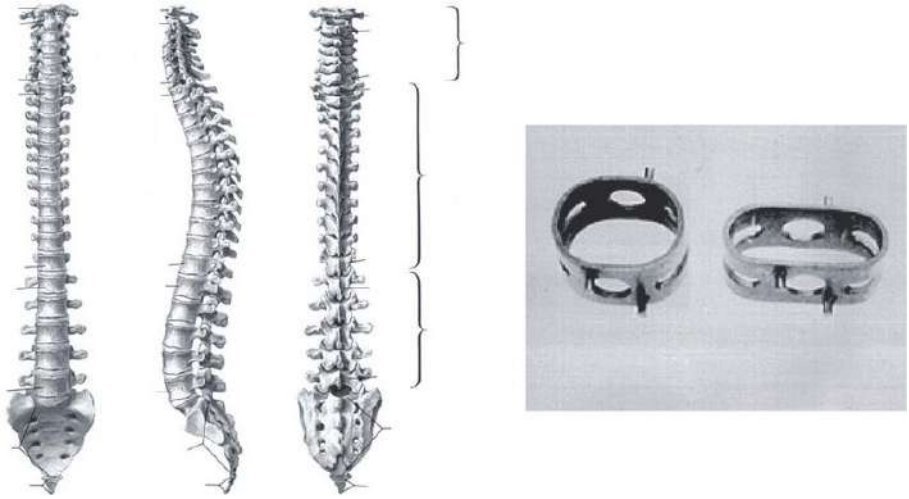

Figure 2.13: Spinal Vertebrae Spacer

Another application in the orthopedic area is related to the healing process of broken and fractured bones. Several types of shape memory orthopedic staples (Figure 2.14) are used to accelerate the healing process of bone fractures, exploiting the shape memory effect. The shape memory staple, in its opened shape, is placed at the site where one desires to rebuild the fractured bone. Through heating, this staple tends to close, compressing the separated part of bones. An external device performs this heating, and not the temperature of the body. The force generated by this process accelerates healing, reducing the time of recovery.

Figure 2.14: Orthopedic staples, staples placed in human bone

With respect to the healing of fractured bones, one can also point out shape memory plates (Figure 2.15) for the recovery of bones. These plates are primarily used in situations where a cast cannot be applied to the injured area, i.e., facial areas, nose, jaw, and eye socket. They are placed on the fracture and fixed with screws, maintaining the original alignment of the bone, and allowing cellular regeneration. Because of the shape memory effect, when heated these plates tend to recover their former shape, exerting a constant force that tends to join parts separated by fractures, helping with the healing process.

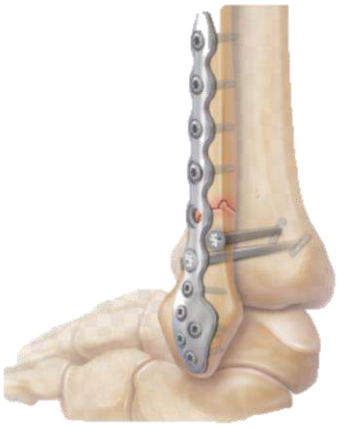

Figure 2.15: Shape memory alloy plate

Orthopedic treatment also exploits the properties of SMA in the physiotherapy of semi-standstill muscle gloves (Figure 2.16) that are composed of shape memory wires on regions of the fingers. These wires reproduce the activity of hand muscles, promoting the original hand motion. The two-way shape memory effect is exploited in this situation. When the glove is heated, the length of the wires is shortened. On the other hand, when the glove is cooled, the wires return to their former shape, opening the hand. As a result, semi-standstill muscles are exercised.

Figure 2.16: Gloves made of shape memory alloy wire

(c) *Surgical instruments:* In recent years, medicine and the medical industry have focused on the concept of less invasive surgical procedures. Following this tendency, shape memory surgical instruments have been created and are becoming noticeable. Among the advantages of these tools, one can emphasize their flexibility as well as their possibility to recover their former shape when heated. The SMA basket is used to remove kidney, bladder and bile duct stones. This basket is inserted into the human body in the same way as the Simon filter. The work principle is shown in Figure 2.17.

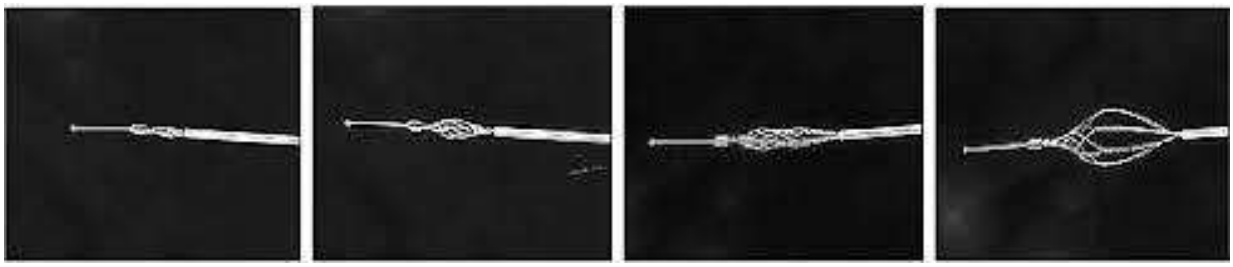

Figure 2.17: Sequence of opening the shape memory basket

The intra-aortic balloon pump (Figure 2.18) is used to unblock blood vessels during angioplasty. The device has an SMA tube whose diameter is reduced compared to polymer materials due to its pseudo elastic effect. Moreover, it also allows greater flexibility and torsion resistance when compared to the same tube made of stainless steel.

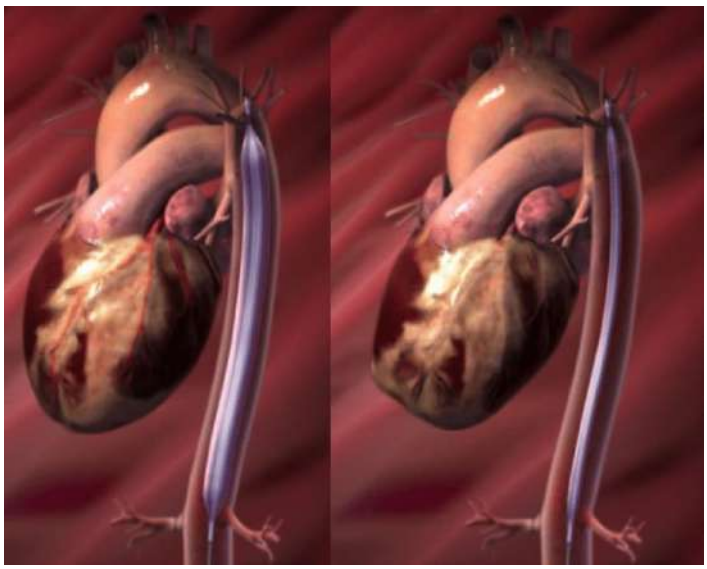

Figure 2.18: Intra-aortic balloon pump

Laparoscopy is another procedure where SMA has been employed. The actions of grippers (Figure 2.19), scissors, tongs, and other mechanisms are performed by SMA. These devices allow smooth movements tending to mimic the continuous movement of muscles. Moreover, these devices facilitate access to intricate regions.

Figure 2.19: Laparoscopy tools used for gripping in surgery

The morphology, metallurgical properties of an alloy play an important role in the biomedical application of the alloy. So, CuAlNi and NiTiCu can be utilized in these applications if the alloys are properly fabricated maintaining the morphology and properties [44].

2.12 Production methods of shape memory alloys:

a) *Melting:* SMA can be produced in many ways. One of the most important methods is vacuum melting. In addition to vacuum melting other melting techniques like electron beam melting and plasma melting can also be adopted. Vacuum induction melting works on Electromagnetic induction works by inducing electrical eddy currents in the graphite crucible and the metallic charges. Furthermore, electrodynamic force is adopted for excellent stirring and mixing of the melt. By using electro graphite crucible SMA can achieve low carbon concentrations. The advantage of VIM is achieving chemical composition homogeneity throughout the ingot and controllability of chemical composition. Vacuum arc re-melting (VAR) doesn't have the problem of contamination of carbon in the alloy due to the absence of graphite crucible and gives high purity. VAR is classified into two types concerning the heating system first method is a non-consumable electrode and is preferred in laboratories and applies to many varieties of alloys in this method raw materials to be melted are placed in a copper mold and irradiated by the argon arc from an electrode made of a tungsten rod. When the alloy melts it resembles a button shape due to the surface tension effect, the button shape is again a re-melted number of times to get homogeneity composition. The second method is a consumable electrode consists of two sources one is the heating source and another one is material source the electrode is heated by the argon arc and the molten alloy drops down onto the mold and forms a cylindrical ingot. A drawback of melting multiple types results in oxygen and carbon pick up if any leakage of vacuum occurs. The double melting process using VIM primary followed by VAR is often used to get further refining. Electron beam melting

utilizes a high voltage electron beam as a heating source this method is mainly adopted for NiTi SMA which doesn't need accurate or definite control of transformation temperature. The plasma melting method uses a low viscosity electron beam discharged from a hollow plasma cathode, this method results in very less loss of the alloy element. Composition distribution is uniform despite the use of water-cooled copper mold.

b) *Powder metallurgy:* Powder metallurgy is an essential technique for producing near net shape components of shape memory alloys. In the case of copper-based shape memory alloys, a grain refinement to enhance fatigue properties is targeted. There are two kinds of powder metallurgy techniques for preparing NiTi alloys, one is raw metal powder sintering and another one is alloy powder sintering. The homogeneity of NiTi alloy can be improved compared with raw metal powder sintering. Different powder metallurgy methods have been developed for Ni-Ti in which both elemental powders and pre-alloyed powders can be used as starting materials by hot isostatic pressing (HIP), hydrating, and pulverization. The HIP is the most adopted sintering technique. Powders are filled in evacuated and gas-tight welded cans will transfer the pressure to the powder. Samples prepared by this method have combined advantages of theoretical density and high homogeneity. If we require a high amount of complex near net shape parts Metal injection molding (MIM) becomes cost-effective. It is a combination of polymer injection molding and powder metallurgy (PM) due to low density their yield strain is only 1%.

c) *Thermal spray:* Thermal spray process is mainly used for producing NiTi foils or NiTi tubes, thin-walled mill products and other 3D shapes. It offers near-net-shape processing to reach the advantage of processing highly reactive materials under controlled conditions. This process can be done by two methods one is low-pressure wire arc spraying and another one is vacuum plasma spraying technique. Smart NiTi alloys are difficult and expensive to manufacture by conventional methods. Low-pressure thermal spraying process technology will reduce lead time, the production cost for semi-finished NiTi foils and tubes. The microstructure of the NiTi foils or tubes can be improved by hot rolling [45, 46].

2.13 Spark plasma sintering of CuAlNi and NiTiCu:

Spark Plasma Sintering refers to the sintering technique involving the contemporaneous use of uniaxial pressure and high-intensity, low-voltage, pulsed current. In general terms, SPS can be considered a modification of hot pressing, where the furnace is replaced by the mold containing the sample, which is heated by a current flowing directly through it and eventually through the sample [47]. For two decades, the spark plasma sintering (SPS) method is of great interest to the powder and powder metallurgy industry and to material researchers of academia for both product manufacturing and advanced material research development. It is generally well known that the SPS is an advanced processing technology to produce homogeneous highly dense Nano structural sintered compacts, functionally graded materials (FGMs), fine ceramics, composite materials, new wear-resistant materials, thermoelectric semiconductors, and biomaterials [47, 52,53].

2.13.1 Principle of Spark Plasma Sintering:

In the spark plasma sintering process, sintering occurs by simultaneous application of mechanical pressure and higher electrical power. The pulsed direct electricity cleans and activates the surface of powders, and the applied pressure is for the resistive sintering process. In the presence of pressure and electric current, localized necking occurs faster due to Joule heating (Figure 2.20) Consequently, the temperature rises very fast (faster than conventional sintering and Hot pressing), and the densification is completed within a few minutes.

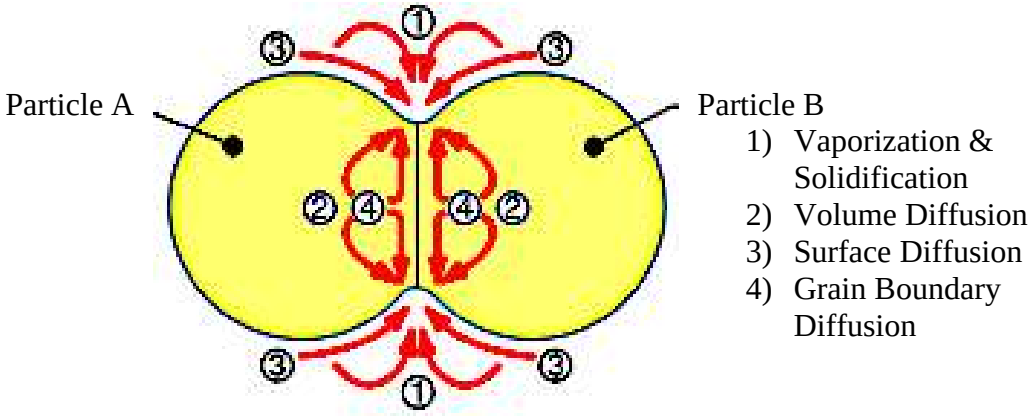

Figure 2.20: Localized heating and neck formation by joule heating [48]

The general principle of SPS is shown Figure 2.21. The typical device consists of a uniaxial hydraulic press with graphite punches and dye fixed in a steel containment. Graphite punches generate pressures (up to ~100 MPa) and serve as electrodes providing a pulsing direct current (up to 10 V and 10 kA) through the powder and dies. Apart from the ongoing scientific discussion concerning the actual mechanisms (presence or absence of plasma during processing by SPS) and the actual effect of the electric field and current, it presents a very efficient technique for powder consolidation compared to classical sintering of green pellets [23].

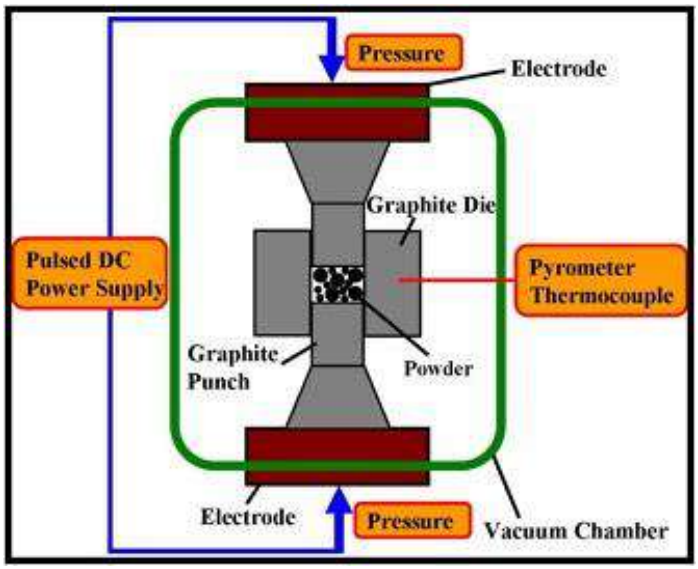

Figure 2.21: Schematic diagram of spark plasma sintering principle

The pulsed discharge is achieved by the application of an on/off low voltage (~ 30 V) and high current (> 600 A). The duration of each pulse varies between 1 and 300 ms, between 2 and 30 ms. The subsequent step comprises the application of a DC current at a level dependent on the powder type. The pulsed and direct current may be applied simultaneously or sequentially. For SPS Process, electrical discharge per se does not consolidate powders and, therefore, some additional effects are needed to increase the final density (pressure application and/or higher temperature than that created by electrical discharge. Pressure applied at constant/variable level during the process. SPS sintering temperatures range from low to over 2000^{o}C, which are typically ~ 200-500^{o}C lower than conventional sintering Vaporization, melting and sintering completed in short periods of ~ 5-20 minutes, including temperature rise and holding times.

2.13.2 Mechanism of solid-state sintering:

When spark discharge appears in the gap between the particles of a material, a local high temperature state occurs. This causes vaporization and the melting of the surfaces of the powder particles during the SPS process. Constricted shapes or "necks" are formed around the contact area between the particles. These necks gradually develop, and plastic transformation progresses during sintering, resulting in a sintered compact of over 99% density. Since only the surface temperature of the particles rises rapidly by self- heating, particle growth of the starting powder materials is controlled.

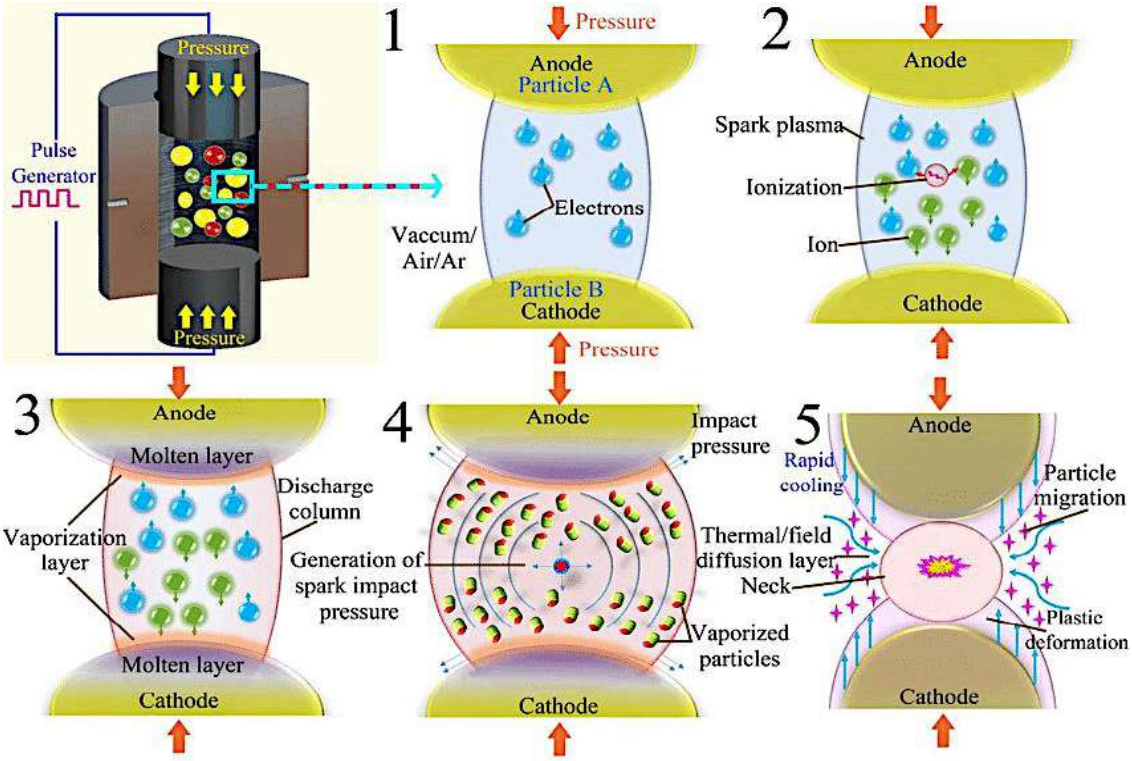

Figure 2.22: Initial stage of spark discharging by ON-OFF pulse energization, Generation of spark plasma, Vaporization and melting action to the particle surface, Generation of spark impact pressure, sputtering of Enhanced neck growth in the presence of vaporized/mol [49]

Figure 2.22 shows the formation of small capacitors at the contact between particles gap around the contact. Electrical discharges are generated across these capacitor gaps. The interfering surface oxide films are pierced beyond a certain voltage level, depending on the dielectric strength of oxide layer. This takes place when the arcing across the particles leads to achieving the breakdown voltage and electrical breakdown of dielectric film on the powder particle surface. Alternatively, the electrical discharges around the contacts may generate plasma, that is, an ionized gas between the powder particles. The above phenomena collectively contribute to the physical activation of the powder particle surface. The physical activation combined with faster densification at lower temperatures reduces grain coarsening and retains a finer microstructure.

Three mechanisms may contribute to field assisted sintering- (a) activation of powder particles by pulsed current (b) resistance sintering (c) pressure application. This activation is unique and provides main difference from more conventional resistance sintering processes (hot pressing). The surface activation results in clean grain boundaries. The grain boundary area shows direct grain-to-grain contact, which is attributed to the physical activation of powder particle surfaces during pulsed current application i.e., enhanced grain boundary diffusion process. Mainly the sintering is done by two effects-

(i) Effects of pulsed DC:

(a) Formation of capacitor banks at the surface insulating films.
(b) Generation of electrical discharges across the capacitors (might result in plasma).
(c) Discharges manifested by the presence of arc, aiding in material transport.
(d) Localized heating of powder surfaces. Breakdown of insulating films due to thermal and electrical breakdown.
(e) Enhanced diffusion (sintering) kinetics, clean interfaces, and good grain to grain bonding.

(ii) SPS effects:

(a) Release of electrical energy through a porous powder compact - breakdown of surface films
(b) Arcing at pores leading to enhanced mass transport to neck

Temperature gradient across powder compact strongly sensitive to both power input and thermal conductivity [49, 50, 51,52].

2.14 Biocompatibility and Spark Plasma Sintering:

Rapid solidification significantly improves the corrosion stability and biocompatibility in vitro of SMAs. SPS has been receiving growing attention in the last two decades due to its

remarkable effectiveness, allowing to obtain fast sintering and densification, particularly in the case of materials considered hard to sinter, such as extremely refractory materials, metastable phases, or nanomaterials. For some of these materials, SPS has already become the sintering technique of choice [47]. SPS process can easily consolidate a homogeneous, high-dense high-quality sintered compact because of the uniform heating, surface purification, and activation made possible by dispersing the spark points (early stage) and/or joule heat points during sintering [50]. Simultaneous application of temperature and pressure leads to high densification and hence a dense compact at sintering temperatures lower by 200 to 250°C than in conventional sintering is easily obtained. In SPS, since no coarsening and grain growth were allowed to occur, high relative densities were reached in a very short time and nano-sized powders can be sintered without considerable grain growth which is not possible in the conventional sintering process. Hence, nanostructured ceramics or nanocomposites can be easily prepared by SPS having more densification and fewer defects. These nano-structured composites exhibit excellent mechanical properties like high strength, high hardness, etc. Besides control while forming any unexpected defects which deteriorate corrosion resistance is possible by the SPS method. Biocompatible Ti-based alloys, Nitinols, hydroxyapatite, alumina have been synthesized by the SPS method in several studies. The control in grain growth, surface modification, porosity formation in SPS made materials offer higher biocompatibility.

Functionally Grated Materials (FGMs) have usually been expected as candidates for a wide variety of industrial applications due to their desirable properties such as high heat resistance capability, good wear resistance, biocompatibility, chemical stability and so on. Scaling-up and three dimensional (3-D) near-net shape forming technique for FGMs are one of the most important key-factor to produce the industrial engineering components and products in practical use. On the other hand, it is generally well known that the Spark Plasma Sintering (SPS) method is a novel process to produce homogeneous FGMs, nano-structural sintered compact, thermoelectric semiconductors and bio-medical materials in shorter sintering time with finer microstructure. In the past, different type of ceramic/metal, ceramic/ceramic, metal/metal, polymer/metal system FGMs have been prepared by SPS. For the bio-material industry's development, fundamental processing technique on 3-D formed ceramic (Al_2O_3)/metal (Ti, Ti-6Al-4V) system functional graded materials were investigated together with multi-layer composition and optimum sintering conditions [51].

Chapter 3 : Experimental Design:

3.1 Material selection:

3.1.1 CuAlNi:

From the ternary phase diagram (Figure 3.1a) in the copper-rich CuAlNi SMAs the aluminium percentage can vary from 10-15wt%. According to the literature review, aluminium has a good impact on these alloys. If aluminum oxide can be formed in the alloy, then it becomes more biocompatible. So, while designing the alloy, aluminium content has been kept higher. On the other hand, Ni ion has harmful effects on the human body. Because of that the Ni amount has been kept low in the alloys. So, the aluminium content has been kept higher and the Ni content has been kept lower in the alloys synthesized during the study.

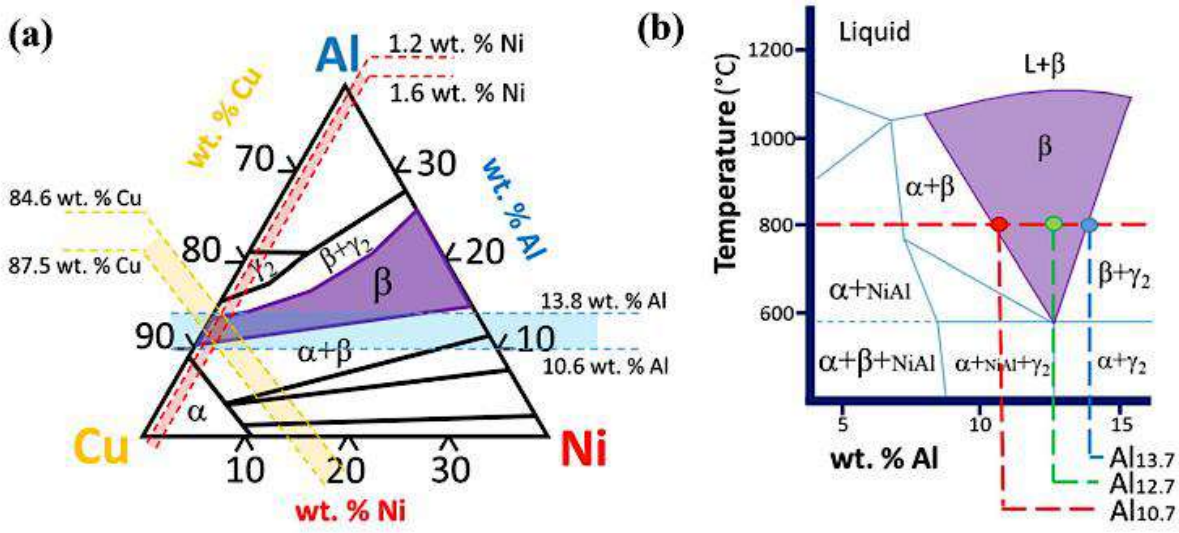

Figure 3.1: CuAlNi ternary phase diagrams (a) isothermal section at 800℃, (b) pseudo-binary phase diagram [52]

The β-phase in the binary Cu-Al alloy system undergoes a eutectoid transformation at 565℃ into α-phase (F.C.C.) and the brittle γ_2-phase (Cu_9Al_4 cubic phase). The presence of ternary element Ni retards the eutectoid transformation into α and γ_2. Ni also shifts the Cu-Al eutectoid to higher Al content. Since the alloys become brittle with increasing Ni content, the content of Ni should be kept around 4 wt% [51, 55].

Ni is added to stabilize the austenite phase and to decrease the high transformation temperatures of the binary system. Furthermore, Ni hinders the precipitation of alpha and stable γ_1 phases, and this is an important point because, in the Cu-Al system and its ternary alloys, the phase is only stable at high temperatures and must be quenched to freeze the metastable austenite phase, avoiding the precipitation of stable phases, which would inhibit any further MT. At the beginning of the SMA research history, the Cu-Al-Ni system was developed because of its outstanding super elastic effect, and the main works regarding thermomechanical properties of

Cu-Al-Ni alloys were focused on alloys whose composition was chosen in the Al-rich area to have low martensitic transformation temperatures. However, these alloys are also prone to the precipitation of the stable phases, and this was an important point in the historic trend of dismissing this SMA system for high-temperature applications. In addition, during the quenching of the austenite, two successive disorder-order transformations take place, and the disordered cubic phase becomes ordered with an L21 structure, as determined by neutron diffraction. After quenching, the transformation temperatures evolve during cycling or low-temperature aging, still adding more confusion. Indeed, some authors attributed the effect of aging on the transformation to precipitation processes, and this is particularly true for alloys with high Al content, far away from the eutectoid composition and prone to the precipitation of the equilibrium phases, which produces an increase of the transformation temperatures and a deleterious impact on the thermomechanical behavior. However, it was further demonstrated that the first stage of such evolution was associated with the slow ordering kinetics during low-temperature aging. This is the dominant effect in the case of Al-poor alloys close to the eutectoid composition of the phase domain [50-51, 55-56].

Analyzing all the literatures and phase diagrams, the following compositions has been chosen to carry out the investigation-

Table 3.1: Chosen composition of CuAlNi alloys

Sample No	**Composition (wt%)**
Sample 1	Cu-85%, Al- 11%, Ni-4%
Sample 2	Cu-84%, Al- 12%, Ni-4%

3.1.2 NiTiCu:

To get the shape memory properties, Ti should be nearly 50wt%. Considering this requirement, the composition of NiTiCu SMAs has been determined.

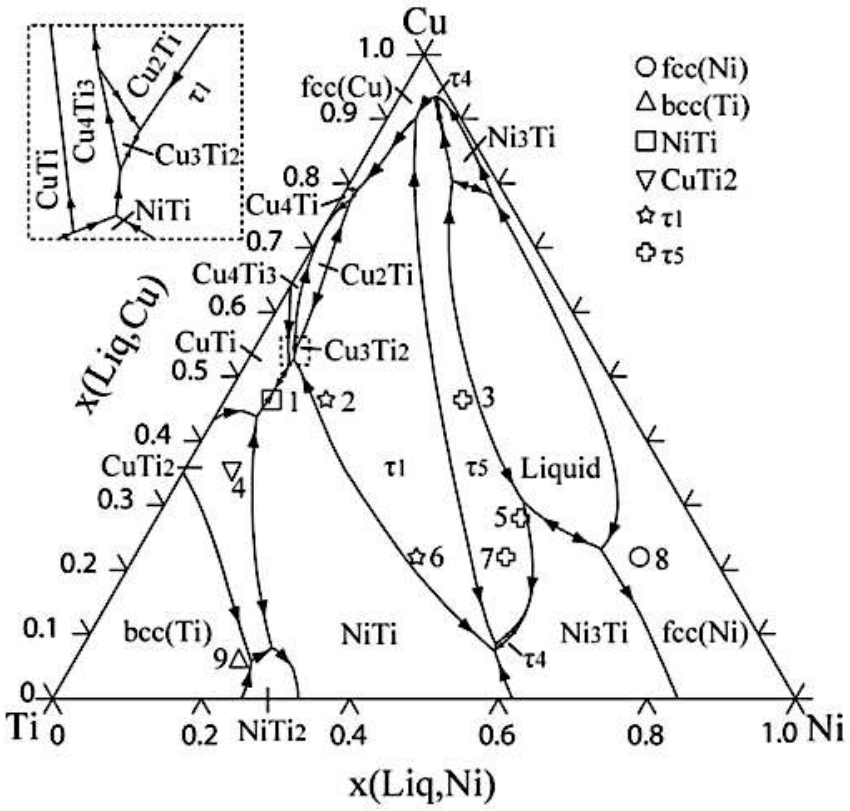

Figure 3.2: Ternary phase diagram of NiTiCu with the liquids and primary crystallization phases [53]

The Cu in the range from 5 to 15 wt% changes the crystallographic structure of the low-temperature phase. Cu >7.7 wt% results in a two-way shape memory effect and Cu<7.7wt% results in a one-way shape memory effect. The thermal hysteresis is reported to decrease from 40 K for the binary alloy to 11 K for NiTi-10 wt% Cu. The stress of the super elastic hysteresis is decreased. Higher unloading plateaus is beneficial for medical application. So, considering the effect of copper added to the NiTinol alloy, the copper percentage has been kept between 7 wt% to 10 wt% [13].

Table 3.2: Chosen composition for NiTiCu alloy

Sample No	Composition (wt%)
Sample 1	Ni-50%, Ti-43%, Cu-7%
Sample 2	Ni-49%, Ti-41%, Cu-10%

3.2 Ball milling parameter selection:

Mechanical alloying (MA) process significantly modifies the characteristics of the powders and shortens the sintering time. According to S.M.Tanga et. al. [54] the pure Cu, Al and Ni powders were milled for 1 hr, 5hrs, l0 hrs, 15hrs, 20hrs and 40hrs at a speed of 100 rpm in a

planetary ball mill machine under a protective argon atmosphere. The microhardness of green and sintered compacts increases with longer MA times and the diffusion of the elements also gets affected. A single phase of fcc structure with lattice parameter close to that of Cu was produced after MA for 40hr of the elemental powder mixtures. The best recovery in the shape memory effect (SME) test was found to be 68% for the quenched compact of 15hr milled specimen with a maximum deformation strain of 1%. The milled powder was subsequently hot pressed and extruded to rods. Chemically homogeneous specimens with nearly full density displaying 100% shape recovery at 4% pre-strain level were attained in these cases. According to Shafeeq et. al. [55] the milling parameters such as ball powder ratio (BPR), milling time and speed have considerable effects on the process of pre-alloying and the properties of Cu–Al–Ni SMAs. A lower BPR and milling speed caused insufficient milling, whereas a higher BPR and speed led to oxidation of the powder. Recently, Vajpai et al. [56] have prepared SMA strips by the milling of the elemental powder mixture for a shorter duration (8 h) followed by secondary processing. However, it was observed that the homogenization treatments required much longer time to produce chemically homogeneous strips. The aim of this present investigation is to focus on the SPS parameter's effect i.e.- low sintering temperature, pressure on the formed phases and physical properties. So, the parameters of ball milling have been chosen accordingly. The modification of property through ball milling has not been focused on this study.

For NiTiCu with 10wt% Cu, the pre-alloying by ball milling had been done for 5hr at 300rpm with a milling media: powder ratio (20:1) [12]. According to Piotr et. al. [57] the use of high-energy ball milling, with an extended grinding time to 100 hr, allowed to obtain both the Ti50Ni50 and Ti50Ni25Cu25 alloys in an amorphous form with few crystallized nano-areas. So too much high period of ball milling may result into amorphous structure. In addition to that, excessive milling can result into severe deformation and originates defects which may accelerate the corrosion of the alloys. So, 8 hours milling time and 5:1 BPR have been fixed for both CuAlNi and NiTiCu.

3.3 SPS Temperature profile and pressure selection:

Since SPS experiments are generally performed in a vacuum chamber, at low temperatures the only significant heat loss is due to the conduction along with the die punches towards the cooler hydraulic cylinders. At higher temperatures, above 700–800^{0}C, radiation losses tend to dominate [47].

3.3.1 CuAlNi:

In SPS the sintering temperature is selected from the melting temperature of the elements of the alloy. In CuAlNi-

Melting Temperature of copper, M_{cu}=1084^{0}C
Melting Temperature of aluminium, M_{Al}=660^{0}C
Melting Temperature of nickel, M_{Ni}=1453^{0}C

Among the elements of the alloy, aluminium has the lowest melting temperature which is 660^0C. So, the sintering should be done at two-thirds of the melting temperature of aluminium, which is 440^0C. The temperature profile has been selected accordingly. The alloys have been sintered up to 475^0C. The determination of the temperature profile has been done by doing multiple trial run.

The temperature profile has been programmed accordingly that; stepwise heat treatment takes place. To trace the start of leaking, the samples have been held for a couple of minutes at a particular temperature. The heating rate is gradually decreased from the initial high heating rate to a lower heating rate. the later step of the sintering gives the heat treatment effect to the alloys. Running the first programmed temperature profile was sufficient to produce the samples without any leakage or melting. The temperature profile in Table 3.3 has been followed for CuAlNi samples.

Table 3.3: SPS Temperature profile for CuAlNi alloys

Temperature (^{0}C)	**Time (min)**	**Heating rate (^{0}C/min)**
300	3	100
350	1	50
410	2	30
430	1	20
455	2	12.5
460	1	5
472	2	4
475	3	1

3.3.2 NiTiCu:

For NiTiCu alloys the melting temperatures of the elements of the alloy are as follows-

Melting Temperature of Copper, M_{cu}= 1084^0C
Melting Temperature of Titanium, M_{Al}= 1668 ^{0}C
Melting Temperature of Nickel, M_{Ni}= 1453^0C

Among the elements, copper has the lowest melting temperature. So, the sintering temperature should be two-thirds of the melting temperature of copper which is around 730^0C. The first temperature profile has been programmed by heating the samples to 730^0C. Like the CuAlNi alloy's temperature profile the initial heating rate has been kept higher and gradually the

heating rate has been decreased. The elements have a higher melting temperature. So, the temperature has been increased more stepwise compared to the CuAlNi alloys. In each step similarly, the sample has been kept for a certain period for getting the heat treatment effect and tracing the leakage. Particularly holding the sample to the highest temperature had been done for heat treatment purposes. The temperature profile in Table 3.3 has been followed for NiTiCu samples. This temperature profile has been fixed after multiple trials.

Table 3.4: SPS Temperature profile for NiTiCu alloys

Temperature (^{0}C)	**Time (min)**	**Heating rate (^{0}C/min)**
500	5	100
550	1	50
600	2	25
640	2	20
710	4	17
725	3	5
730	3	1.67

The pressure for CuAlNi sintering has been kept at 50 MPa. The NiTiCu samples have been sintered with an applied pressure of 42 MPa.

3.4 Corrosion Media Selection:

Among the simulated solutions shown in Table 2.5, Phosphate Buffer Solution (PBS) is mostly recommended because it maintains the constant pH throughout the corrosion study. It has been studied that; inorganic solutions based on diluted NaCl are the satisfactory corrosion media solution alike human body fluid when studying the behavior of passive materials. Thus, for the in-vitro corrosion study, simple saline solution, PBS (0.9wt% NaCl in DI water) is a good option [58, 59].

Chapter 4 : Methodology:

The chapter describes the experimental procedure stepwise for fabricating the shape memory alloys. The powder preparation, spark plasma sintering of two types of alloy powders, and characterization techniques for property analysis have been described in this chapter. This section also evaluates and justifies the parameters used in investigation and characterization and the different necessary steps taken during research work. The following experimental works have been carried out:

I. The alloy powder for each selected composition has been prepared separately by the wet ball milling process.
II. The required amount of powder has been measured for each sample. Then the measured powder has been sintered in the SPS machine according to the programmed temperature profile. Each sintered sample has a dimension of 10mm diameter and 4mm thickness.
III. The DSC test has been carried out to find the transformation temperature of the prepared powder samples.
IV. The micro hardness of the prepared samples has been measured by Vickers hardness tester.
V. The XRD test of the prepared samples has been carried out.
VI. To evaluate the microstructures and compositions of the phases, SEM-EDS has been performed on samples.
VII. Corrosion behavior of the samples in the human body fluid condition has been studied from the corrosion test.

4.1 Ball milling for producing the powders:

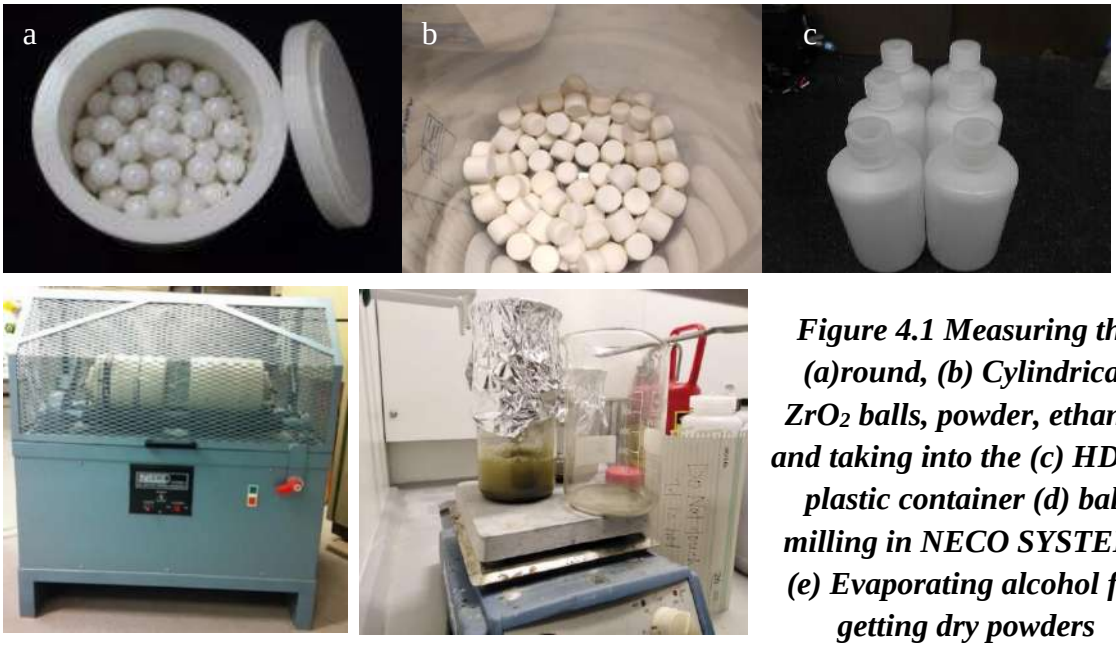

Figure 4.1 Measuring the (a)round, (b) Cylindrical ZrO_2 balls, powder, ethanol and taking into the (c) HDPE plastic container (d) ball milling in NECO SYSTEM, (e) Evaporating alcohol for getting dry powders

The powders of CuAlNi and NiTiCu have been homogenized and mixed by wet ball milling technique. 25 gm of CuAlNi powder and 20gm of NiTiCu powder have been produced for each composition of SMAs. For preparing CuAlNi powder of each composition, the Milling media: powder ratio is 5:1 (125gm: 25gm). Again, for NiTiCu powder of each composition the Milling media: powder= 5:1 (100gm: 20gm). As milling media, cylindrical, spherical (3mm and 6mm diameter) ZrO_2 balls have been taken. The ratio is Cylindrical: 6 mm diameter ball: 3mm diameter ball (according to weight) = 1:1.6:9. The pure element powder weight for preparing the alloy powder is given in Table 4.1 and Table 4.2.

(a) CuAlNi:

Milling media: powder= 5:1 (125gm: 25gm)
Cylindrical: 6 mm diameter ball: 3mm diameter ball (according to weight) = 1:1.6:9

Table 4.1: weight of pure elements and prepared CuAlNi alloy powder

Sample No	Cu(gm)	Al(gm)	Ni(gm)	Total powder
1	21.25	2.75	1	25gm
2	21.25	3.25	0.5	

(b) NiTiCu:

Milling media: powder= 5:1 (100gm: 20gm)
Cylindrical:6 mm diameter ball: 3mm diameter ball (according to weight) = 1:1.6:9

Table 4.2: weight of pure elements and prepared NiTiCu alloy powder

Sample No	Cu (gm)	Ni (gm)	Ti (gm)	Total
1	1.7	10.7	7.6	20gm
2	2.4	10.4	7.2	

According to the table, 25 gm of CuAlNi and 20 gm of NiTiCu powder for each composition have been prepared from the 99.99% pure powders of copper, aluminium, nickel, titanium. All the pure elemental powder used for making the SMA powders have the size of 20 µm.

The HDPE container and milling media have been washed properly at first. The required amount of pure element powder and milling media have been measured on a weight scale. Then the measured amounts have been taken into HDPE containers. The ethanol has been added to the containers. Then, the containers have been inserted into the Ball milling machine: NECO SYSTEM 3, DC Motor speed control after making those airtight using paratapes. Maintaining a rotation speed of 80-85 RPM, the containers have been continuously rotated in one direction for 4 hours and then rotated to the reverse direction for another 4 hours. After a total of 8 hours of rotation, the containers have been brought out from the machine. From the HDPE container, the powder and ethanol mixtures have been transferred to a glass beaker covered with aluminum foil paper. The glass beakers then have been placed on a hot plate inside a fume hood chamber to get the dry powder. After drying, the powder weight is measured again.

4.2 DSC:

The transformation temperatures of the prepared powdered sample have been measured using NETZSCH STA 449 F3 STA449F3A-1580-M. The heating rate is 10^0C/min. Nitrogen gas has been purged to create a vacuum atmosphere. Al_2O_3 crucibles have been used as DSC pans. Both the CuAlNi and NiTiCu powdered samples for the DSC test weighed below 0.1gm.

4.3 Spark Plasma Sintering and characterizations:

4.3.1 Die preparation:

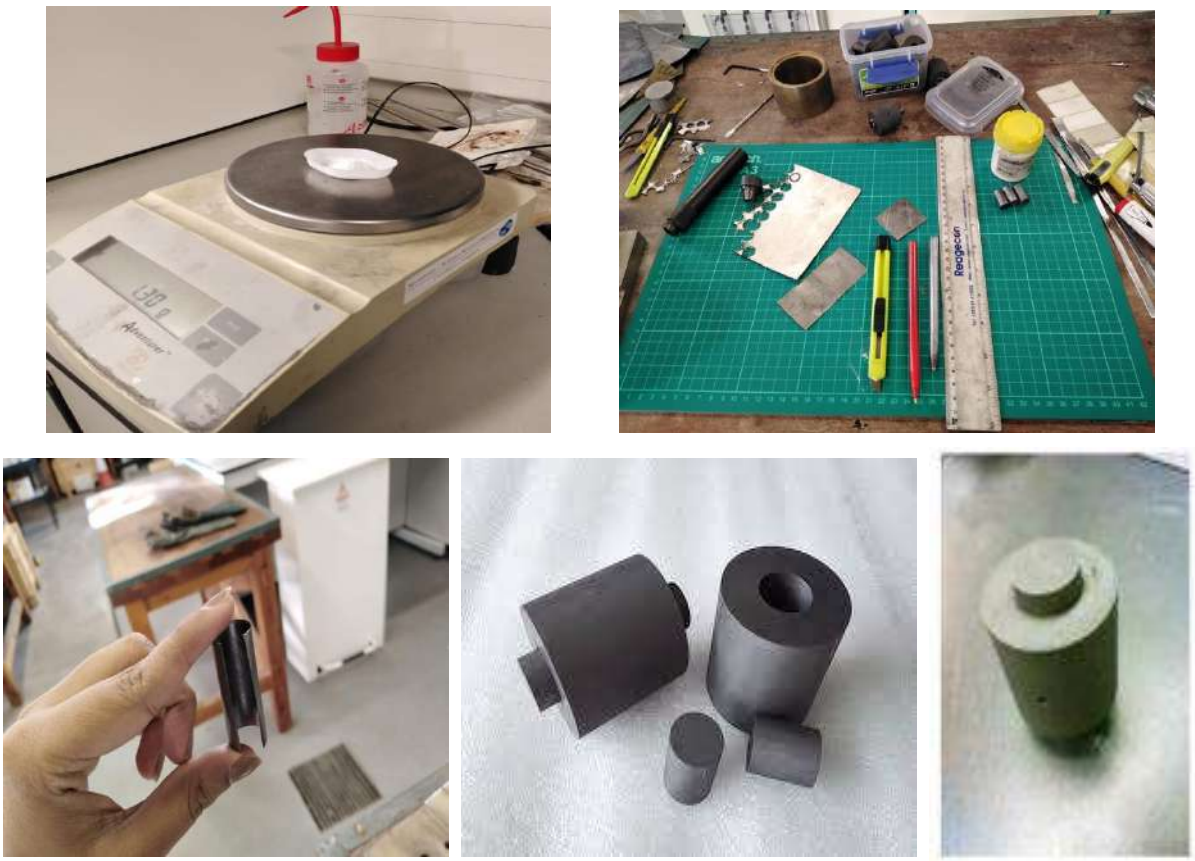

Figure 4.2: Die preparation before Sintering

One of the important steps in the SPS method is die preparation. If the die is not properly prepared, then there are chances of leaking. The measured amount of powder is poured into a graphite mold and then the mold is placed into the SPS machine for sintering. Before pouring the measured amount of powder, the mold needs to be prepared.

For each 10mm diameter punch, 0.2mm thick graphite paper has been cut into 40mm length and 38mm width. The electrical conductivity nature of carbon paper is helpful to transmit electric current uniformly throughout the powder taken inside the mold for sintering. After cutting the 40mm×38mm graphite paper, the paper is curved into a hollow cylindrical shape and is placed into the die. This paper works as a liner for the die's inner diameter (ID) to protect

the die and the sample from the deterioration during the sintering process. The same graphite paper has been used to make disks. These discs are used as spacers between the powder and both punch faces. Because of that, the die can be fully fitted without any porosity. One punch is inserted into the die cavity from the bottom side and the powder is carefully transferred to the die cavity. The die sides have been gently tapped to allow powder to settle. The remaining punch has been inserted into the die. Then it has been pressed with hand to pre-compact the powder in the die. The powder column has been kept as close as possible to the center of the die cavity.

Table 4.3 and Table 4.4 list the weights of the powders according to their composition.

CuAlNi:

Table 4.3: Theoretical density wise weight of each CuAlNi sample's powder before sintering

Sample No	Composition (wt%)	Density of the mixed powder (gm/cc)	Weight of the powder (gm)
Sample 1	Cu-85%, Al- 11%, Ni-4%	8.27	2.59
Sample 2	Cu-84%, Al- 12%, Ni-4%	8.21	2.58

NiTiCu

Table 4.4: Theoretical density wise weight of each NiTiCu sample's powder before sintering

Sample No	Composition (wt%)	Density of the mixed powder (gm/cc)	Weight of the powder (gm)
Sample 1	Ni-50%, Ti-43%, Cu-7%	7.23	2.27
Sample 2	Ni-49%, Ti-41%, Cu-10%	7.32	2.3

4.3.2 Sintering of the samples in the SPS machine:

After preparing the die, the SMA powders have been sintered into pallets in the spark plasma sintering furnace. After turning on the chiller of the SPS machine the prepared die have been set inside the vacuum chamber. For setting up the die with sample powder, the lower ram has been pulled down. The prepared die has been mounted on top of the lower ram with a graphite spacer. Then another graphite spacer has been put on top of the upper punch to make it symmetrical.

Figure 4.3: Dr. Sinter, SPS-515S, SPS Syntax Inc., Kawasaki, Japan Model SPS-511 with optional High Vacuum System and no Analysis Unit

After placing the die properly in between the lower and upper ram, a thermocouple is inserted into the graphite die to regulate the temperature. Any deflection from the programmed temperature indicates leaking or any other unwanted circumstances. The whole chamber is closed, and a vacuum environment is created by the Pirani vacuum gauge. Vacuum pump-1 is set as on, and vacuum pump-2 is set as open. The lower chamber is pushed tightly for two seconds after the vacuum. The valve is opened. Previously determined patterns have been set in the PID controller. From the initial displacement, the Z-axis displacement is converted to zero. The sintering temperature and pressure is applied to the sample once the machine is commanded to run. The whole operation is monitored on a computer screen and PID controller. Then, the thermal controller is reset, and the P set value is made zero before opening the chamber. SPS pressure is lowered by stop buttons. When the chamber returns to the atmospheric pressure, the sintering chamber is opened, and the thermocouple is removed carefully. Then the lower ram is put down to remove the die from the chamber by a tong. After removing the sample, the chamber is closed again, the power of the machine is turned off, and the water-cooling valve is closed before further SPS operation.

4.3.3 XRD:

To identify the phases in the prepared alloys and to investigate the presence of desired phases for shape memory property, XRD has been carried out on the prepared alloys. The phase identification of the samples was conducted at the XRD machine model: Empyrean, PANalytical-Netherlands. For doing the test, 2mm sample thickness has been maintained. The Bragg's angle has been regulated within 0 to 70 degrees. For NiTiCu samples, the count time was double that of the CuAlNi samples.

4.3.4 SEM:

A field emission scanning electron microscope (JEOL JSM-7600F) has been used to scan and reveal different phases. Microstructures have been observed both in secondary mode and backscattering mode. This test has been carried out for both CuAlNi and NiTiCu samples. Along with the SEM, the system enables obtaining chemical information from a specimen by using an X-ray energy-dispersive spectrometer (EDS). The EDS micro-analyzer in an SEM uses a primary electron beam to excite the emission of characteristic X-rays from the sample atoms. Since the electron beam can be readily focused on a microscopic area on a sample, the EDS micro-analyzer can examine chemical compositions in a tiny space.

4.3.5 Hardness Test:

The Vickers hardness tester has measured the microhardness of the samples. The primary load of 2kg was applied for 10 seconds and removed. The resulting Vickers hardness numbers are inversely related to the additional depth, to which the indenter is forced by the significant load beyond the depth of the zero-load condition. The Vickers hardness results have been seen as a digital output.

4.3.6 Corrosion Test:

The corrosion rate of the prepared SMAs has been measured by the weight loss method. It is a process that involves the placement of the samples in a specific environment, removal of the samples after a designated time interval, cleaning them for net weight, and recording the weight difference in accordance with the time intervals. It is a suitable method for determining corrosion levels in intricate structures. The corrosion of the samples is evident in Figure 4.4 and Figure 4.5.

Before corrosion:

Figure 4.4: CuAlNi and NiTiCu submerged in PBS solution before corrosion

After corrosion:

Figure 4.5: CuAlNi and NiTiCu submerged in PBS solution after corrosion

The simple immersion technique has been carried out to determine the corrosion rate. According to the immersion technique, the corrosion rate can be measured by the following formula-

$$\text{MDD}= \frac{\Delta\text{wt.(mg)}}{(\Delta Area(\text{dm2})* \text{Time(day)})}$$

As the samples are in pelleted form, the total surface area of the samples is measured by-

$$\text{Area}= 2\pi r\text{^}2 + 2\pi rh$$

At first two CuAlNi and two NiTiCu samples have been weighed. The measured initial weights and dimensions of CuAlNi and NiTiCu are listed respectively in Table 4.5 and Table 4.7. The

dimensions of the sample before corrosion have also been measured. Then the samples are kept inside the PBS solution for 20 days. The area and the weight of the samples have been measured again after the 20th day of corrosion test. Table 4.6 and 4.8 lists out the weights and dimensions of the samples after 20 days of corrosion test. The corrosion rate in milli inch per year (MPY) has been calculated from these data.

Table 4.5: Initial specifications of the CuAlNi samples

Sample No	Diameter (dm)	Radius (dm)	Height (dm)	Area (dm^2)	Average Area (dm^2)	Initial weight (mg)
1	0.103	0.0513	0.065	0.03742	0.04606	1560
	0.135	0.0675	0.063	0.05511		
	0.118	0.0588	0.065	0.04566		
2	0.105	0.0525	0.060	0.03710	0.03756	2090
	0.110	0.0550	0.063	0.04060		
	0.103	0.0513	0.058	0.03500		

Table 4.6: Specifications of CuAlNi Samples after 20 days of Corrosion

Sample No	Diameter (dm)	Radius (dm)	Height (dm)	Area (dm^2)	Average Area (dm^2)	Final weight (mg)
1	0.102	0.0508	0.063	0.03614	0.03830	1553
	0.115	0.0575	0.063	0.04333		
	0.103	0.0510	0.060	0.03555		
2	0.093	0.0464	0.060	0.03096	0.03280	2077
	0.110	0.0498	0.063	0.03507		
	0.110	0.0500	0.053	0.03230		

Table 4.7: Initial specifications of NiTiCu samples

Sample No	Diameter (dm)	Radius (dm)	Height (dm)	Area (dm^2)	Average Area (dm^2)	Initial weight (mg)
1	0.108	0.0538	0.040	0.0316	0.0339	2080
	0.113	0.0563	0.048	0.0366		
	0.110	0.0550	0.042	0.0333		
2	0.100	0.0500	0.048	0.0306	0.0314	1670
	0.105	0.0525	0.045	0.0321		
	0.105	0.0525	0.043	0.0313		

Table 4.8: Specifications of NiTiCu Samples after 20 days of Corrosion

Sample No	Diameter (dm)	Radius (dm)	Height (dm)	Area (dm^2)	Average Area (dm^2)	Final weight (mg)
1	0.103	0.0513	0.040	0.0294	0.0329	2073
	0.112	0.0562	0.047	0.0363		
	0.110	0.0547	0.042	0.0330		
2	0.110	0.0498	0.048	0.0304	0.0285	1655
	0.098	0.0492	0.039	0.0272		
	0.098	0.0488	0.042	0.0278		

Chapter 5 : Results and Discussions:

5.1 DSC of ball milled powder:

To clearly understand the effect of sintering temperature on the formed phases in the SMAs the DSC tests have been carried out on the powder samples prepared by wet ball milling. The results are as follows-

5.1.1 CuAlNi powder:

The heating cycle curves shown in Figure 5.1 for both Sample-1 and Sample-2 powder are similar.

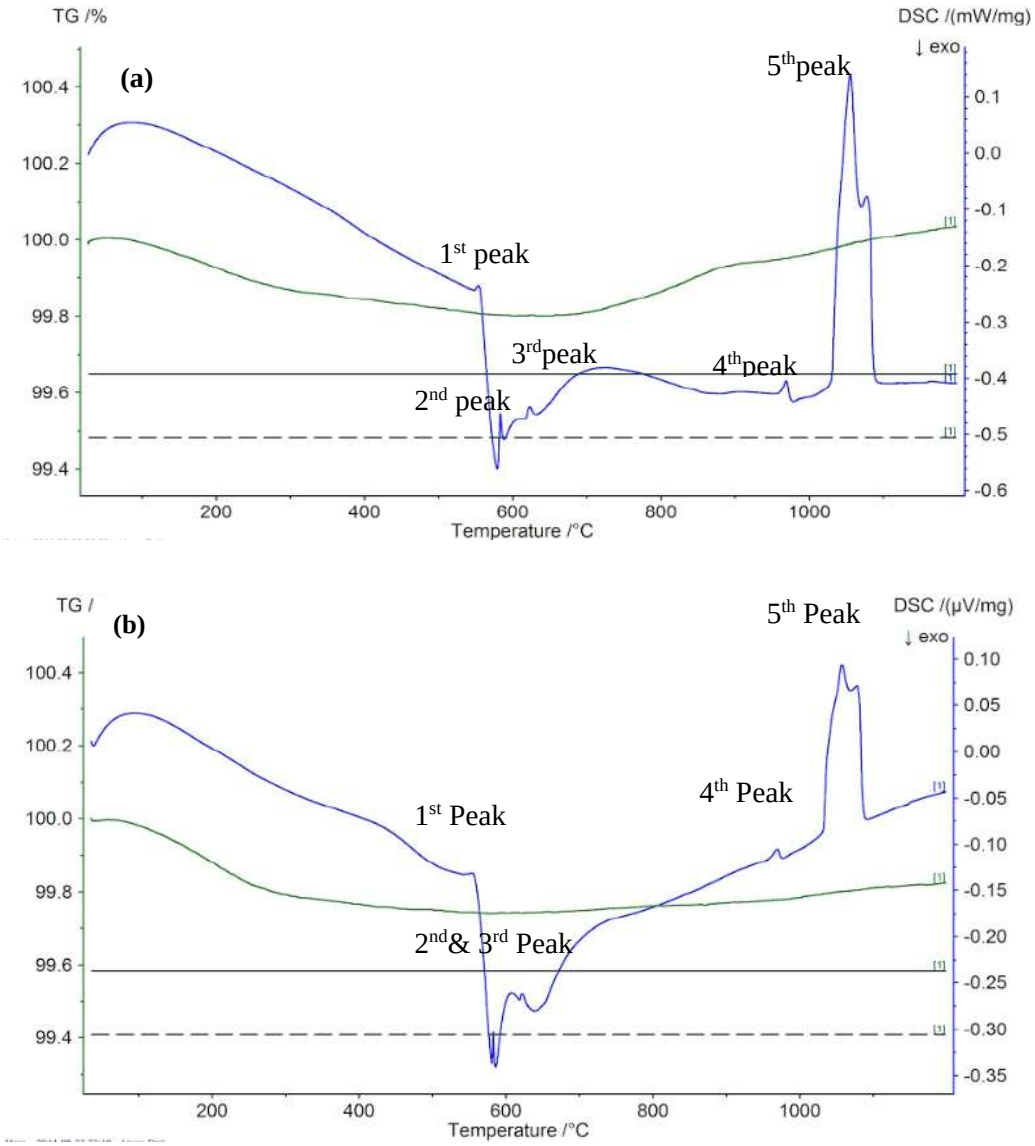

Figure 5.1: DSC Curve (Heating cycle) of ball milled CuAlNi (a) sample-1 (b) sample-2 powders ball milled for 8hrs

For both samples, the first exothermic peak is at around 550^0C, which corresponds to the eutectoid reaction $\beta = \alpha + \gamma_2$. The 2nd and 3rd peak denotes the formation of NiAl intermetallic compound [60, 61, 62, 63, 64]. The 4th peak is for the change of the crystal orientation of the phases [65, 61, 66]. The endothermic peaks are due to the transformation of the martensitic phases to β phases [66]. The melting peak is at approximately 1100^0C. Based on the temperature range of the melting peak, the selected sintering temperatures should be 950^0C and 1060^0C. These temperatures were chosen considering that at 950^0C only solid-state sintering should take place, whereas at 1060^0C the presence of some proportion of liquid would be expected. Liquid phase sintering is a commonly applied sintering aid and is widely used in commercial powder metallurgy products [67]. But in the present study, around one-third of this temperature has been selected as the sintering temperature. The low-temperature sintering was sufficient to produce the phases in the sintered sample.

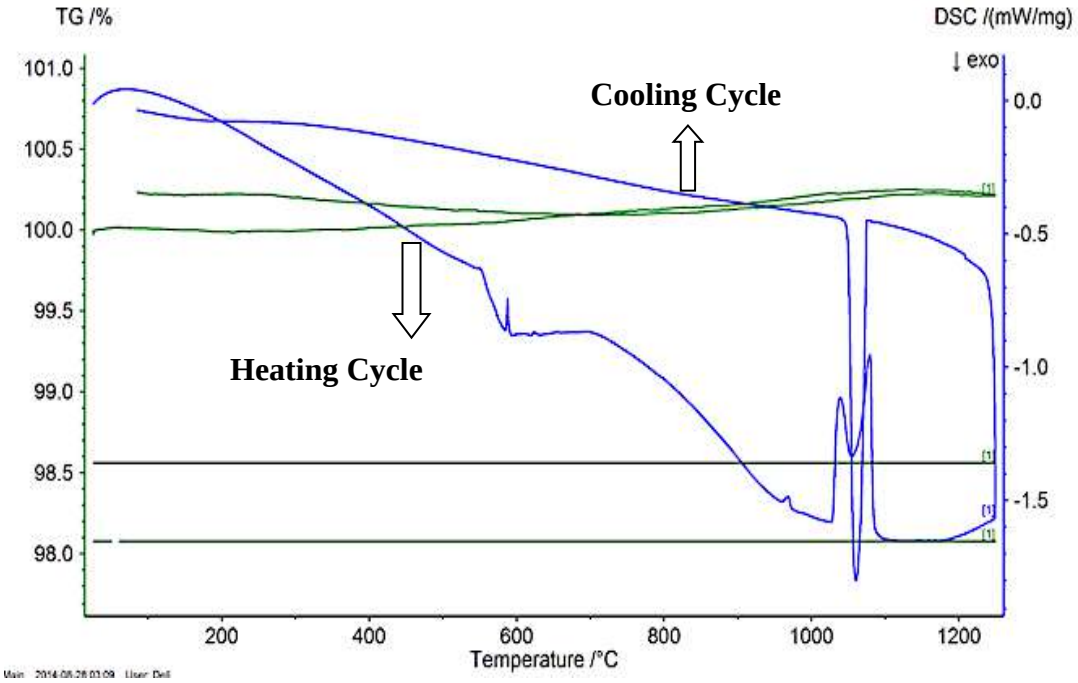

Figure 5.2: DSC curves of heating and cooling cycle of ball milled CuAlNi powder

From Figure 5.2, the transformation temperature for the CuAlNi sample 1 and sample 2 powders are identical. The cooling curve in Figure 5.2 shows the endothermic peak which denotes the dissolution of the formed precipitations and the formation of the disordered β phase. From this DSC curve, the transformation temperature for the prepared CuAlNi powders is in between 550 to 1100℃.

5.1.2 NiTiCu powder:

Like the CuAlNi samples, the heating cycle curves for both Sample-1 and Sample-2 are similar which is evident in Figure 5.3.

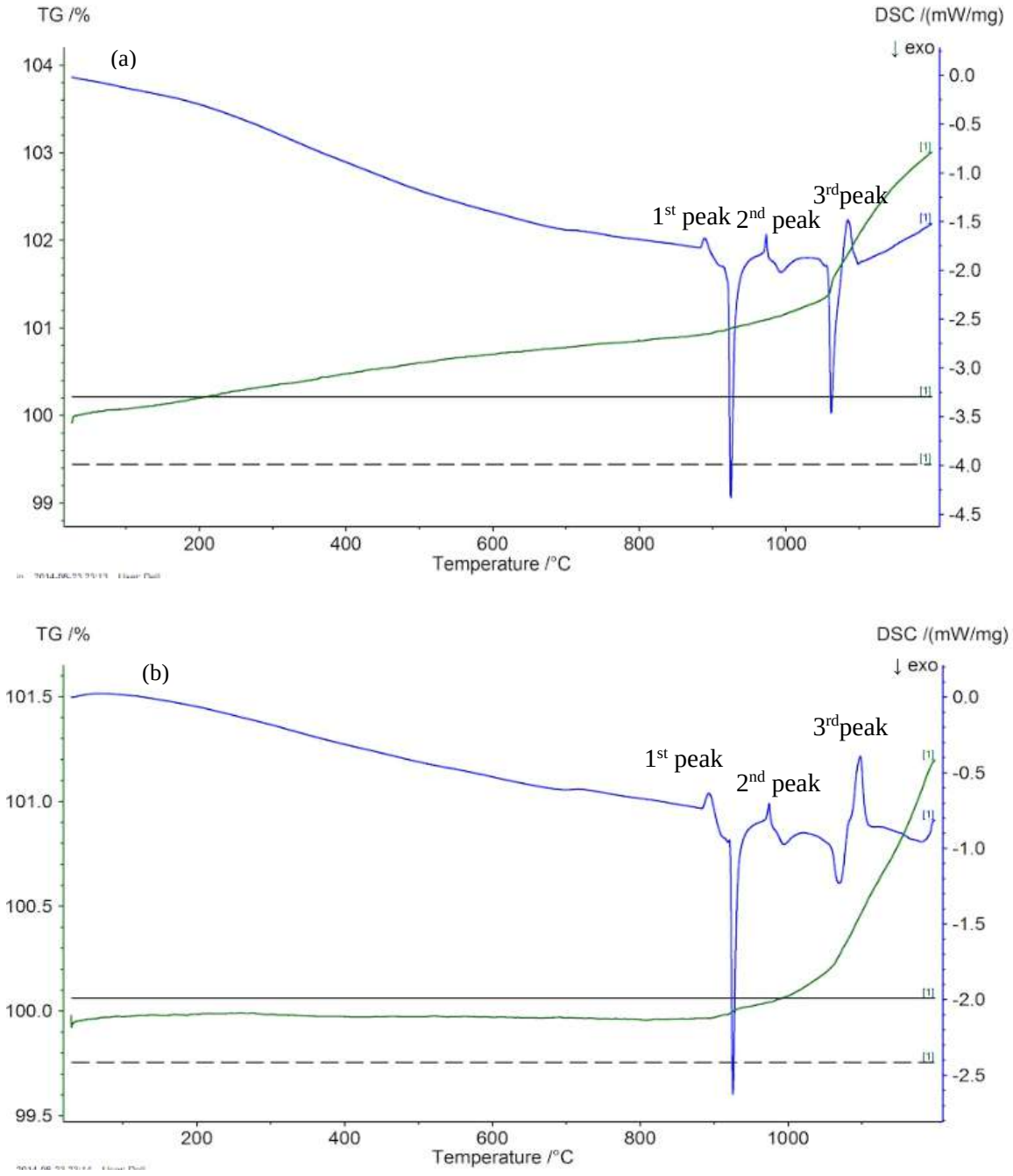

Figure 5.3: DSC Curve (heating cycle) of ball milled NiTiCu (a) Sample-1 (b) Sample-2 powders ball milled for 8hrs

From the heating curve of the powdered samples (Figure 5.3), the 1st, 2nd, and 3rd peaks denote respectively Ti_2Ni, Ti_2Cu, and Ni_4Ti_3 precipitation formation [68, 69, 70, 71]. The endothermic peak denotes the allotropic transformation of Titanium at around 880^0C [72]. The melting temperature of the sample is higher than 1200^0C. The precipitation has started at 850^0C. The sintering temperature has been chosen as around two third of 1200^0C. This solid-state sintering has enabled the desired phase formation in the NiTiCu SMAs at this lower sintering temperature.

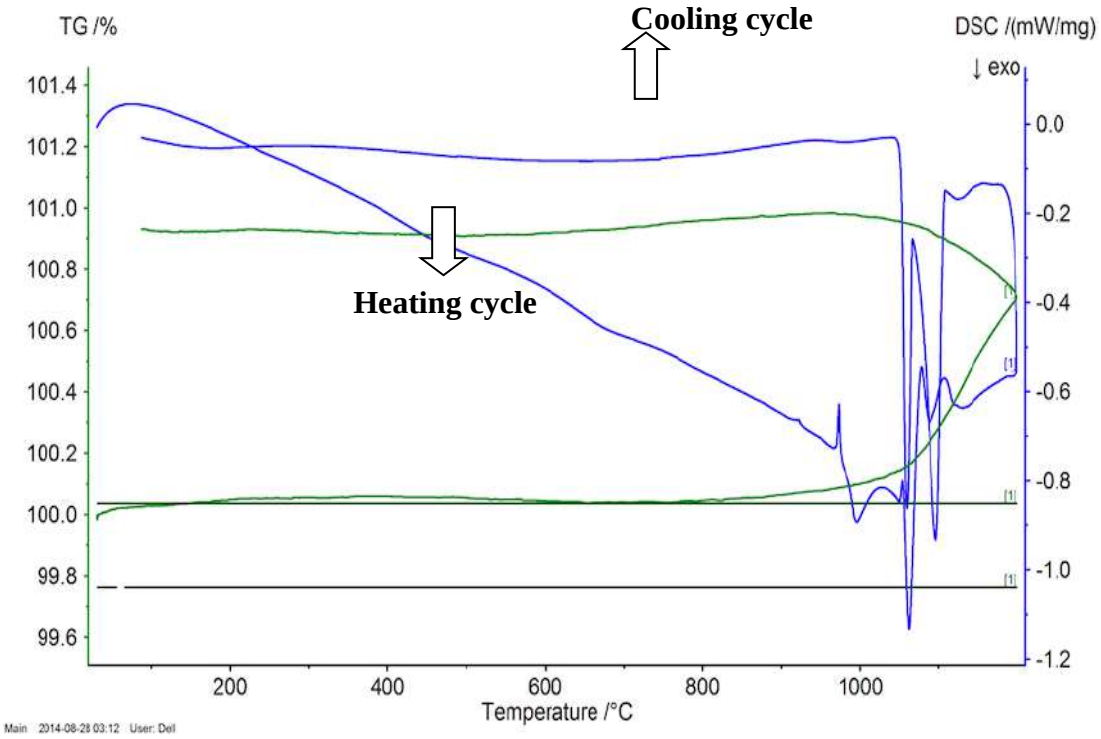

Figure 5.4: DSC Curve (heating and cooling cycle) of ball milled NiTiCu powder

From the DSC curve in Figure 5.4, the transformation temperature for the NiTiCu ranges from 880^0C to 1200^0C.

5.2 Hardness:

The Vickers hardness values of the CuAlNi and NiTiCu SMAs listed in Table 5.1 are the average values of three different hardness points.

Table 5.1: Hardness data of CuAlNi and NiTiCu Samples

Hardness of CuAlNi samples sintered at 475^0C	
Sample No	**Hardness (HV)**
Sample 1	60.5
Sample 2	114.6
Hardness of NiTiCu samples sintered at 730^0C	
Sample No	**Hardness (HV)**
Sample 1	476.4
Sample 2	484.7

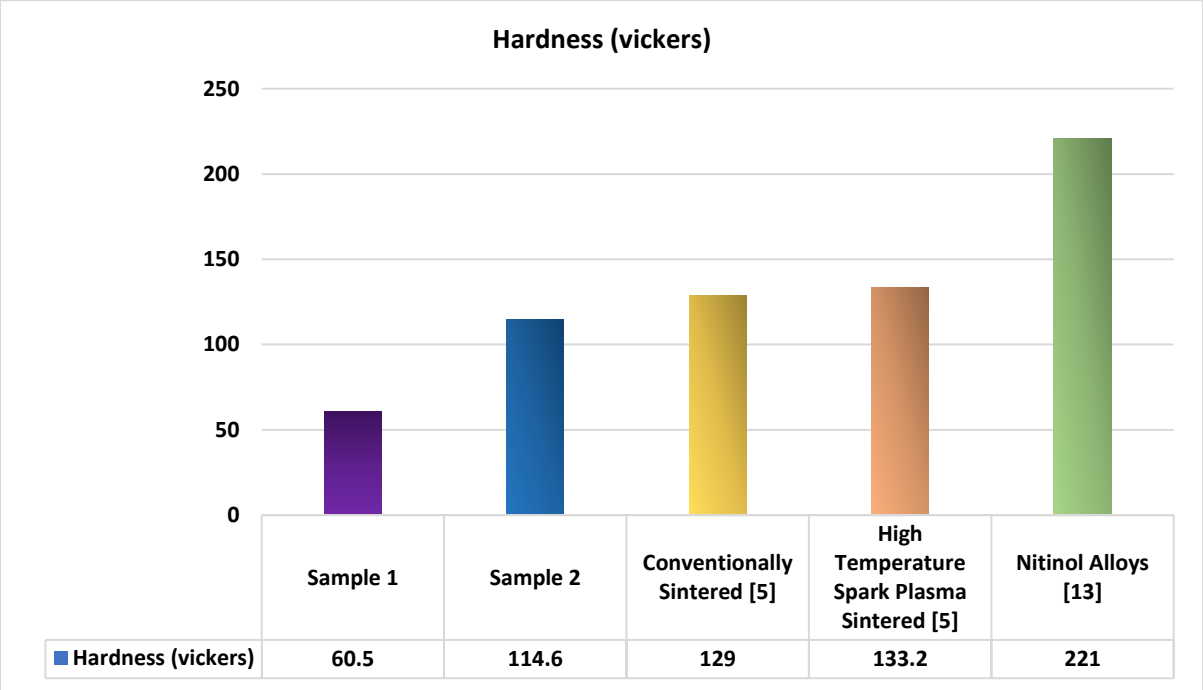

Figure 5.5: Comparison of the hardness of CuAlNi SMAs with the existing biomaterials

From Table 5.1 and Figure 5.5 for CuAlNi, sample 1 has comparatively less hardness than sample 2. Previous studies on CuAlNi, prepared by conventional sintering method and high temperature spark plasma sintering method denote that the hardness values of those samples are higher than sample 1. But the hardness value of sample 2 is close to the hardness of the samples studied in the past. Thiruppathi et. al. [11] have studied the spark plasma sintered Cu-11.85%Al-Ni at 700^0C, which is higher than the present study. So, in addition to the aluminium

content, the sintering temperature has a role in increasing the hardness of the sintered sample. If the microhardness values of the samples are compared to the mostly used SMA for biomedical applications, NiTinol, the hardness of Sample-2 is a bit lower. But the referenced NiTi [73] has orthopedic, orthodontic, and cardiovascular applications. For these applications, the hardness of the alloy is improved by coating, heat treatment or by alloying. So, if the presently studied samples are treated with any of these additional methods, then better hardness can be expected.

Taher et. al. [74] have analyzed that when there is an increase in Al and Ni concentration in alloy lead, it will automatically increase the hardness and porosity. But the increase in Al ratio shows more effect than the increase in Ni. When Al>14 wt%, it leads to the production of a single martensitic phase. This type of martensite is brittle and causes a heavy increase in its hardness. The increment causes the alloys to lose its ability to recover its original shape and limits its use in high temperatures applications. In addition, Al is an alpha-phase stabilizer that increases the hardness.

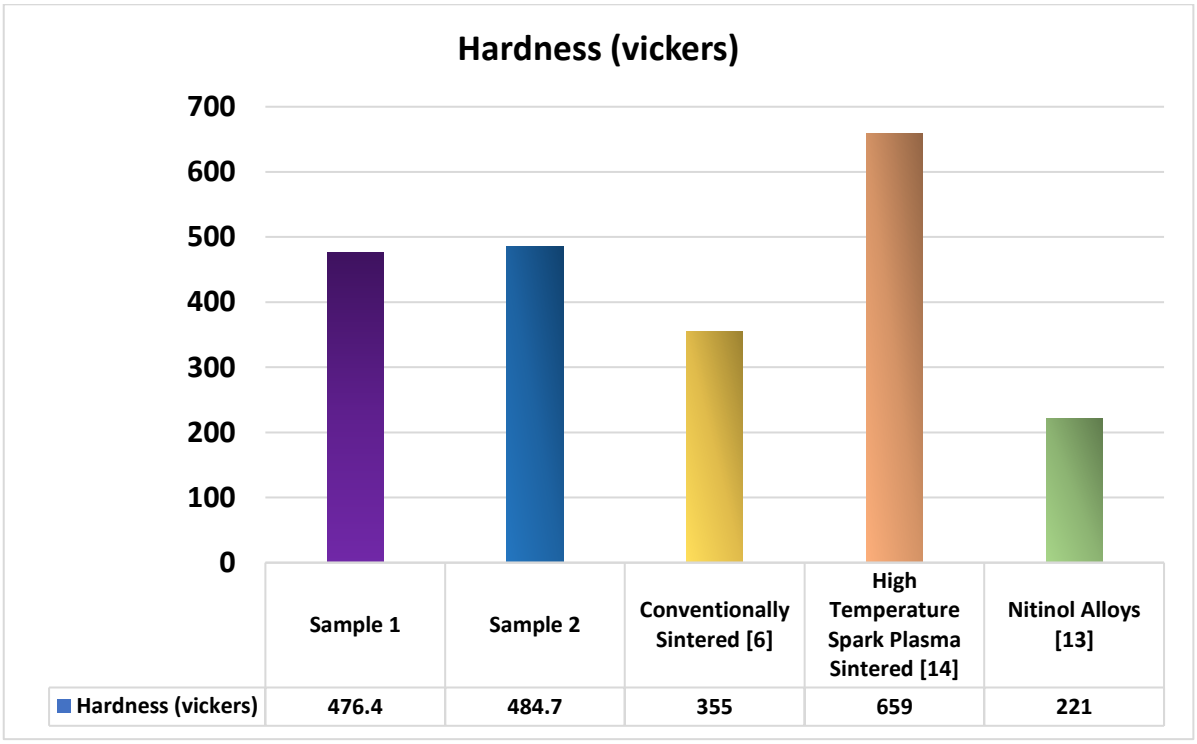

Figure 5.6: Comparison of the hardness of NiTiCu SMAs with the existing biomaterials

SPS made NiTiCu samples in this study, have higher hardness values than the previously studied conventionally sintered [75] and high temperature SPS made CuAlNi [76]. NiTiCu samples have shown a better hardness than NiTi SMA [73]. In the previous studies [77, 78, 79, 80], it has been found that, the addition of copper to the NiTi increases the hardness of the alloy. In this study, the samples of NiTiCu have been prepared from pure element powders and the hardness is better in sample 2 with higher copper content than sample 1. 3 wt% of increment in Cu content in sample 2 than in Sample 1 increases the hardness around 8.3 HV. The NiTiCu samples in the study have a feasible hardness for biomedical applications.

5.3 SEM results of the Samples:

5.3.1 CuAlNi:

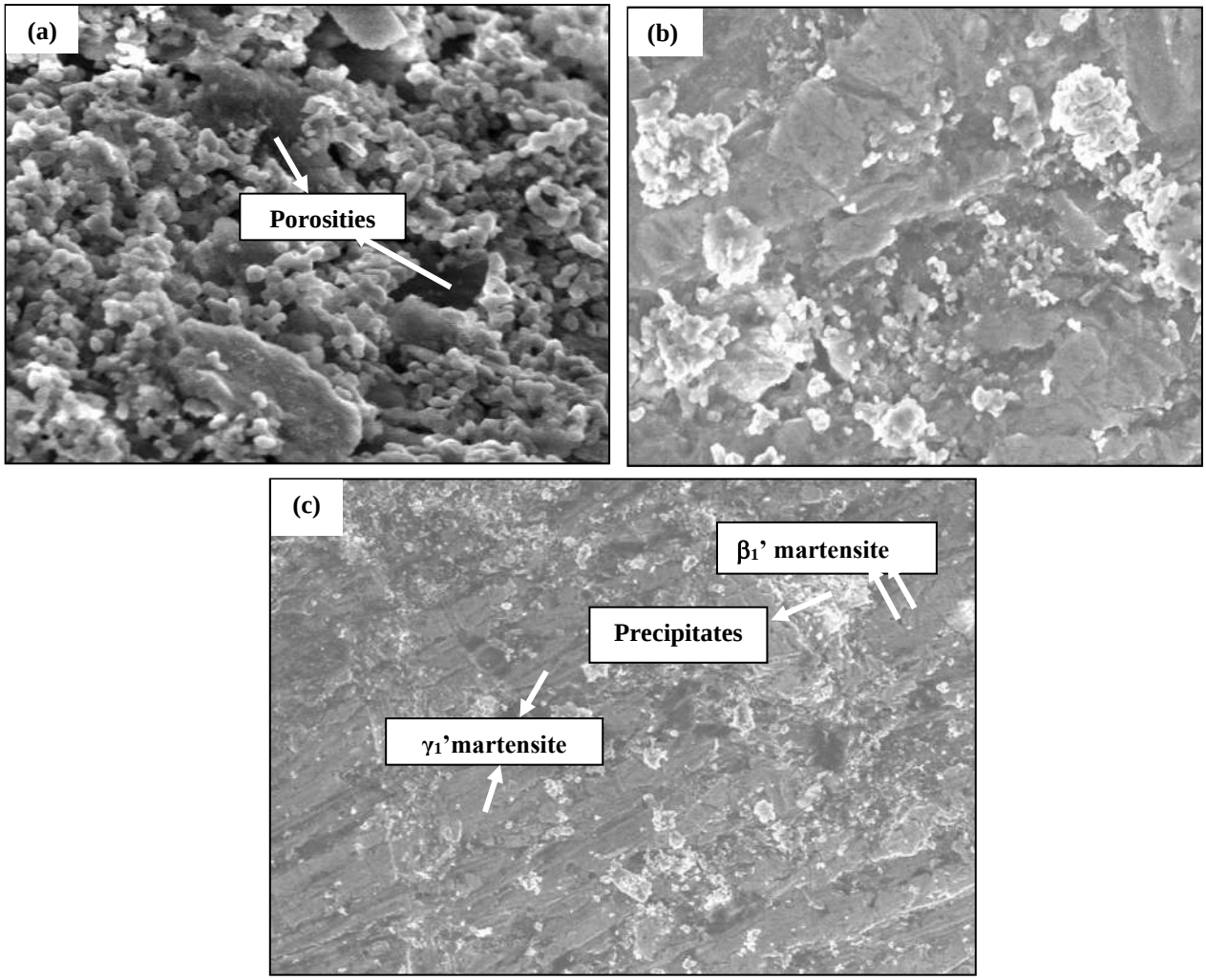

Figure 5.7: SEM micrograph of CuAlNi Sample-1 sintered at 475℃ (a) 10000x (b) 10,000 x (c) 2,000x

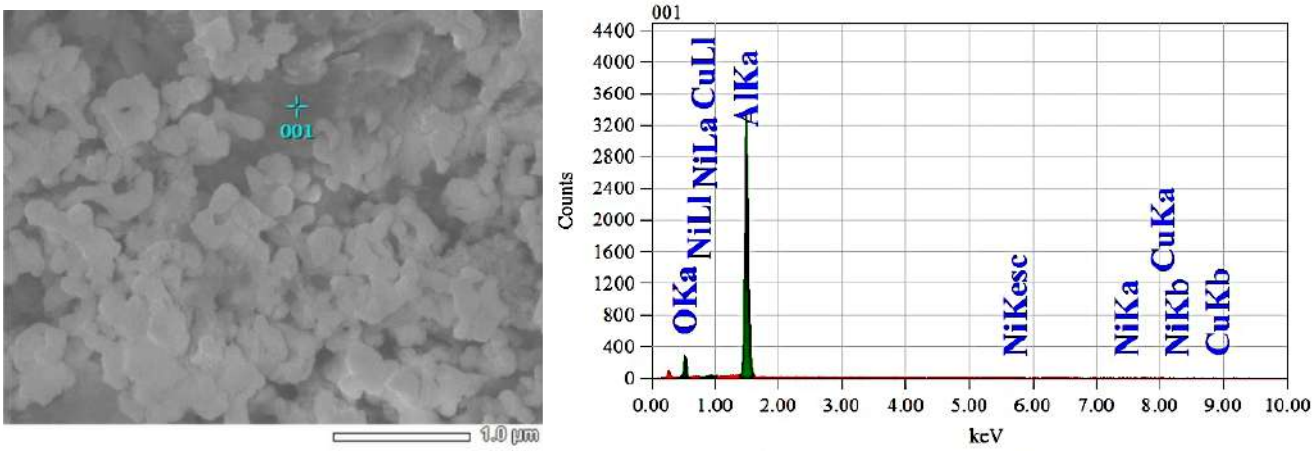

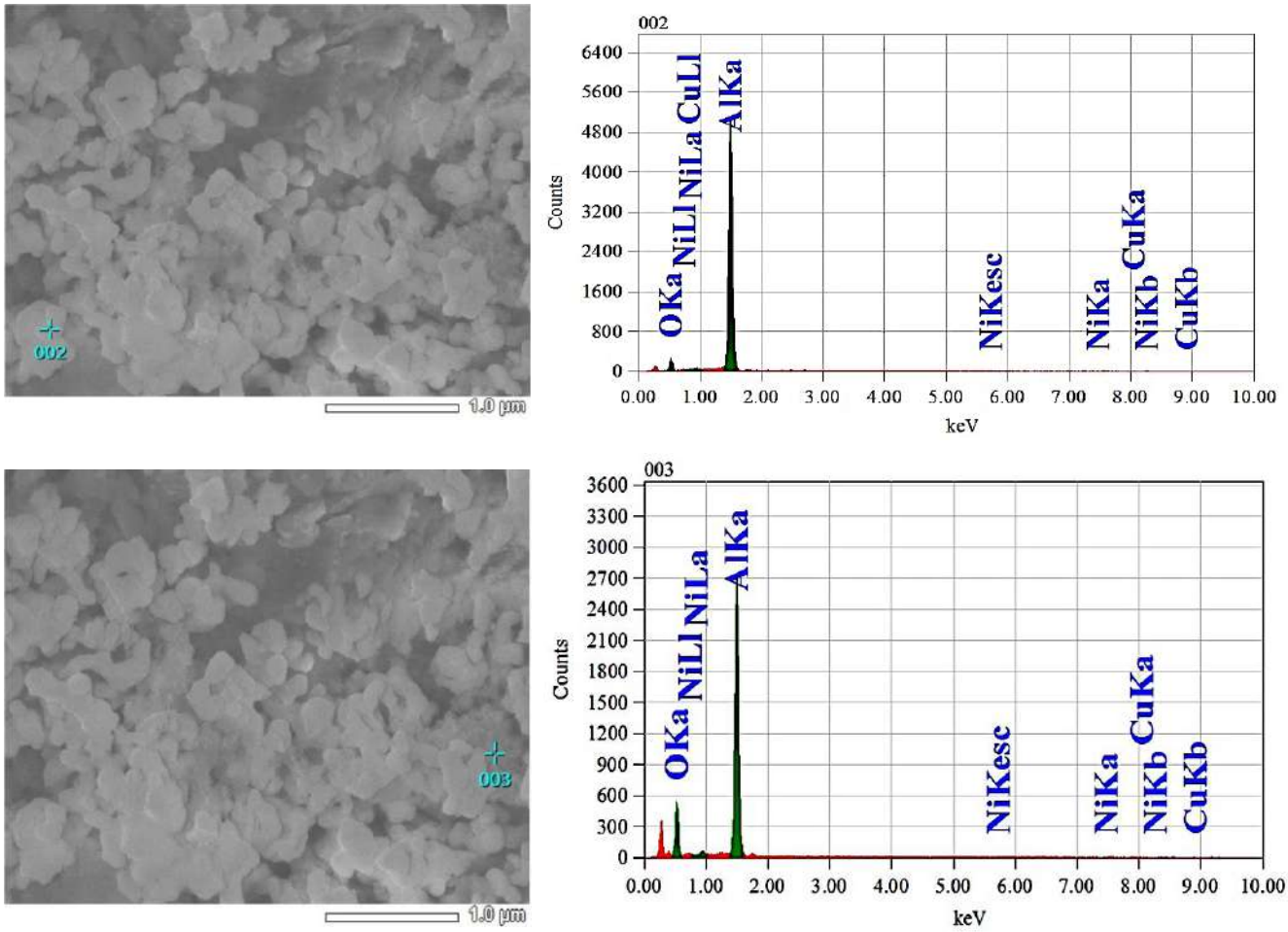

Figure 5.8: EDS of CuAlNi sample 1

Table 5.2: Elemental Composition Analysis of CuAlNi Sample 1 by EDS

Point 1 EDS Result		**Point 2 EDS Result**		**Point 3 EDS Result**	
Element	**Mass%**	**Element**	**Mass%**	**Element**	**Mass%**
O	15.48%	O	10.08%	O	28.41%
Al	83.23%	Al	88.78%	Al	70.53%
Cu	0.72%	Cu	0.60%	Cu	0.21%
Ni	0.57%	Ni	0.54%	Ni	0.85%

From the SEM micrograph of sample 1 (Figure 5.7), it is evident that the dominant phase of the sample is γ_1' martensite. The γ_1'phase form as coarse variants/plate-like phase. From Figure 5.7 (c), between the γ_1'phases the needle-like phase of the β_1' martensite is in a very small amount. The martensite phase's growth has been done in an identical direction. The growth process of the martensite involves the accommodation of the local stress field. Therefore, it requires forming other plate-like groups [81]. The two-type martensite is a unique property of copper rich Cu-Al-Ni SMAs. Copper-based alloys exhibit shape memory within a certain range of composition, which has the disordered bcc structure, called β phase. The phase is stable at

high temperature and goes through two successive ordering transitions during cooling. The transformation happens very rapidly and brings all the metal to the set shape. Usually β' retains for further transformation to γ_1'martensite [79]. As the sample has been cooled slowly inside the SPS machine, the β phase has gone through the eutectoid decomposition. So, sample 1, while being sintered at 475^0C has formed the β phases which after the cooling formed two types of martensite and α and γ_2 precipitates.

In sample-1 Along with the martensite phases, the SEM images indicate the presence of precipitations. The precipitates have irregular shapes and are distributed in between the martensite phases. Saud et al. [19] identified that the precipitation phase is the γ_2 phase. These precipitates tend to isolate the martensite phases lengthways, as shown in Figure 5.7(c). From the EDS data of the sample 1 (Figure 5.8), the finding is that the amount of Al is higher than other elements. The amount of Al is higher in the matrix as well as in the precipitations. Another significant finding is the oxygen content in the precipitate clusters. So, Al_2O_3 is present in sample 1.

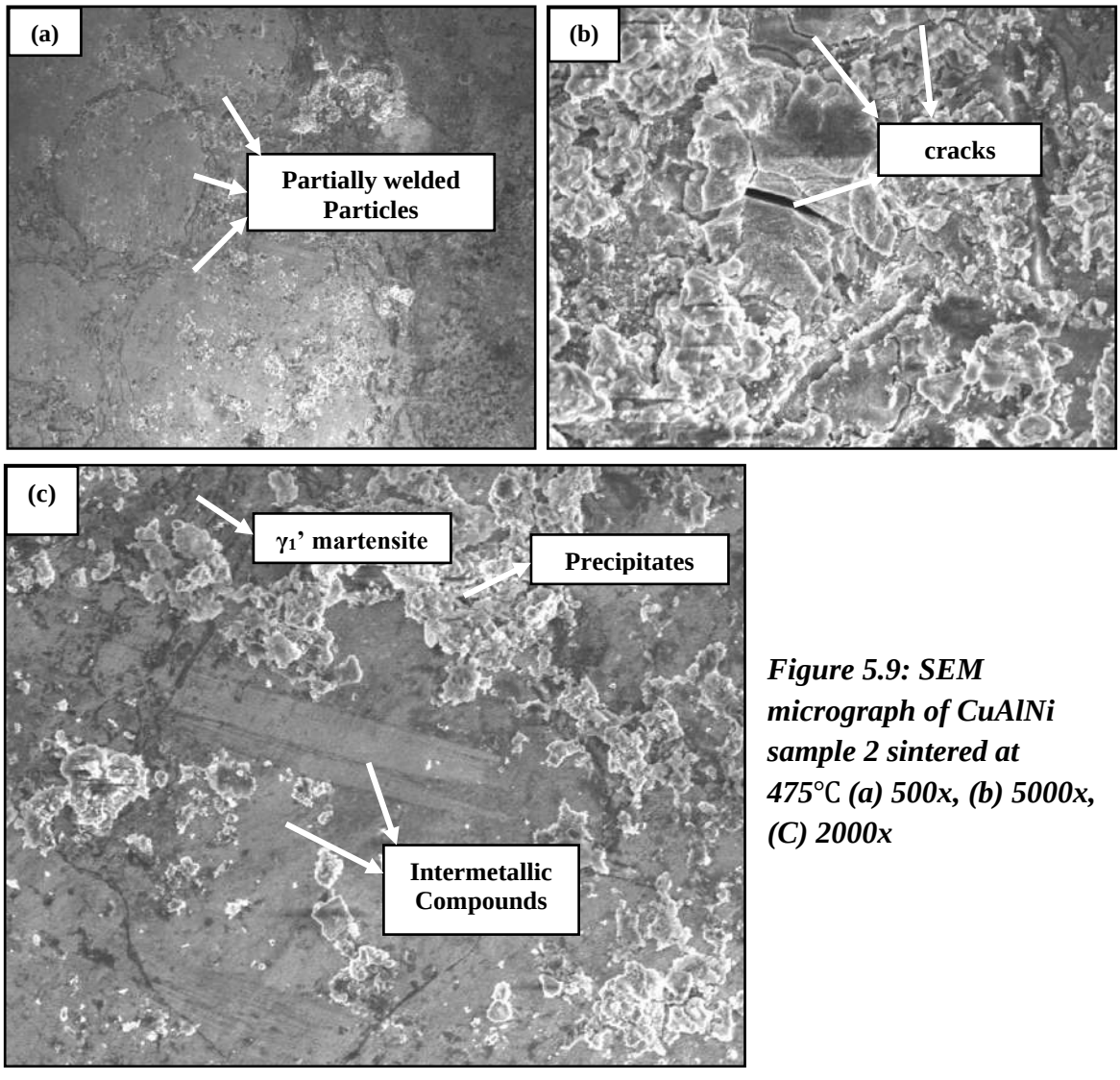

Figure 5.9: SEM micrograph of CuAlNi sample 2 sintered at 475℃ (a) 500x, (b) 5000x, (C) 2000x

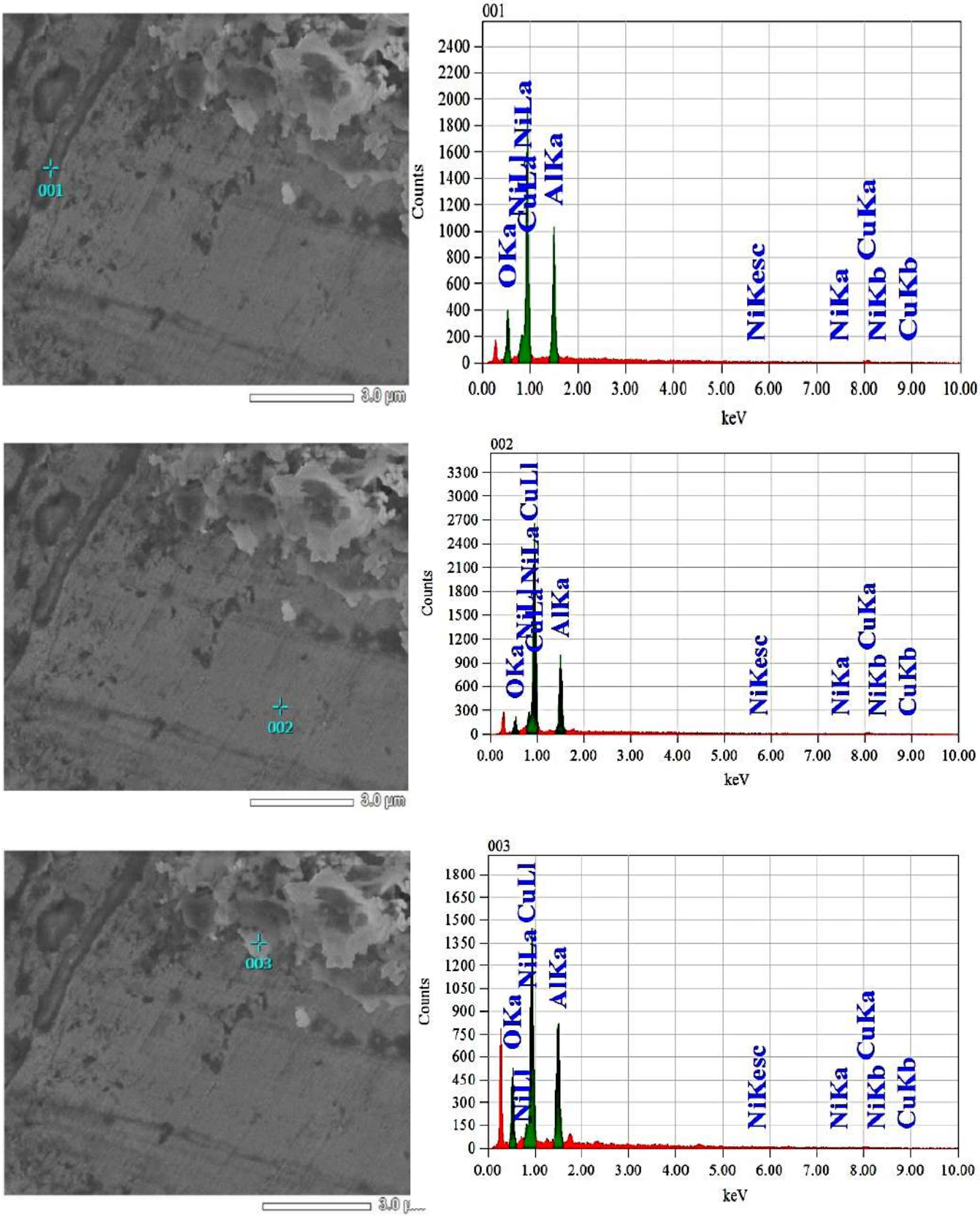

Figure 5.10: EDS of CuAlNi sample 2

Table 5.3: Elemental Composition Analysis of CuAlNi Sample 2 by EDS

Point 1 EDS Result		**Point 2 EDS Result**		**Point 3 EDS Result**	
Element	**Mass%**	**Element**	**Mass%**	**Element**	**Mass%**
O	12.45%	O	4.81%	O	17.95%
Al	24.56%	Al	19.76%	Al	23.16%
Cu	56.63%	Cu	6.82%	Cu	50.40%
Ni	6.35%	Ni	68.61%	Ni	8.49%

From the SEM images of the CuAlNi sample 2 (Figure 5.9), different intermetallic compounds, plate like γ_1' martensite and irregular precipitations have been formed in this sample. Figure 5.9 (a) shows the region where the particles are partially welded. Figure 5.9 (b), (c) represents respectively presence of cracks and different precipitations in the sample. According to Richard et. al. [82], Mirko et. al. [83], and Nawal et. al. [84] studies, the probable phases are the γ_2 phase, CuO, CuNi, NiAl, and Al_2O_3. The EDS result indicates that the amount of copper and oxygen is comparatively higher than in sample 1.

From the EDS data of both samples of CuAlNi, different oxides are present in the samples. The oxygen contamination of the sample may have occurred while drying the powders in an open environment. Redox reactions can take place in Cu-Al-Ni powders as was discussed in [85]. In that case two type of reaction are possible:

- $4CuO + 2Al + \frac{1}{2}O = 2Cu_2O + Al_2O_3$
- $2Al + 6CuO = 3Cu_2O + Al_2O_3$.

Both reactions are highly exothermic resulting in the mixture of oxides binding the micron sized particles. However, this oxide is a dominant phase filling the interspaces between the micron sized particles. Similar (may be more complex) reactions can occur during the sintering mechanism [10].

5.3.2 NiTiCu:

The way of densification of the alloy powders plays an important role that what types of precipitations will be formed in the shape memory alloys. Formed porosities and precipitates have significant effect on the corrosion and shape memory properties of NiTiCu [6,94,98]

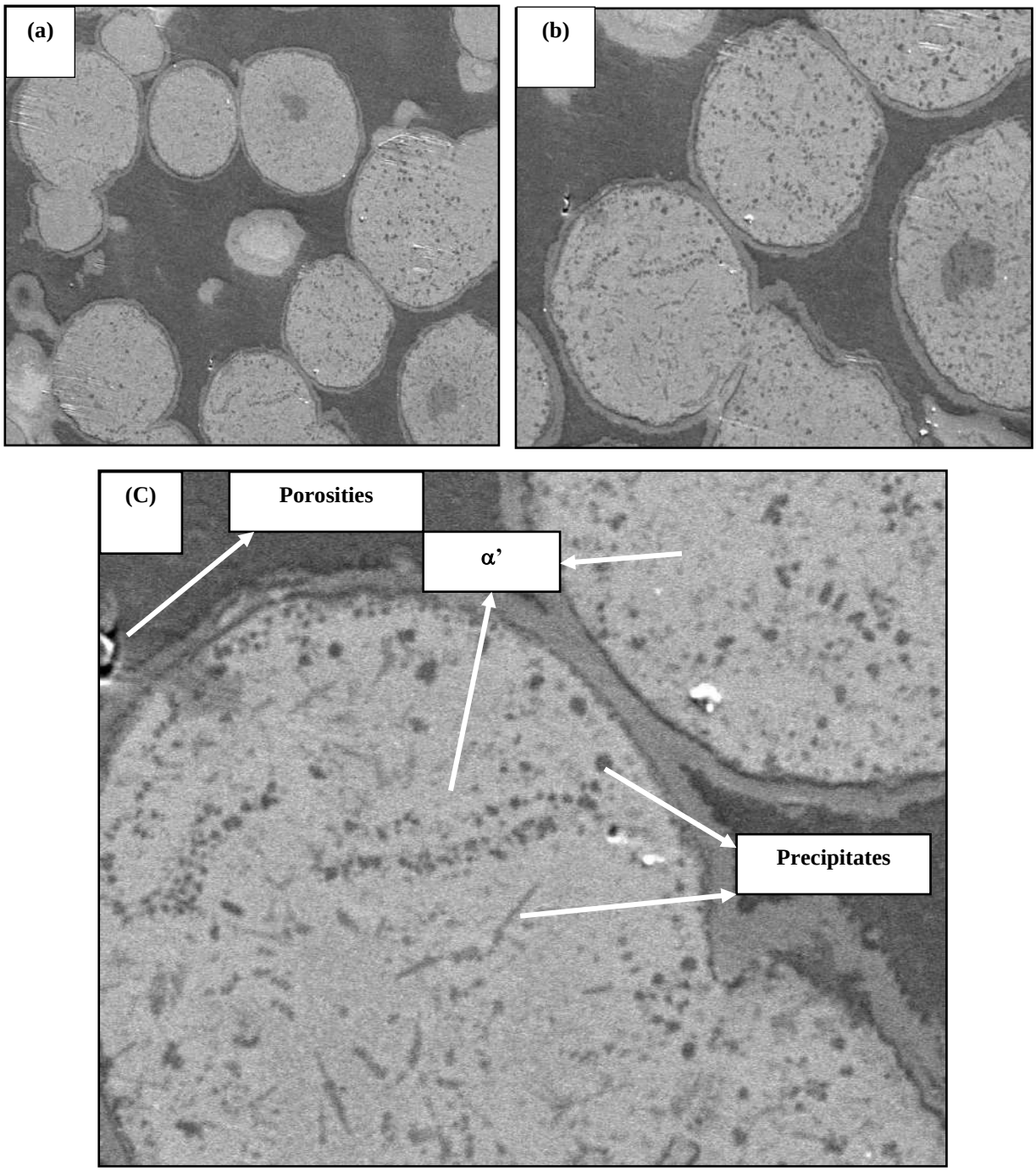

Figure 5.11: SEM image of NiTiCu Sample-1 sintered at 730℃ (a) 300x, (b) 500x, (c) 1000x.

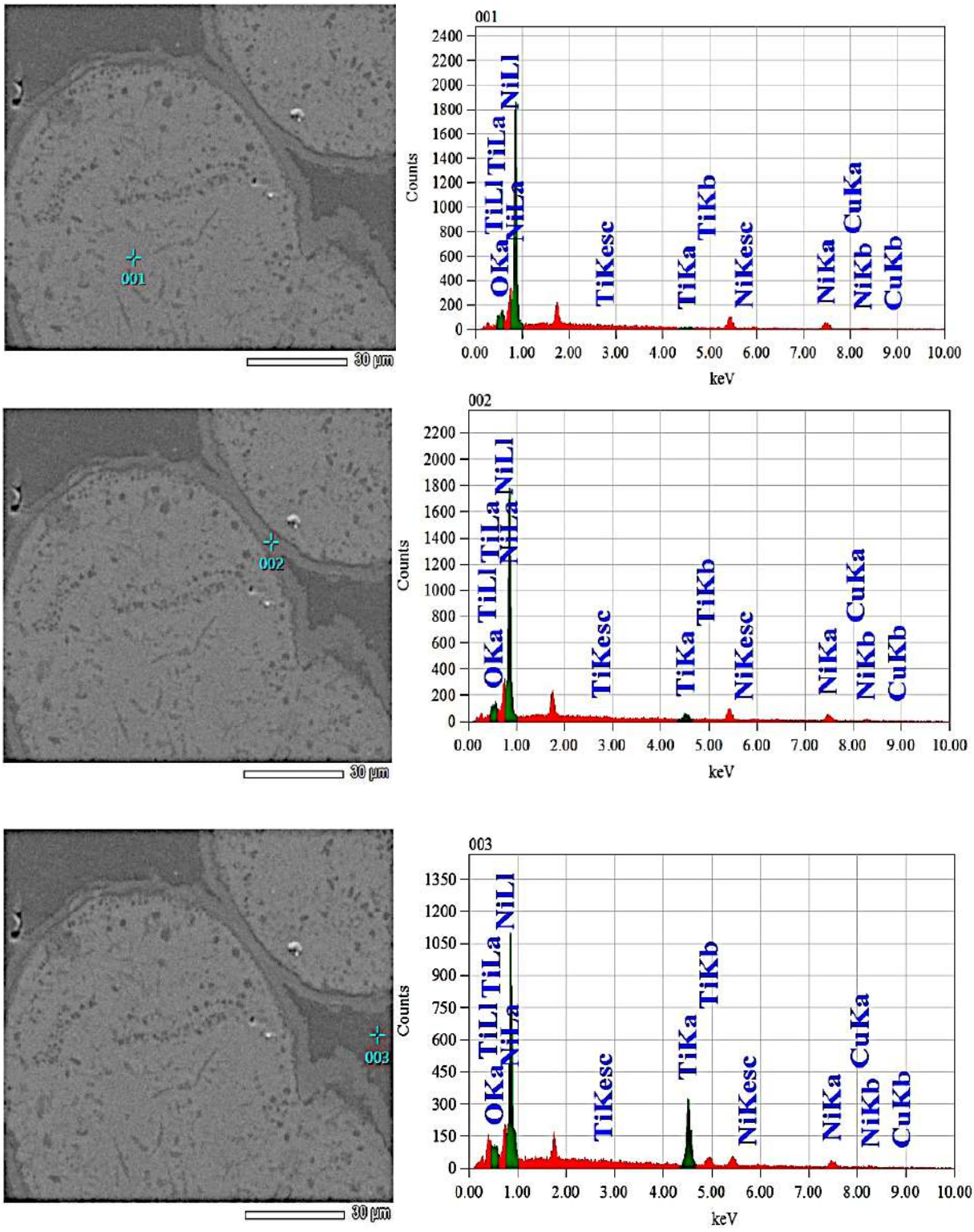

Figure 5.12: EDS result of NiTiCu Sample-1

Table 5.4: Elemental Composition Analysis of NiTiCu Sample 1 by EDS

Point 1 EDS Result		**Point 2 EDS Result**		**Point 3 EDS Result**	
Element	**Mass%**	**Element**	**Mass%**	**Element**	**Mass%**
O	0.00%	O	0.38%	O	0.57%
Ti	0.00%	Ti	5.60%	Ti	31.72%
Ni	100.00%	Ni	94.02%	Ni	64.82%
Cu	0.00%	Cu	0.00%	Cu	2.90%

From Figure 5.11, the particles of the NiTiCu sample 1 have not been fully deformed. Needle-like fine precipitations have been formed. Porosities can also be seen in the SEM images of sample 1. By observing the samples at higher magnification, voids are more prominent with the adjoining particles in sample 1 [24]. From the EDS result of the sample (Figure 5.12), nickel is more dominant than other elements and oxygen is nearly absent in the sample. Analyzing the EDS data, the matrix phase composition is like the Ni_2Ti, and Ni_4Ti_3 phases [73, 86].

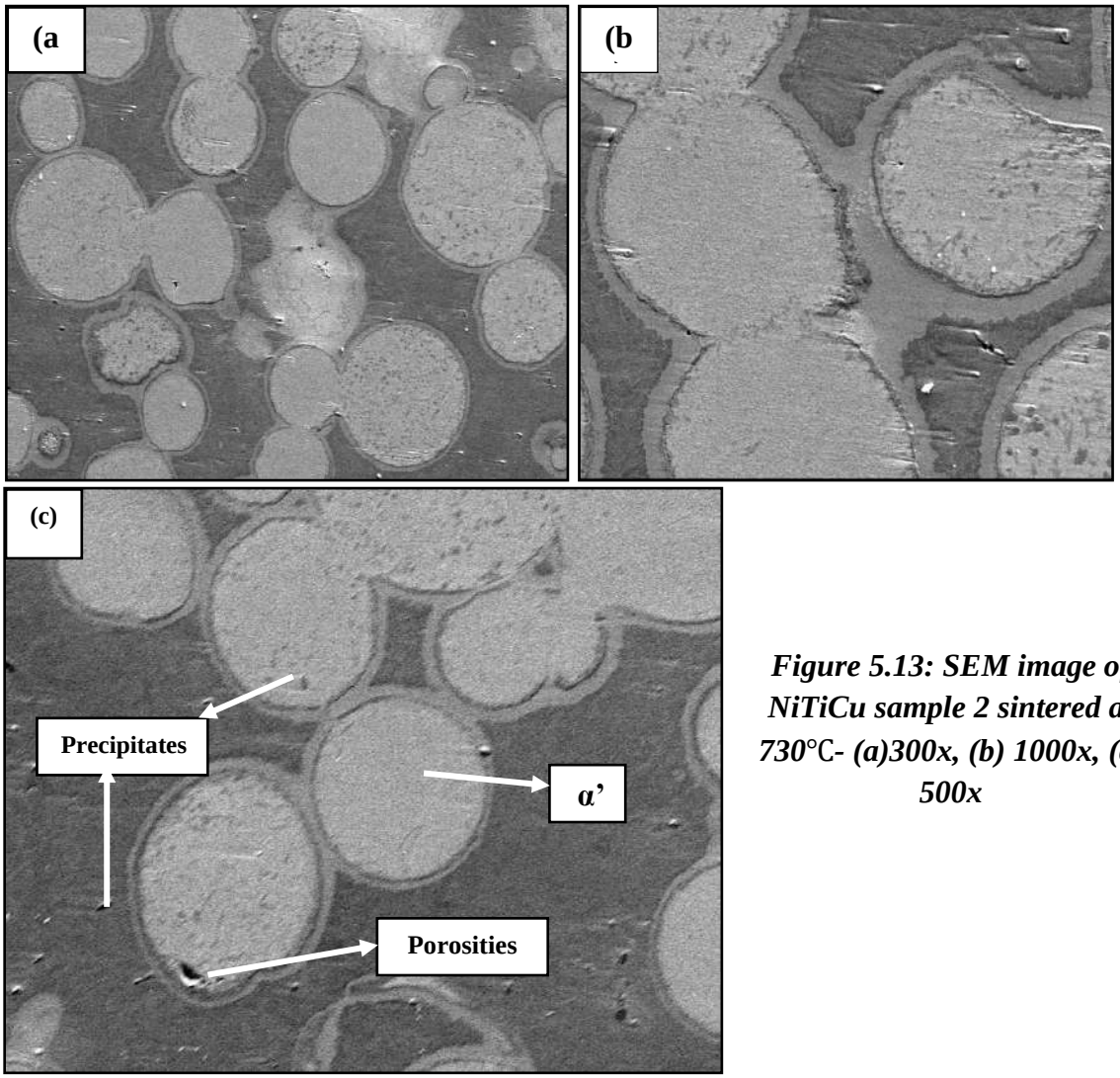

Figure 5.13: SEM image of NiTiCu sample 2 sintered at 730℃- (a)300x, (b) 1000x, (c) 500x

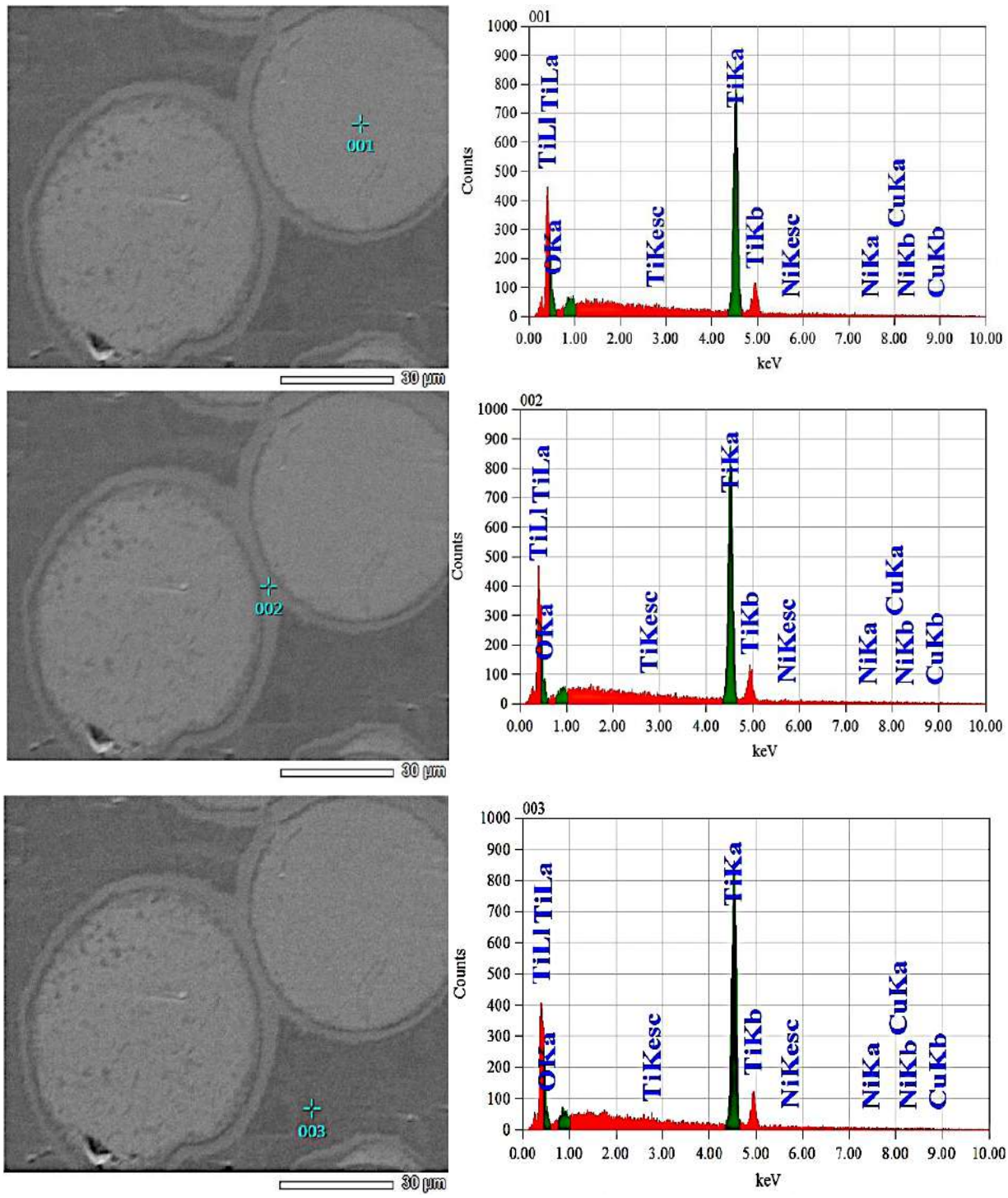

Figure 5.14: EDS result of NiTiCu sample 2

Table 5.5: Elemental Composition Analysis of NiTiCu Sample 2 by EDS

Point 1 EDS Result		Point 2 EDS Result		Point 3 EDS Result	
Element	**Mass%**	**Element**	**Mass%**	**Element**	**Mass%**
O	0.97%	O	0.74%	O	0.00%
Ti	94.51%	Ti	98.21%	Ti	96.25%
Ni	3.87%	Ni	0.75%	Ni	3.34%
Cu	0.66%	Cu	0.30%	Cu	0.42%

From Figure 5.14, sample 2 of NiTiCu has not been fully deformed. No significant phases have also been formed in the sample. From the EDS data (Figure 5.14), Ti is the dominating element at all three analysis points. The SEM images and EDS analysis are in line with the fact that, the NiTiCu sample 2 is incompletely sintered.

5.4 XRD analysis of the samples:

5.4.1 CuAlNi:

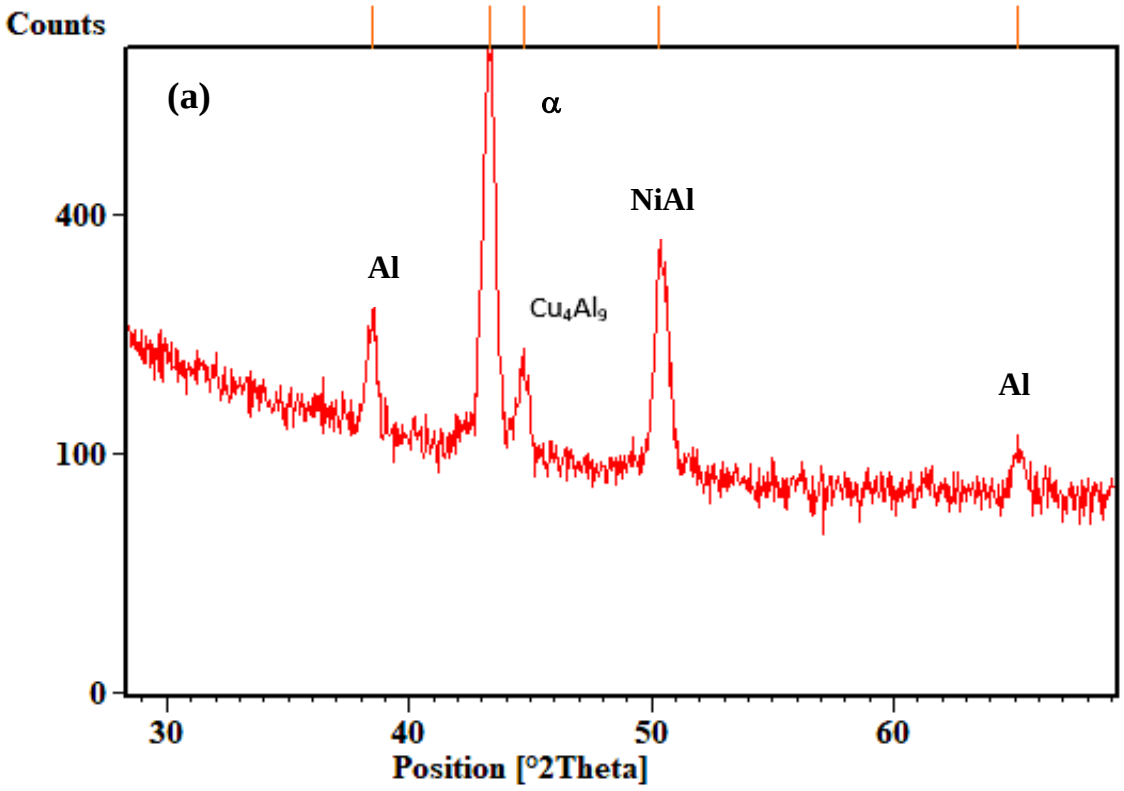

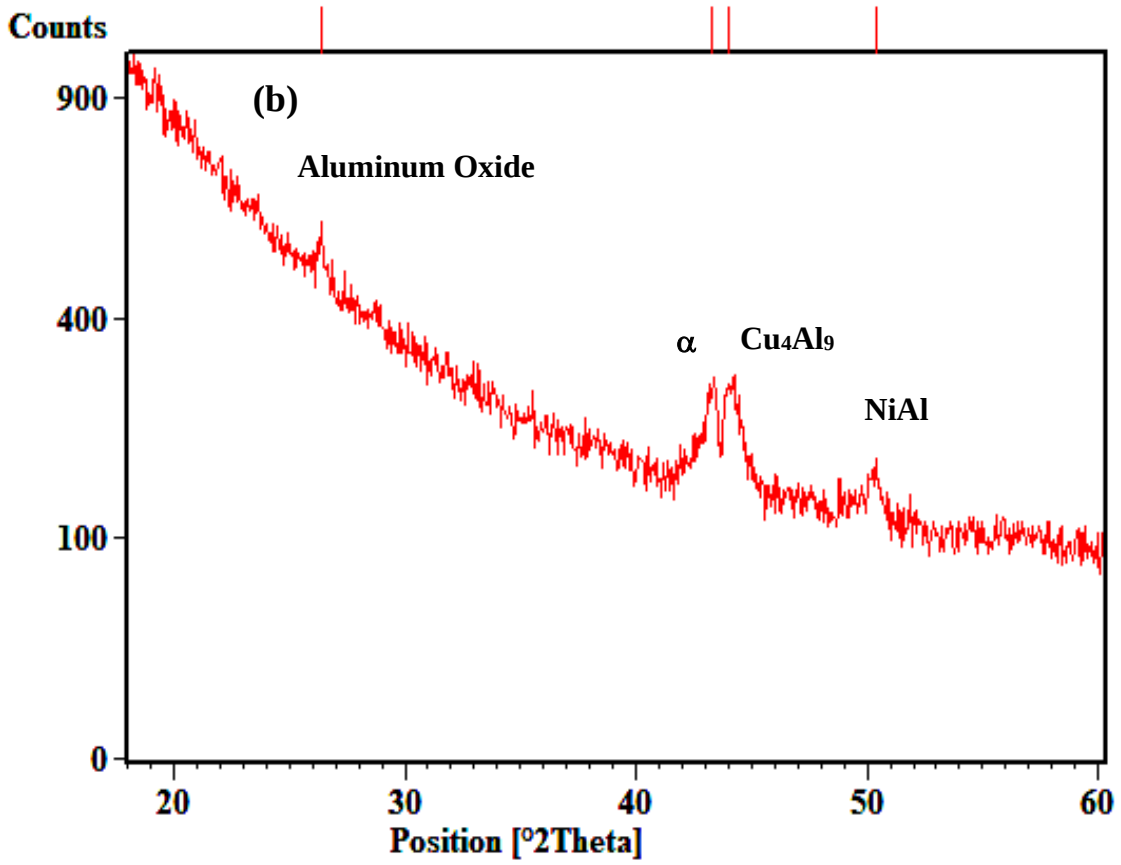

Figure 5.15: XRD pattern of (a) Sample 1, (b) Sample 2

From the XRD graph of CuAlNi sample 1 (Figure 5.15) the phases that are present in the sample are NiAl, Cu_4Al_9 and Al. Sample 2 contains Al_2O_3, NiAl, Cu_4Al_9 phase. The samples have been sintered at 475^0C. So according to the phase diagram, the identified phases should be present at the samples. The XRD graph of sample 1 (Figure 5.15 (a)) is showing the sharp peaks. Whereas in the XRD graph of sample 2 (Figure 5.15 (b)), the peaks are not sharp. So, the XRD result indicates that sample 1 is more crystalline than sample 2. The samples were prepared from very fine powder particles from ball milling, which can also be a reason for the comparatively less sharp peak.

5.4.2 NiTiCu:

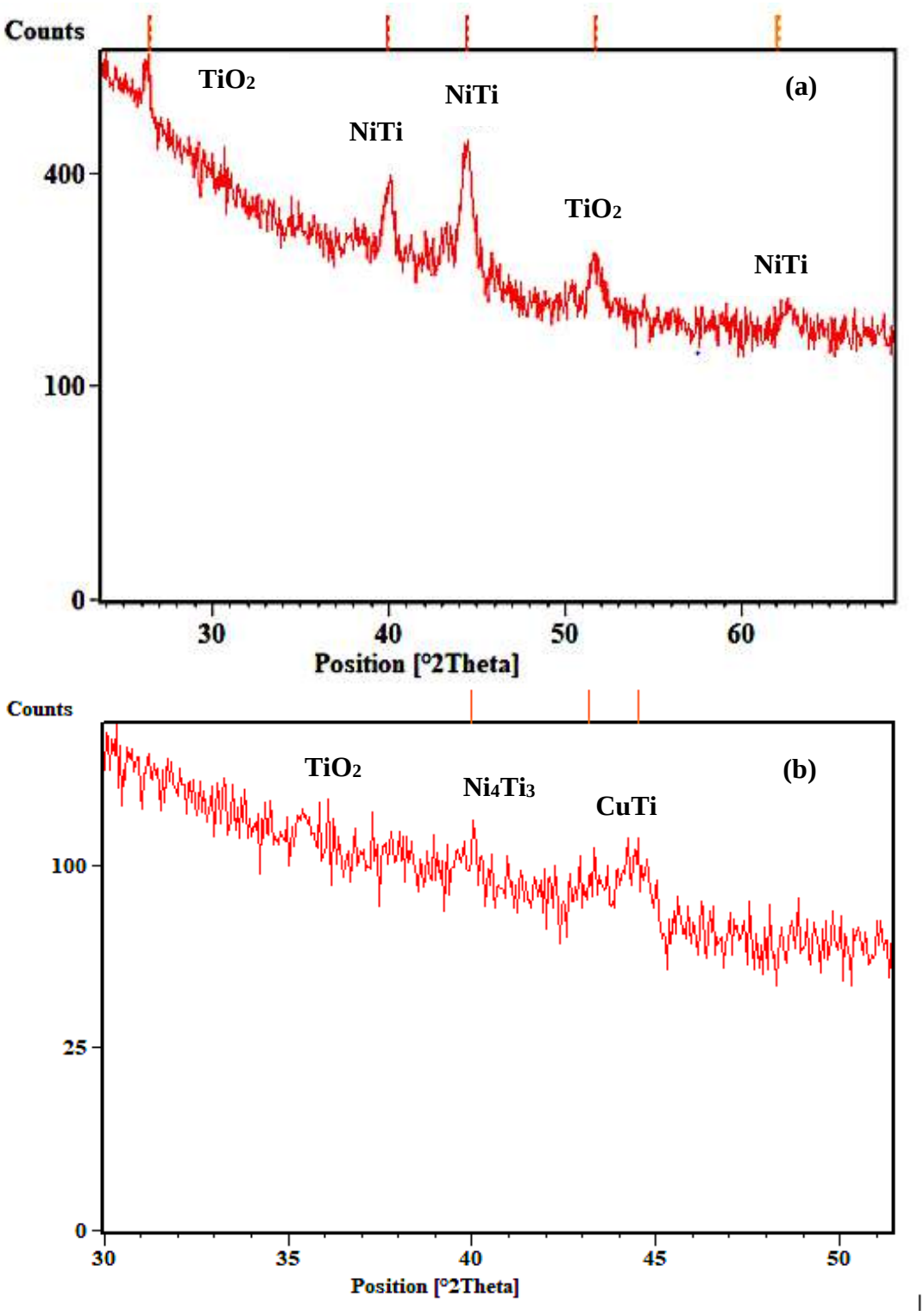

Figure 5.16: XRD pattern of NiTiCu (a) sample 1 (b) sample 2

From the XRD graphs of sample-1 and 2 it can be postulated that, the phases that had been formed while sintering is in nanophase. Fine shaped phases have been formed all over the sample. That is why the peaks are not sharp. From the XRD pattern of sample 2 for NiTiCu (Figure 5.16 (b)), no significant peak has been found, which justifies the partial welding state of the sample.

Identifying the smaller peaks of the samples, sample-1 contains the NiTi phase and TiO_2 phase. The NiTi phases are the desirable phase for shape memory properties. Analyzing the peaks of the XRD graph of NiTiCu sample 2 (Figure 5.16 (b)) with Xpert highscore plus software, smaller amount of Ni_4Ti_3, TiO_2 and CuTi phases are found. Oxygen should not be present in the sample as the samples have been prepared in a vacuum environment. But during the ball milling, the powders have been wet milled with ethanol. The oxygen may have come from the ethanol. The Ti in NiTiCu alloys has the tendency of forming TiO_2 [65].

5.5 Corrosion rate:

5.5.1 CuAlNi:

Table 5.6: After 20 days corrosion rate of the CuAlNi samples

Sample No	weight difference *Δw* (mg)	Average Area difference *ΔA* (dm^2)	MDD	MPY
Sample 1	7	0.00776	45	6
Sample 2	13	0.00476	136	19

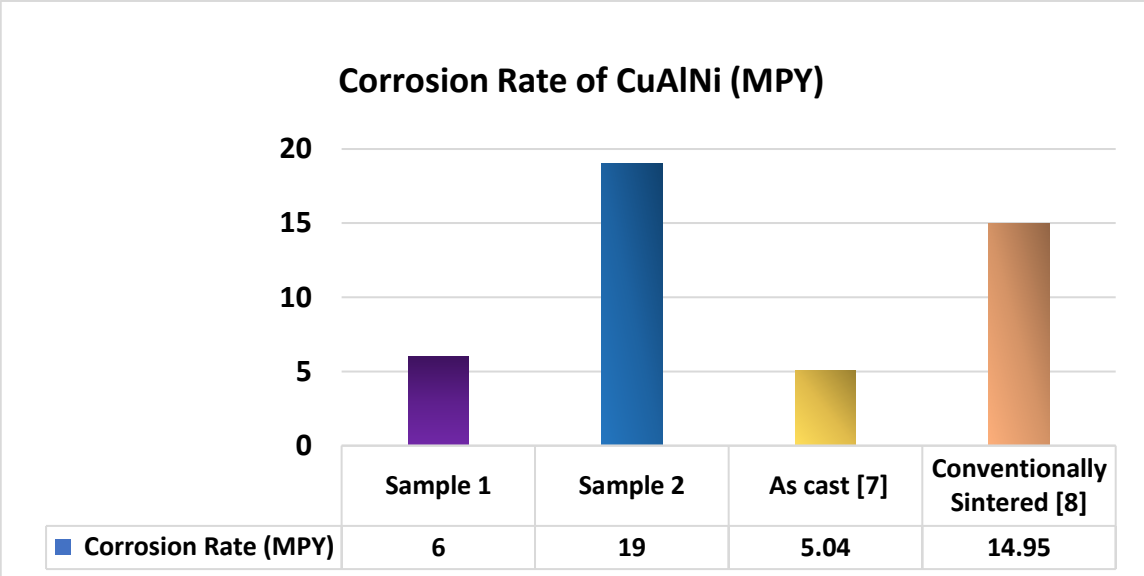

Figure 5.17: Comparison of the corrosion rate of prepared CuAlNi samples

The CuAlNi sample-1 and sample-2 have the corrosion rate of respectively 6 MPY and 19 MPY according to Table 5.6. From Figure 5.17, both CuAlNi sample 1 and sample 2 have comparatively higher corrosion rate than the CuAlNi made by the casting method [87, 65]. But sample 1 has better corrosion resistance than conventionally sintered CuAlNi alloys [87]. Sample 1 is comparatively more crystalline than sample 2. Better crystallinity offers better corrosion resistance to the CuAlNi sample 1 [88, 89, 90].

5.5.2 NiTiCu:

Table 5.7: After 20 days corrosion rate of the NiTiCu samples

Sample No	weight difference Δw (mg)	Average Area difference ΔA (dm^2)	MDD	MPY
Sample 1	3	0.003	150	24
Sample 2	15	0.003	250	39

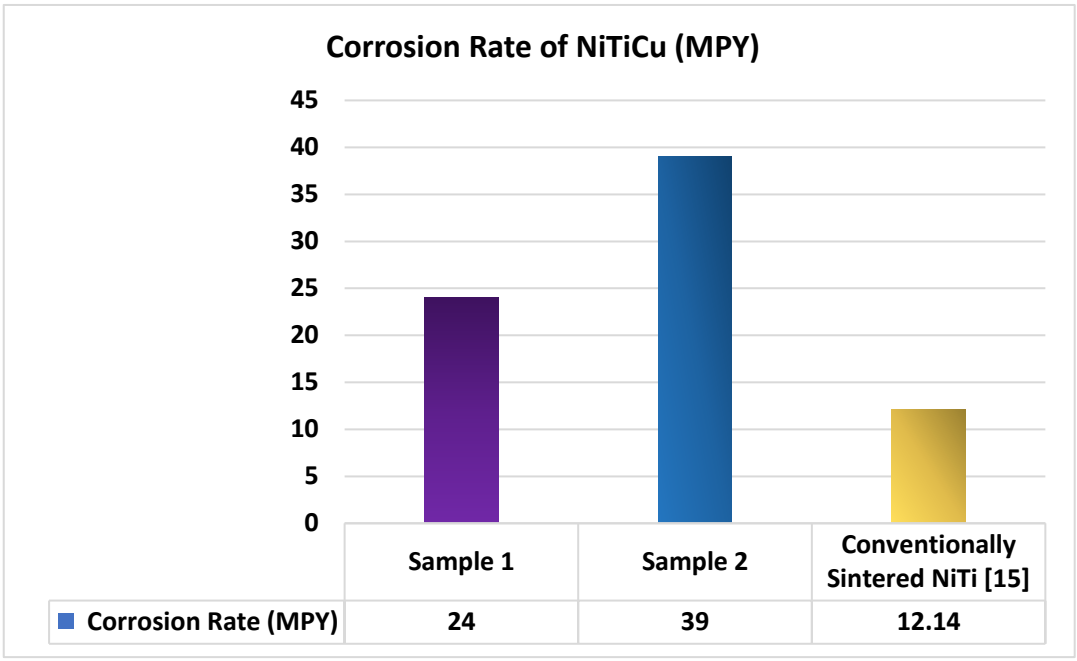

Figure 5.18: Comparison of the corrosion rate of NiTiCu with NiTi

The NiTiCu sample-1 and sample-2 have the corrosion rate of respectively 24 MPY and 39 MPY according to Table 5.7. To compare the corrosion resistance of the prepared NiTiCu samples, there is a lack of available reference data. So, the sample's corrosion rate can be compared with the NiTi SMA fabricated by the powder metallurgy route. From Figure 5.18, both NiTiCu sample 1 and sample 2 have comparatively higher corrosion rate than the conventional sintered NiTi.

Conclusion:

- The CuAlNi and NiTiCu Shape memory alloys with desired phases can be sintered at lower temperature & pressure by SPS.
- Different oxides have been found in the samples which improves the corrosion resistance of the SMAs
- The crystalline samples of CuAlNi and NiTiCu showed better corrosion resistance
- The crystalline samples of CuAlNi and NiTiCu showed comparatively less hardness
- Increasing the Al content in the CuAlNi samples increases the hardness.
- Increasing the Cu content in the NiTiCu samples increases the hardness.

Future Scope of work:

The potential future work can be carried out on the samples:

- The sample's amorphous structure can be improved by heat treatment. As an extension of this work, the samples can be heat treated to get the desired crystallinity. After heat treatment the changes in the mechanical and corrosion properties can be observed.
- The CuAlNi samples in this study have already shown promising properties. Surface treatment of the samples and investigating the improvements of biocompatibility can be done as an extension of this work.

References

[1] C. Wen, X. Yu1, W. Zeng, S. Zhao, L. Wang, G. Wan, S. Huang, H. Grover and Z. Chen, "Mechanical behaviors and biomedical applications of shape-memory materials: A review," *AIMS Materials Science,* vol. 5, no. 4, pp. 559-590, 2018.

[2] L. Petrini and F. Migliavacca, "Biomedical Applications of Shape Memory Alloys," *Journal of Metallurgy, Article ID 501483,* p. 15, 2011.

[3] Trepanier, Venugopalan and Pelton, "Corrosion Resistance and Biocompatibility of Passivated Nitinol," *ndc,* pp. 35-45, 2000.

[4] F. J. Gil and J. A. Planell, "Shape memory alloys for medical applications," *Sage journals, Proceedings of the Institution of Mechanical Engineers, Part H: Journal of Engineering in Medicine,* vol. 212, no. 6, p. 473–488.

[5] Al-Humairi and S. N. Saud, "Cu-Based Shape Memory Alloys: Modified Structures and Their Related Properties," *Recent Advancements in the Metallurgical Engineering and Electrodeposition, 10.5772/intechopen.77535 (Chapter 3).*

[6] M. Cˇolic and S. Tomic, "The Response of Macrophages to a Cu–Al–Ni Shape Memory Alloy," *Journal of Biomaterials Applications,* vol. 25, pp. 269-286, 2010.

[7] S. S. Mohammed, M. Kök, I. N. Qader and M. Coşkun, "A review study on biocompatible improvements of NiTi-based shape memory alloys," vol. 5, no. 2, pp. 125 - 130, 31 12 2021.

[8] W. Haider, N. Munroe, C. Pulletikurthi, P. K, S. Gill and S. Amruthaluri, "A Comparative Biocompatibility Analysis of Ternary Nitinol Alloys," *J Mater Eng Perform,* p. 760–764, 1 August 2009 18(5-6).

[9] C. D. Cirstea, M. Mihai, V. Cirstea, D. Patroi, H. Chivu, F. Radulescu, V. tsakiris, A. o. culicova and A. M. balagurov, "Phase relations in the NiTiCu shape-memory materials used in medicine applications," *Rev. Roum. Chim.,* Vols. 62(6-7), pp. 539-544, 2017.

[10] G. E. Monastyrsky, P. Ochin, A. V. Gilchuk, V. I. Kolomytsev and Y. Koval, "The Role of Nano-sized Fraction on Spark Plasma Sintering the Pre-Alloyed Spark-Erosion Powders," *Journal of Nano- and Electronic Physics 4(1),* March 2012.

[11] T. K, R. M. R and R. S, "Study on the densification behaviour of copper with aluminum and nickel powders through spark plasma sintering," *Journal of Mechanical Science and Technology 34 (8),* 2020.

[12] C. Velmurugan and V. Senthilkumar, "Optimization of spark plasma sintering parameters for NiTiCu shape memory alloys," *Materials and manufacturing processes.*

[13] M. Es-Souni and M. Es-Souni, "On the transformation behaviour, mechanical properties and biocompatibility of two NiTi-based shape memory alloys: NiTi42 and NiTi42Cu7," *Biomaterials,* August 2001 22(15):2153-61, PMID: 11432595.

[14] X. Huang, G. J. Ackland and K. M. Rabe, "Crystal structures and shape memory behavior of NiTi," *Nature Materials,* vol. 2, p. 307–311, 2003.

[15] H. Hermawan, D. Ramdan and J. R. P. Djuansjah, "Metals for Biomedical Applications," *Biomedical Engineering,* 2011.

[16] O. Bazaka, K. Bazaka, P. Kingshott, R. J. Crawforda and E. P. Ivanovaa, "Metallic Implants for Biomedical Applications," *The Chemistry of Inorganic Biomaterials,* pp. 1-98, 2021.

[17] R. Dasgupta, "A look into copper-based shape memory alloys- present scenario and future prospects," *Journal of Materials Research,* vol. 29, no. 16, pp. 1681-1698, 28 August 2014.

[18] M. C˘olic, R. Rudolf, D. Stamenkovic, I. Anz˘el, Vuc˘evic, Dragana, M. Jenko, V. Lazic and G. Lojen, "Relationship between microstructure, cytotoxicity and corrosion properties of a Cu–Al–Ni shape memory alloy," *Acta Biomater,* January 2010;6(1):308-17. doi: 10.1016/j.actbio.2009.06.027. Epub 2009 Jun 21..

[19] S. Saud, E. Hamzah, T. Abubakar and H. Bakhsheshi-Rad, "Thermal aging behavior in Cu-AlNi-xCo shape memory alloys," *J Therm Anal Calorim,* p. 1273–1284, 2015 119(2).

[20] J. M. G. Fuentes, "Phase changes behavior of NiTinol shape memory alloys," *Advanced Engineering Materials,* p. 4, 2002.

[21] Johnson.United States Patent (10) Patent US 8,556,969 B2, 15 October 2013.

[22] F. J. GIL and J. A. PLANELL, "Comparison between the mechanical behavior of Ti-Ni and Ti-Ni-Cu shape memory alloys used for orthodontic applications," *ISRN Dent.,* 2011, PMID: 21991455.

[23] V. Tyrpekl, C. Berkmann, M. Holzhäuser, F. Köpp, M. Cologna, T. Wangle and J. Somers, "Implementation of a spark plasma sintering facility in a hermetic glovebox for compaction of toxic, radiotoxic, and air sensitive materials," *Review of Scientific Instruments,* vol. 86, no. 2, 2015.

[24] S. Samal, O. Molnárová, F. P. ˚uša, J. Kope˘cek, L. ˇ. Heller, P. Šittner, M. Škodová, L. Abate and I. Blanco, "Net-Shape NiTi Shape Memory Alloy by Spark Plasma Sintering Method," *Appl. Sci.,* vol. 11, 2021, 1802.

[25] M. l. young, J. d. Defouw, J. Frenzel and a. D. c. Durand, "Cast-Replicated NiTiCu Foams with Superelastic Properties," *The Minerals, Metals and Materials Society and ASM International,* 2012.

[26] D. Ghosh, S. Godeshala, R. Nitiyanandan, M. S. Islam, J. R. Yaron, D. Dicaudo, J. Kilbourne and K. Rege, "Copper-eluting Fibers for Enhanced Tissue Sealing and Repair," *ACS Applied Materials and Interfaces,* vol. 12, no. 25, pp. 27951-27960.

[27] L. A. Volodina, A. N. Zhigach, I. O. Leypunsky, E. S. Zotova and N. N. Glushchenko, "The influence of physical-chemical characteristics of surface modified copper nanoparticles on E. coli cell population growth suppression and on electrostatic properties of their membranes," *Biophysics,* vol. 58, p. 394–401, 2013.

[28] M. Valodkar, P. S. Rathore, R. N. Jadeja, M. Thounaojam, R. V. Devkar and S. Thakore, "Cytotoxicity evaluation and antimicrobial studies of starch capped water-soluble copper nanoparticles," *J Hazard Mater,* 30 January 2012 201-202:244-9, Epub 2011 Dec 1.

[29] Y. h. Y. Peng Wang, K. Xu, H. Zhong, Y. Yang, S. Jin, KeYang and X. Qi, "Biological applications of copper-containing materials," *Bioactive Materials,* vol. 6, no. 4, pp. 916-927, April 2021.

[30] C. Exley, "The toxicity of aluminum in humans," *Morphologie,* June 2016; 100(329):51-5, Epub 2016 Feb 28.

[31] R. D. Mantcheva, D. D. Kiradzhiyska, Y. Feodorova and K. I. Draganova, "Biocompatibility of aluminium alloys and anodic Al2O3," *Bulgarian Chemical Communications,* Vols. 49, Number 2, pp. 371-376, 2017.

[32] M. Anke, L. Angelow, M. Glei, M. Müller and H. Illing, "The biological importance of nickel in the food chain," *Fresenius' Journal of Analytical Chemistry*, vol. 352, pp. 92-96, 1995.

[33] G. Laing and P. E. Dupont, "Beating-heart mitral valve chordal replacement," *Annual International Conference of the IEEE Engineering in Medicine and Biology Society*, 2011.

[34] J. Ryhänen, "Biocompatibility of Nitinol," *Minimally Invasive Therapy and Allied Technologies*, vol. 9, pp. 99-105, 2000.

[35] D. Mantovani, "Shape memory alloys: Properties and biomedical applications," *JOM*, vol. 52, pp. 36-44, 2000.

[36] A. T. Sidambe, "Biocompatibility of Advanced Manufactured Titanium Implants—A Review," *Materials (Basel)*, 19 December 2014; 7(12):8168-8188.

[37] H. Matsuno, AtsuroYokoyama, FumioWatari, MotohiroUo and TakaoKawasaki, "Biocompatibility and osteogenesis of refractory metal implants, titanium, hafnium, niobium, tantalum and rhenium," *Biomaterials*, vol. 22, no. 11, pp. 1253-1262, June 2001.

[38] T. Albrektsson, P. I. Brånemark, H. A. Hansson and J. Lindström, "Osseointegrated titanium implants. Requirements for ensuring a long-lasting, direct bone-to-implant anchorage in man," *Acta Orthop Scand*, 1981;52(2):155-70.

[39] K. McNamaraa, S. Beloshapkina, K. M. Hossain, M. S. Dhoubhadel and S. A. M. Tofail, "Tantalum Oxide Films on NiTi Plates," *Applied Surface Science*, vol. 535, 1 January 2021, 147621.

[40] W. Geurtsen, "Biocompatibility of Dental Casting Alloys," vol. 13, no. 1, pp. 71-84, 1 January 2002.

[41] L. Vrsalović, a. S. Gudić, a. L. Terzić, a. I. Ivanić, S. Kožuh, M. Gojić and E. E. Oguzie, "Intergranular Corrosion of Cu-Al-Ni Alloy in 0.5 mol dm−3 H2SO4 Solution," *Chemists and Chemical Engineers*, pp. 457-464, 63(9-10).

[42] N. Sharma, G. Singh, H. Hegab, M. Mia and N. K. Batra, "Tribo-corrosion characterization of NiTiCu alloy for bioimplant applications," *Materials Research Express*, vol. 6, no. 9, 2019.

[43] T. Volkov-Husovíc, I. Ivaníc, S. Kožuh, S. Stevanovíc, M. Vlahovíc, S. Martinovíc, S. Stopic and a. M. Gojíc, "Microstructural and Cavitation Erosion Behavior of the CuAlNi Shape Memory Alloy," *Metals*, vol. 11, no. 7, p. 997, 2021.

[44] L. G. Machado and M. A. Savi, "Medical applications of shape memory alloys," *Braz J Med Biol Res*, vol. 36, no. 6, pp. 683-691, June 2003.

[45] V. Ricarte, I. Hurtado, J. Herreros, MLNo and J. S. Juan, "Precipitation of the stable phases in the Cu-Al-Ni Shape Memory Alloys," *Scripta Materialia*, vol. 6, 1996.

[46] A. Agrawal and R. K. Dube, "Methods of fabricating Cu-Al-Ni shape memory alloys," *Journal of Alloys and Compounds*, vol. 750, pp. 235-247, 25 June 2018.

[47] C. Naresh, "Shape memory alloys: a state of art review," *IOP Conf. Series: Materials Science and Engineering 149*, 2016.

[48] M. Suarez, A. Fernandez, J. L. Menendez, R. Torrecillas, H. U. Kessel, J. Hennicke, R. Kirchner and T. Kessel, "Challenges and Opportunities for Spark Plasma Sintering: A Key Technology for a New Generation of Materials," *Sintering Applications*, 2013.

[49] B. Basu, "Some Fundamentals on Spark Plasma Sintering as a processing tool to fabricate biomaterials," *Slides (44), Department of Materials Science & Engineer, Indian Institute of Technology, Kanpur.*

[50] D. J. Blackwood, "Biomaterials: Past Successes and Future Problems," *Corros. Rev.*, vol. 21, no. 2, pp. 97-124, 2003.

[51] M. Tokita, "The potential of Spark Plasma Sintering (SPS) method for the fabrication," *Advances in Science and Technology,* vol. 63, pp. 322-331, 2010, Online available since 2010/Oct/27 at www.scientific.net © (2010) Trans Tech Publications, Switzerland on an industrial scale of Functionally Graded Materials.

[52] L. Peltier, O. Perroud, P. Moll, J. Slowensky, P. Charbonnier, A. Eberhardt and A. Hautcoeur, "Production and Mechanical Properties of Cu-Al-Ni-Be Shape Memory Alloy Thin Ribbons Using a Cold Co-Rolled Process," *Shape Memory and Super elasticity, Springer,* p. 10, 2021.

[53] W. J. Zhu, L. I. Duarte and C. Leinenbach, "Experimental study and thermodynamic assessment of the Cu–Ni–Ti system," *Calphad,* vol. 47, p. 9–22.

[54] S. M. Tanga, C. Y. Chunga and W. G. Liu, "Preparation of Cu single bond Al single bond Ni-based shape memory alloys by mechanical alloying and powder metallurgy method," *Journal of Materials Processing Technology,* vol. 63, no. 1-3, pp. 307-312, January 1997.

[55] M. Shafeeq, G. K. Gupta, Hirshikesh and M. M. M. a. O. P. Modi, "Effect of milling parameters on processing, microstructure and properties of Cu–Al–Ni–Ti shape memory alloys".

[56] S. K. Vajpai, R. K. Dube and S. Sangal, Metall. Mater. Trans. A 42A (2011) 3178–3189.

[57] P. Salwa and T. Goryczka, "Crystallization of Mechanically Alloyed Ni50Ti50 and Ti50Ni25Cu25 Shape Memory Alloys," *JMEPEG,* vol. 29, p. 2848–2852, 2020.

[58] B. G. Pound, "Corrosion behavior of metallic materials in biomedical applications. I. Ti and its alloys," *Corros. Rev.*, vol. 32, no. 1-2, pp. 1-20, 2014.

[59] N. Eliaz, "Corrosion of metallic biomaterials: A review," *Materials (Basel),* vol. 12, no. 3, 2019.

[60] A. Aydogdu, Y. Aydogdu and O. Adigiize, "Improvement of Hardness and Microstructures by Ageing in Shape Memory CuAINi Alloys," *J. PHYS. IV FRANCE 7,* 1997.

[61] C. A. Canbay and Z. Karagoz, "Effects of Annealing Temperature on Thermomechanical Properties of Cu–Al–Ni Shape Memory Alloys," *Int J Thermophys,* vol. 34, p. 1325–1335, 2013.

[62] Suru, Marius-Gabriel, Lohan, Nicoleta-Monica, Pricop, Bogdan, Mihalache, Elena, Mocanu, Mihai, Bujoreanu and Leandru-Gheorghe, "Precipitation Effects on the Martensitic Transformation in a Cu-Al-Ni Shape Memory Alloy," *Journal of Materials Engineering and Performance,* vol. 25, no. 4, pp. 1562-1569.

[63] M. Cˇolic, R. Rudolf, D. Stamenkovic, I. A. b, D. Vucˇevica, M. Jenko, V. Lazicc and G. Lojen, "Relationship between microstructure, cytotoxicity and corrosion properties of a Cu–Al–Ni shape memory alloy," *Acta Biomater,* pp. 308-317, January 2010; 6(1).

[64] S. P. Alisova, P. B. Budberg and R. A. Nauk, "The Cu-Ni-Ti (Copper-Nickel-Titanium) system," *Metally,* vol. 4, no. 218, 1992 (in Russian).

[65] M. Abedi, A. Asadi, S. Vorotilo and A. S. Mukasyan, "A critical review on spark plasma sintering of copper and its alloys," *Journal of Materials Science,* vol. 56, no. 7, December 2021.

[66] A. E. Svirid, V. G. Pushin, N. N. Kuranova, V. V. Makarov and Y. M. Ustyugov, "Structural and Phase Transformations and Physical and Mechanical Properties of Cu-Al-Ni Shape Memory Alloys Subjected to Severe Plastic Deformation and Annealing," *Materials,* 2021, 14, 4394.

[67] D. B. Gera, J. Soyama, R. D. Cava, J. E. Spinelli and C. S. Kiminami, "The Influence of Sintering Parameters in the Microstructure and Mechanical Properties of a Cu–Al–Ni–Mn–Zr Shape Memory Alloy," *Adv. Eng. Mater.,* 2018, 1800372.

[68] N. Ye and X. Ren, "Corrosion Behaviors of Sputtered NiTiCu Shape Memory Films," *Journal of Materials Science and Chemical Engineering,* vol. 8, pp. 7-15, 2020.

[69] C. Yang, Q. R. Cheng, L. H. Liu, Y. H. Li and Y. Y. Li, "Effect of minor Cu content on microstructure and mechanical property of NiTiCu bulk alloys fabricated by crystallization of metallic glass powder," *Intermetallics,* vol. 56, p. 37–43.

[70] C. Tatar, R. Acar and I. N. Qader, "Investigation of thermodynamic and microstructural characteristics of NiTiCu shape memory alloys produced by arc-melting method," *Eur. Phys. J. Plus,* 2020, 135:311.

[71] N. A. Tanışa, H. Gökmeşe and B. Bostanc, "Effect of Cu addition on microstructure and mechanical properties of NiTi based shape memory alloy," *International Advanced Researches and Engineering Journal,* vol. 02, no. 01, pp. 020-026, 2018.

[72] T. Goryczka and J. V. Humbeeck, "NiTiCu shape memory alloy produced by powder technology," *Journal of Alloys and Compounds,* vol. 456, pp. 194-200, 2008.

[73] C. D. Cirstea, M. LUNGU, A. M. BALAGUROV, V. MARINESCU, O. CULICOV, G. Sbarceaa and V. CIRSTEA, "Shape memory NiTi and NiTiCu alloys obtained by spark plasma sintering process," *Advanced Engineering Forum,* vol. 13, pp. 83-90, 20 10 2014, ISSN: 2234-991X.

[74] T. M. Ammar and A. A. R. Al-khafaji, "Effect of (Al-Ni) and (Cu-Ni) Concentrations Ratios on the Hardness and Porosity of Ternary (CuAl-Ni) Smart Alloys," *Australian Journal of Basic and Applied Sciences,* vol. 12, no. 2, pp. 36-48, February 2018.

[75] K. D. Salman, "Manufacture of shape memory alloys NiTi and NiTiCu by casting method and studying the effect of adding the copper element in different proportions to the binary alloy on the microstructure, phase transformations and conductivity," *Journal of Physics: Conference Series 1973,* 2021.

[76] S. N. Alnomani, E. Z. Fadhel and A. A. Mehatlaf, "Prepare Nitinol Alloys and Improve their Hardness Using Copper as an Alloying Element," *International Journal of Applied Engineering Research ISSN 0973-4562,* vol. 12, no. 14, pp. 4299-4308, 2017.

[77] M. Navarro, A. Michiardi, O. Castaño and J. A. Planell, "Biomaterials in orthopaedics," *J R Soc Interface,* vol. 5, no. 27, p. 1137–1158, 6 October 2008.

[78] G. Szcz¸esny, M. Kopec, D. J. Politis, Z. L. Kowalewski, A. Łazarski and T. Szolc, "A Review on Biomaterials for Orthopaedic Surgery and Traumatology: From Past to Present," *Materials,* vol. 15, 2022, 3622.

[79] S. Alavi and M. Kachuie, "Assessment of the hardness of different orthodontic wires and brackets produced by metal injection molding and conventional methods," *Dent Res J (Isfahan),* vol. 14, no. 4, p. 282–287, Jul-Aug 2017.

[80] M. Hans, "Mechanical properties of biomaterials," *J Biotechnol Biomater,* vol. 11, no. 6, 2021.

[81] S. Saud, E. Hamzah, T. Abubakar and M. K. Ibrahim, "Effect of a fourth alloying element on the microstructure and mechanical properties of Cu–Al–Ni shape memory alloys," *Journal of Materials Research,* June 2015.

[82] R. A. Portier, P. Ochinb, A. Pasko, G. E. Monastyrskyc, A. V. Gilchukc, V. I. Kolomytsev and Y. N. Koval, "Spark plasma sintering of Cu–Al–Ni shape memory alloy".

[83] M. Gojic, L. Vrsalovic, S. Kozuh, A. Kneissl, I. Anzel, S. Gudic, B. Kosec and M. Kliski, "Electrochemical and microstructural study of Cu–Al–Ni shape memory alloy".

[84] N. m. Dawood and A. R. A. Ali, "The Effect of Boron Addition on The Microstructure and Corrosion Resistance of Cu-Al-Ni Shape-Memory Alloys Prepared by Powder Technology," *Key Engineering Materials,* vol. 911, pp. 96-102.

[85] P. Ochin, A. Pasko, G. E. Monastyrsky, A. V. Gilchuk, V. I. Kolomytsev, Y. Koval and R. Portier, "Spark plasma sintering of Cu-Al-Ni shape memory alloy, to be published in J. Alloy Compd".

[86] E. Omrani, A. Shokuhfar, A. Etaati, A. D. M and A. Saatian, "The Effects of Homogenization Time and Cooling Environment on Microstructure and Transformation Temperatures of Ni-42.5wt%Ti-7.5wt%Cu Alloy," *Defect and Diffusion Forum,* Vols. 297-301, pp. 344-350, 2010, Switzerland.

[87] A. Raheem, K. A. Ali and N. M. Dawood, "The Effect of Boron Addition on The Microstructure and Corrosion Resistance of Cu-Al-Ni Shape-Memory Alloys Prepared by Powder Technology," *IOP Conf. Series: Materials Science and Engineering 987,* 2020, 012028.

[88] V. Recarte, I. Hurtado, J. Herreros, M. L. Nb and J. S. Juan, "Precipitation of the stable phases in cu-al-ni shape memory alloys," *Materials Science, Scripta Materialia,* 15 January 1996.

[89] V. Recarte, J. Pérez-Landazábal, A. Ibarra, M. Nó and J. S. Juan, "High-temperature phase decomposition process in a Cu–Al–Ni shape memory alloy," *Materials Science and Engineering A 378,* p. 238–242, 2004.

[90] V. P.-L. Recarte, J. I, J. Campo, R. B. Pérez-Saez, M. L. No and J. S. Juan, "In situ study of the β phase decomposition process in a Cu-Al-Ni shape memory alloy processed by powder metallurgy," *Journal de Physique IV (Proceedings),* vol. 112, no. 1, pp. 605-609, October 2003.